

# Massive Color-Octet Bosons: Bounds on Effects in Top-Quark Pair Production

ULRICH HAISCH<sup>a,c</sup> AND SUSANNE WESTHOFF<sup>a,b</sup>

<sup>a</sup>*Institut für Physik (THEP), Johannes Gutenberg-Universität  
D-55099 Mainz, Germany*

<sup>b</sup>*Helmholtz-Institut Mainz, Johannes Gutenberg-Universität  
D-55099 Mainz, Germany*

<sup>c</sup>*Rudolf Peierls Centre for Theoretical Physics, University of Oxford  
OX1 3PN Oxford, United Kingdom*

## Abstract

A critical survey of the existing direct and indirect constraints on massive spin-one color octets is presented. Since such new degrees of freedom appear in any extension of the color gauge group to a product of at least two  $SU(3)$  factors, we keep our discussion as independent as possible from the underlying theory. In the framework of scenarios that involve flavor non-universal couplings, we show that excessive flavor-changing neutral currents can be avoided by a suitable alignment in flavor space. Constraints from electroweak precision observables and direct production at hadron colliders still leave space for sizable new-physics effects in top-quark pair production, in particular a large forward-backward asymmetry. In this context, we derive a model-independent upper bound on the asymmetry that applies whenever top-antitop production receives the dominant corrections from  $s$ -channel exchange of a new single color-octet resonance.

# Contents

<b>1</b>	<b>Introduction</b>	<b>1</b>
<b>2</b>	<b>Flavor Non-Universal Axigluon Model</b>	<b>3</b>
<b>3</b>	<b>Flavor Physics</b>	<b>5</b>
<b>4</b>	<b>Precision Measurements</b>	<b>11</b>
<b>5</b>	<b>Collider Observables</b>	<b>19</b>
<b>6</b>	<b>Numerical Analysis</b>	<b>27</b>
<b>7</b>	<b>Conclusions</b>	<b>42</b>
<b>A</b>	<b>Form Factors for <math>Z \rightarrow q\bar{q}</math></b>	<b>44</b>
<b>B</b>	<b>Corrections to Oblique Parameters</b>	<b>45</b>
<b>C</b>	<b>Contributions to <math>t\bar{t}</math> Observables</b>	<b>48</b>
<b>D</b>	<b>Matrix Elements for Dijet Production</b>	<b>50</b>

## 1 Introduction

The CERN Large Hadron Collider (LHC) has launched a new era of particle physics research. With the first  $45\text{ pb}^{-1}$  of luminosity recorded by both ATLAS and CMS during stable  $pp$  beams at 7 TeV center-of-mass (CM) energy, it has started to supersede the Fermilab Tevatron at the energy frontier. While much of the attention concerning new-physics searches has centered around theories that offer new insights into the mechanism of electroweak symmetry breaking (EWSB), all initial states at hadron colliders consist of particles that are charged under the color gauge group. Any new strongly-coupled colored resonance with TeV-scale mass will therefore be copiously produced at the LHC. Experimental studies of the properties of such resonances will provide us with valuable information about the underlying theory and may also give us some clues about the dynamics of EWSB and/or other deep questions left unanswered by the standard model (SM) of particle physics.

Of general phenomenological interest are massive color-octet vector bosons, whose production channels interfere with the dominant parton decay channels of quantum chromodynamics (QCD). Resonances of this kind arise in a wide spectrum of new-physics models, for instance in extra dimension scenarios of Randall-Sundrum type [1], which explain the gauge hierarchy by gravitational red-shifting, or in technicolor theories, where EWSB is triggered by new strong dynamics (for a review see [2]). Many of these models have in common that they involve an extension of the SM color gauge group  $SU(3)_c$  to a chiral product group of two (or more)  $SU(3)$  factors, which is spontaneously broken to its diagonal subgroup at energies above the

electroweak scale. The most important model-independent prediction of the original proposal of chiral color [3], as well as its numerous variations, is the existence of a massive color-octet vector boson. This new resonance, dubbed axigluon [3, 4, 5], interacts strongly and possesses axial-vector couplings to fermions, whose chiral states are charged under different  $SU(3)$  factors. While the earliest chiral color models were treating the different quark flavors universally, it is also possible to construct flavor non-universal scenarios by choosing anomaly-free fermion representations with appropriate color quantum numbers. In fact, in concepts like topcolor [6, 7] and certain coloron models [8, 9], the massiveness of the top quark and/or the mechanism of EWSB are explained by the exchange of a TeV-scale gluon-like object with enhanced couplings to heavy quarks. Due to the compositeness of the top quark, the very same feature is shared by Kaluza-Klein (KK) gluons in warped extra dimensions and their dual conformal field theory interpretations [10, 11, 12]. In flavor non-universal set-ups, the existence of a massive colored octet might hence serve a higher purpose, rather than being an accident.

Another more pragmatic motivation to study the physics of flavor non-universal color-octet bosons is provided by the puzzling picture of results in top-quark pair production obtained at the Tevatron: the accurately measured total cross section [13, 14] and the spectrum in bins of the invariant mass of the top-antitop pair [15] are both in good agreement with their SM predictions, but the inclusive  $t\bar{t}$  forward-backward asymmetry and its distribution at high invariant masses  $M_{t\bar{t}} > 0.45$  TeV [16] are not. The inclusive asymmetry has been measured several times in the lepton plus jets channel [17, 18, 19, 20] and very recently also in the dilepton channel [21]. The central values of all measurements turned out to be larger than expected from the sole presence of SM physics. The experimental situation is tantalizing because the anomaly at high  $M_{t\bar{t}}$  has a statistical significance of  $3.4\sigma$ , which translates into a discrepancy of about  $2\sigma$  in the inclusive measurements. The sharp growth of the excess with the invariant mass of the  $t\bar{t}$  system suggests the presence of a new heavy particle in top-quark pair production. By its very nature a heavy color-octet resonance with appropriate axial-vector couplings to the top quark and the light quarks seems to be able to generate a sizable  $t\bar{t}$  forward-backward asymmetry. But how big can the effect of such a flavor non-universal colored resonance in the asymmetry be, given the strong constraints imposed by the symmetric top-quark observables? How restrictive are other constraints that follow from flavor physics, precision measurements at the  $Z$  pole, and direct production? In particular, do they leave enough space to explain the anomaly?

The purpose of this article is to provide quantitative answers to these questions by critically assessing the existing direct and indirect constraints on axigluons and their doppelgänger. We find that the dominant indirect constraints arise from the electroweak precision observables (EWPOs) [22]. At the one-loop level, the presence of heavy gluon partners alters the  $Z$ -boson couplings to quarks, which are tightly constrained by the precise measurements of the bottom-quark pseudo observables (POs), as well as the total and hadronic decay widths of the  $Z$  boson. Less significant, but nevertheless non-trivial, are the constraints that stem from two-loop contributions to the Peskin-Takeuchi parameters which encode oblique corrections to the weak gauge boson propagators [23]. While axigluon models with flavor non-universal couplings are rife with new and dangerous tree-level flavor-changing neutral currents (FCNCs), the constraints resulting from neutral meson mixing turn out to be highly model-dependent. Nevertheless, there exists a minimal, though quite weak, constraint from  $D$ -meson mixing that

has to be respected by any scenario with flavor non-universal interactions. Direct constraints derive from resonance searches and analyses of angular distributions in dijet production at hadron colliders. The recent LHC bounds [24, 25, 26] significantly restrict the properties of any strongly-coupled  $s$ -channel resonance produced by the annihilation of light quarks and antiquarks. Taking direct and indirect constraints into account, we show that the effects of a flavor non-universal axigluon in top-quark pair production yield a satisfactory fit to the data, but that the size of effects is limited by direct searches. Throughout the article, we try to keep our discussion as general as possible by presenting analytic formulas that are applicable to a wide class of scenarios involving massive color-octet bosons. Other recent studies that discuss the physics of heavy gluon partners, which partially overlap with our work, include [27, 28, 29, 30, 31, 32, 33, 34, 35, 36].

This article is organized as follows. After reviewing in Section 2 the basic ingredients of the flavor non-universal axigluon model, we study in Section 3 the additional sources of flavor breaking present in the scenario and calculate their impact on  $K-\bar{K}$ ,  $B_{d,s}-\bar{B}_{d,s}$ , and  $D-\bar{D}$  mixing. Section 4 is devoted to a discussion of the indirect constraints coming from the EWPOs. In Section 5, we elaborate on effects of heavy colored resonances at hadron colliders. After setting the scene for new physics in top-quark observables, we derive the constraints from dijet production at the LHC. The actual bounds on the parameter space of models with massive color-octet vectors are presented in Section 6, which also contains a detailed study of axigluon effects in top-quark pair production. We conclude in Section 7. A series of appendices contains useful details concerning some technical aspects of our calculations.

## 2 Flavor Non-Universal Axigluon Model

We consider the extended gauge group  $SU(3)_A \times SU(3)_B$  with coupling constants  $g_A$  and  $g_B$ , which is spontaneously broken<sup>1</sup> at a scale of  $f = \mathcal{O}(1 \text{ TeV})$  down to the QCD gauge group  $SU(3)_c$ . This breaking pattern yields two mass eigenstates of color-octet gauge bosons. A massless particle  $g$ , which can be identified with the regular gluon, and an axigluon  $G$ , that acquires a mass  $M_G = gf$  with  $g = \sqrt{g_A^2 + g_B^2}$ . The corresponding fields are related to the gauge eigenstates  $A_\mu$  and  $B_\mu$  via

$$\begin{pmatrix} G_\mu \\ g_\mu \end{pmatrix} = \begin{pmatrix} \sin \theta & -\cos \theta \\ \cos \theta & \sin \theta \end{pmatrix} \begin{pmatrix} A_\mu \\ B_\mu \end{pmatrix}, \quad \tan \theta = \frac{g_A}{g_B}. \quad (1)$$

Notice that physical predictions are symmetric under the exchange of  $g_A$  with  $g_B$ , so that only half of the parameter space in the mixing angle  $\theta$  is physical. This means that instead of considering values of  $\theta$  in the range  $[0^\circ, 90^\circ]$ , one can restrict  $\theta$  to lie within  $[0^\circ, 45^\circ]$ . The gauge sector of the model is therefore fully characterized by two parameters only, the axigluon mass  $M_G$  and the mixing angle  $\theta$ .

If left- and right-chiral quarks carry different charges under the  $SU(3)_A$  and  $SU(3)_B$  gauge factors, the axigluon exhibits axial-vector couplings  $g_A^q$  to quarks. This is an interesting feature because it leads to a non-zero forward-backward asymmetry  $A_{\text{FB}}^t$  in  $t\bar{t}$  production at

---

<sup>1</sup>We ignore possible effects of the scalar sector responsible for this breaking in our work.

	$Q_{1,2}$	$u_{1,2}^c$	$d_{1,2}^c$	$Q_{3,4}$	$u_{3,4}^c$	$d_{3,4}^c$
$SU(3)_A$	3	1	1	1	$\bar{3}$	$\bar{3}$
$SU(3)_B$	1	$\bar{3}$	$\bar{3}$	3	1	1

Table 1: Charge assignments of the quark fields under the  $SU(3)_A$  and  $SU(3)_B$  gauge factors. The symbols  $Q_p$  and  $u_p^c$ ,  $d_p^c$  with  $p = 1, 2, 3, 4$  denote electroweak doublets and conjugate singlets, respectively.

tree level [37, 38]. In order to achieve a positive shift in  $A_{\text{FB}}^t$  the axigluon has to couple to the first and the third generation of quarks with opposite axial-vector couplings [39], implying  $g_A^q g_A^t < 0$ .<sup>2</sup> This observation motivates us to choose the charge assignments for the quark fields as in Table 1, following the proposal in [27].

We emphasize that in order to cancel the gauge anomaly our flavor non-universal axigluon model contains a sequential fourth generation of heavy quarks and leptons (the charge assignments of the lepton fields have not been reported in Table 1 for brevity). While the absolute mass scale of the new fermions is bounded from below by direct searches,<sup>3</sup> both the mass splitting and inter-generational mixing of extra chiral matter is strongly constrained by EWPOs and flavor physics. The latter constraints as well as those following from the bottom-quark POs, are readily evaded by setting the mixing between the first three and the fourth generation to zero. In this case, one is left with the constraints that arise from the oblique parameters  $S$  and  $T$ , which are mostly sensitive to the mass splitting of the fourth-generation up- and down-type quarks  $u_4$  and  $d_4$ . We will be more precise below (see the discussion in Section 4), but suffice to say that the wide spread of possible fourth-generation contributions to  $S$  and  $T$  does not allow to derive any model-independent bound on the parameter space of the flavor non-universal axigluon model from the oblique corrections.

In the further discussion, we will restrict ourselves for most of the time, to the first three generations of quarks. Their couplings to the axigluon are given by  $(i, j = 1, 2, 3)$

$$\mathcal{L} \supset g_s \left[ (\Gamma_L^u)_{ij} \bar{u}_L^i \not{G} u_L^j + (\Gamma_L^d)_{ij} \bar{d}_L^i \not{G} d_L^j + (\Gamma_R^u)_{ij} \bar{u}_R^i \not{G} u_R^j + (\Gamma_R^d)_{ij} \bar{d}_R^i \not{G} d_R^j \right], \quad (2)$$

where  $g_s = g \sin \theta \cos \theta$  is the strong coupling constant,  $u_{L,R}^i$  ( $d_{L,R}^i$ ) are left- and right-handed chiral up-type (down-type) quark fields of generation  $i$ . We use the abbreviation  $\not{G} = \gamma^\mu G_\mu^a T^a$ , where  $T^a$  is a generator of  $SU(3)_c$  in the adjoint representation. In the weak interaction basis indicated by a superscript “ $I$ ”, the axigluon couplings are diagonal  $3 \times 3$  matrices in flavor space,

$$\Gamma_L^I = (\Gamma_L^{u,d})^I = \text{diag} (g_L^\ell, g_L^\ell, g_L^h), \quad \Gamma_R^I = (\Gamma_R^{u,d})^I = \text{diag} (g_R^\ell, g_R^\ell, g_R^h). \quad (3)$$

<sup>2</sup>Strictly speaking, this is true only under the assumption that the interference between the SM and the new-physics  $q\bar{q} \rightarrow t\bar{t}$  amplitudes gives the dominant contribution to the asymmetric cross section.

<sup>3</sup>The 95% confidence limits (CLs) on the masses of fourth-generation leptons obtained by LEP II are  $m_{\nu_4} > 101.5 \text{ GeV}$  and  $m_{\ell_4} > 101.9 \text{ GeV}$  [40], while the latest published Tevatron bounds on the fourth-generation up- and down-type quark masses read  $m_{u_4} > 311 \text{ GeV}$  [41] and  $m_{d_4} > 372 \text{ GeV}$  [42] at 95% CL. The first LHC bounds [43] on the masses  $m_{u_4}$  and  $m_{d_4}$  are still weaker than those from the Tevatron.

If the quark charge assignments are chosen as in Table 1, the coupling strengths for light ( $\ell$ ) and heavy ( $h$ ) quarks are given by

$$g_L^\ell = g_R^h = \tan \theta, \quad g_L^h = g_R^\ell = -\cot \theta. \quad (4)$$

Notice that for  $\theta \in [0^\circ, 45^\circ]$  these couplings fulfill

$$g_A^\ell g_A^h = (g_L^\ell - g_R^\ell)(g_L^h - g_R^h) = -\frac{4}{\sin^2(2\theta)} < 0, \quad (5)$$

$$\frac{|g_V^{\ell,h}|}{|g_A^{\ell,h}|} = \frac{|g_L^{\ell,h} + g_R^{\ell,h}|}{|g_L^{\ell,h} - g_R^{\ell,h}|} = \cos(2\theta) < 1.$$

In particular, one has  $g_A^\ell g_A^h \rightarrow -4$  and  $|g_V^{\ell,h}|/|g_A^{\ell,h}| \rightarrow 0$  in the limit  $\theta \rightarrow 45^\circ$ , which is crucial to obtain a large forward-backward asymmetry in  $t\bar{t}$  production, while leaving the symmetric cross section largely unaffected.

### 3 Flavor Physics

Naively one might think that the number of additional flavor parameters in our axigluon model is given by  $4 \cdot 6 = 24$  mixing angles and  $4 \cdot 3 = 12$  CP-violating phases, *i.e.*, the number of elements of the hermitian matrices  $\Gamma_L^{u,d}$  and  $\Gamma_R^{u,d}$ . Yet, most of the parameters which appear in the axigluon couplings are unphysical. In order to determine the number of physical degrees of freedom in (2), we first recall that in the absence of the Yukawa couplings,

$$\mathcal{L} \supset -(Y_u)_{ij} \bar{Q}_L^i \tilde{\phi} u_R^j - (Y_d)_{ij} \bar{Q}_L^i \phi d_R^j + \text{h.c.}, \quad (6)$$

the SM would possess a large global non-abelian  $SU(3)_{Q_L} \times SU(3)_{u_R} \times SU(3)_{d_R}$  flavor symmetry. Here  $\phi$  denotes the SM Higgs doublet and  $\tilde{\phi} = i\tau_2 \phi^*$ .

Before spontaneous EWSB, the terms that lead to (2) can be written in the following way

$$\mathcal{L} \supset g_s \left[ (\Gamma_L)_{ij} \bar{Q}_L^i \not{G} Q_L^j + (\Gamma_R)_{ij} \bar{Q}_R^i \not{G} Q_R^j \right], \quad (7)$$

where  $Q_{L,R}^i = (u_{L,R}^i, d_{L,R}^i)^T$  are  $SU(2)_{L,R}$  doublets. Using now the  $SU(3)_{Q_L} \times SU(3)_{u_R} \times SU(3)_{d_R}$  symmetry transformations, one can choose (without loss of generality) to work in the basis with

$$Y_u = V^\dagger \lambda_u, \quad Y_d = \lambda_d, \quad \Gamma_L = U_d^\dagger \Gamma_L^I U_d, \quad \Gamma_R = \Gamma_R^I, \quad (8)$$

where  $V$  denotes the Cabibbo-Kobayashi-Maskawa (CKM) matrix and  $\lambda_{u,d}$  are of the form

$$\lambda_u = \frac{\sqrt{2}}{v} \text{diag}(m_u, m_c, m_t), \quad \lambda_d = \frac{\sqrt{2}}{v} \text{diag}(m_d, m_s, m_b), \quad (9)$$

with  $v \approx 246$  GeV being the Higgs vacuum expectation value (VEV) and  $m_u, m_d$ , *etc.* denoting the quark masses. The unitary matrix  $U_d$  in (8) parametrizes the misalignment of the left-handed operator appearing in (7) relative to the down-type quark mass basis.

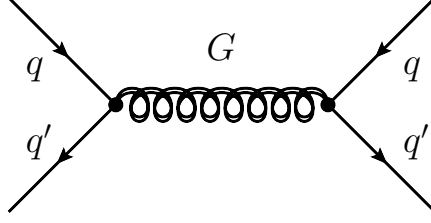


Figure 1: Tree-level axigluon contribution to the mixing of neutral mesons.

Alternatively, one can choose to work in a basis where

$$Y_u = \lambda_u, \quad Y_d = V \lambda_d, \quad \Gamma_L = U_u^\dagger \Gamma_L^I U_u, \quad \Gamma_R = \Gamma_R^I, \quad (10)$$

and  $U_u$  is a unitary matrix which parametrizes the misalignment of the left-handed operator in (7) with the up-type quark mass basis. Importantly, the unitary matrices  $U_{u,d}$  are not independent from each other, but related via the CKM matrix. Explicitly, one has

$$U_u = U_d V^\dagger. \quad (11)$$

By appropriate rotations of the chiral quark fields, we can choose a basis where the mass matrices are diagonal and the axigluon couplings take the form

$$\Gamma_L^{u,d} = U_{u,d}^\dagger \Gamma_L^I U_{u,d}, \quad \Gamma_R^{u,d} = \Gamma_R^I, \quad (12)$$

with  $U_u$  and  $U_d$  satisfying (11). We conclude that the total number of additional real and imaginary flavor parameters amounts to 6 mixing angles and 3 phases. These appear all in the sector of left-handed quarks, namely in  $\Gamma_L^{u,d}$ . In contrast, the right-handed quark sector does not involve new sources of flavor breaking, since the corresponding chiral rotations are not observable in the SM. This allows one to diagonalize the axigluon couplings  $\Gamma_R^{u,d}$  simultaneously.

The structure of (12) implies that the non-universality of the axigluon couplings induces tree-level FCNCs among both left-handed up- and down-type quarks. However, the flavor-breaking terms in the two sectors are connected via

$$\Gamma_L^u = V \Gamma_L^d V^\dagger. \quad (13)$$

This equation implies that the axigluon couplings  $\Gamma_L^u$  and  $\Gamma_L^d$  are to first approximation identical, since the CKM matrix is close to a unit matrix. Explicitly, we find that the left-handed axigluon coupling to down-type quarks takes the form

$$\Gamma_L^d = g_L^\ell \mathbf{1} + (g_L^h - g_L^\ell) \begin{pmatrix} |(U_d)_{31}|^2 & (U_d^*)_{31}(U_d)_{32} & (U_d^*)_{31}(U_d)_{33} \\ (U_d)_{31}(U_d^*)_{32} & |(U_d)_{32}|^2 & (U_d^*)_{32}(U_d)_{33} \\ (U_d)_{31}(U_d^*)_{33} & (U_d)_{32}(U_d^*)_{33} & |(U_d)_{33}|^2 \end{pmatrix}, \quad (14)$$

where  $\mathbf{1}$  denotes the  $3 \times 3$  identity matrix. Notice that the splitting of heavy- and light-quark couplings,  $(g_L^h - g_L^\ell)$ , determines the overall strength of flavor breaking and that all of these

terms arise from the mixing with the third generation. For example, the  $s_L \rightarrow d_L$ ,  $b_L \rightarrow d_L$ , and  $b_L \rightarrow s_L$  processes involve the combinations  $(U_d^*)_{31}(U_d)_{32}$ ,  $(U_d^*)_{31}(U_d)_{33}$ , and  $(U_d^*)_{32}(U_d)_{33}$  of mixing-matrix elements.

The presence of the new unitary matrix  $U_d$ , which (together with  $V$ ) controls the amount of flavor mixing in the left-handed quark sector, can have a considerable impact on particle-antiparticle mixing of neutral mesons. The relevant Feynman diagram is shown in Figure 1. In order to determine the structure of the mixing matrix  $U_d$ , we could use the present knowledge on the  $\Delta F = 2$  amplitudes and obtain upper bounds on most of the elements of  $U_d$  for given values of  $M_G$  and  $\theta$ . In particular, we could investigate which pattern of  $U_d$  would cure potential SM inconsistency concerning the size of CP violation in  $K-\bar{K}$  and  $B_{d,s}-\bar{B}_{d,s}$  mixing.<sup>4</sup> In the following, we will however take a different path in order to work out the weakest possible bounds on  $M_G$  and  $\theta$  by minimizing the amount of flavor violation in the  $\Delta F = 2$  sector. By virtue of (12), the axigluon contributions to  $K-\bar{K}$  and  $B_{d,s}-\bar{B}_{d,s}$  mixing can be set to zero by alignment in the down-type quark sector, *i.e.*,  $U_d = 1$ . Corrections to  $D-\bar{D}$  mixing can be removed by alignment in the up-type quark sector, *i.e.*,  $U_u = 1$  or equivalently  $U_d = V$ . However, it is not possible to set the contributions to both down- and up-type quark  $\Delta F = 2$  amplitudes simultaneously to zero by any choice of  $U_d$ . This feature has also been observed independently in [31]. Notice that if the down-type (up-type) quark sector is aligned one has  $\Gamma_L^u = V \Gamma_L^I V^\dagger$  ( $\Gamma_L^d = V^\dagger \Gamma_L^I V$ ). This implies that the  $c_L \rightarrow u_L G$ ,  $t_L \rightarrow u_L G$ , and  $t_L \rightarrow c_L G$  ( $s_L \rightarrow d_L G$ ,  $b_L \rightarrow d_L G$ , and  $b_L \rightarrow s_L G$ ) amplitudes are to leading order proportional to the combinations  $V_{cb}^* V_{ub}$ ,  $V_{tb}^* V_{ub}$ , and  $V_{tb}^* V_{cb}$  ( $V_{td}^* V_{ts}$ ,  $V_{td}^* V_{tb}$ , and  $V_{ts}^* V_{tb}$ ) of CKM elements. In this case the flavor-changing axigluon contributions follow the pattern of minimal flavor violation (MFV). In particular, there will be no new sources of CP violation beyond the CKM phase. Flavor alignment is crucial to respect the severe constraints arising from the quark flavor sector, especially from CP-violating  $\Delta F = 2$  observables. This requirement constrains the structure of viable non-universal axigluon models that are accessible at the existing hadron colliders.

Before deriving and comparing the constraints on  $M_G$  and  $\theta$  from the relevant  $\Delta F = 2$  mixing amplitudes in the two scenarios of flavor alignment, let us briefly comment on partial misalignment in the down-type quark sector. Generically partial flavor alignment implies axigluon effects in both up- and down-type quark sectors. Given the freedom in the choice of  $U_d$ , it is of course possible to set the axigluon contributions to  $K-\bar{K}$ ,  $B_d-\bar{B}_d$ , and/or  $B_s-\bar{B}_s$  mixing to zero. For example, choosing<sup>5</sup>

$$U_d = \begin{pmatrix} 1 + \mathcal{O}(\lambda^2) & 0 & V_{td}^* \\ 0 & 1 & 0 \\ V_{td} & 0 & V_{tb} + \mathcal{O}(\lambda^2) \end{pmatrix}, \quad (15)$$

---

<sup>4</sup>Recent measurements of the CDF and DØ collaborations of both the mixing-induced CP asymmetry in  $B_s \rightarrow J/\psi \phi$  and the like-sign di-muon charge asymmetry in  $B_{d,s}$ -meson samples show deviations from their SM predictions. A tension also exists in  $|\epsilon_K|$  if the exclusive determination of  $|V_{cb}|$  is used. Yet, the disagreements are not large enough to exclude the possibility of statistical and/or systematic origins of the deviations.

<sup>5</sup>Textures of this type arise in the context of topcolor models from the requirement to produce the observed non-degenerate quark masses [44, 45, 46]. The possible textures are controlled by the breaking patterns of horizontal global flavor symmetries, which we leave unspecified.



one arrives at  $(\Gamma_L^d)_{13} = (g_L^h - g_L^\ell) V_{td}^* V_{tb} + \mathcal{O}(\lambda^5)$  and  $(\Gamma_L^d)_{12} = (\Gamma_L^d)_{23} = 0$ , *i.e.*, new-physics effects of MFV pattern in  $B_d$ - $\bar{B}_d$  mixing and no corrections in the  $K$ - $\bar{K}$  and  $B_s$ - $\bar{B}_s$  observables. Since  $\Gamma_L^d$  and  $\Gamma_L^u$  necessarily have to obey (13), the choice (15) will fix the pattern of flavor violation in the  $D$ -meson sector. Explicitly, we find

$$\begin{aligned} (\Gamma_L^u)_{12} &= (g_L^h - g_L^\ell) \left[ V_{cb}^* V_{ub} |V_{tb}|^2 + V_{cb}^* V_{ud} V_{td}^* V_{tb} + V_{cd}^* V_{ud} |V_{td}|^2 + V_{cd}^* V_{ub} V_{tb}^* V_{td} \right] + \mathcal{O}(\lambda^5) \\ &= (g_L^h - g_L^\ell) A^2 \lambda^5 + \mathcal{O}(\lambda^7), \end{aligned} \quad (16)$$

where in the second line we have parametrized the CKM elements in terms of the Wolfenstein parameters  $A$ ,  $\lambda$ ,  $\bar{\rho}$ ,  $\bar{\eta}$ , and expanded in  $\lambda \approx 0.23$ . This result has to be compared with the expression  $(\Gamma_L^u)_{12} = (g_L^h - g_L^\ell) V_{cb}^* V_{ub} = A^2 \lambda^5 (\bar{\rho} - i\bar{\eta}) + \mathcal{O}(\lambda^7)$  obtained in the case of flavor alignment,  $U_d = 1$ . We see that MFV effects in  $B_d$ - $\bar{B}_d$  mixing of  $\mathcal{O}(\lambda^3)$  imply flavor violation in  $D$ - $\bar{D}$  mixing of  $\mathcal{O}(\lambda^5)$ , but can lead to new CP violation with respect to the case of flavor alignment. Yet, unless the element  $(U_d)_{13}$  in (15) is smaller than  $\mathcal{O}(\lambda^5)$ , the constraints on the axigluon parameters  $M_G$  and  $\theta$  from  $B_d$ - $\bar{B}_d$  mixing turn out to be more stringent than those arising from the  $D$ - $\bar{D}$  observables. Notice that a scenario of partial flavor alignment in the down-type quark sector similar to the one in (15) has been considered in [29]. The bound on  $M_G$  and  $\theta$  derived in the latter article from  $B_d$ - $\bar{B}_d$  mixing is thus the relevant constraint for the specific pattern of flavor violation, but not the weakest constraint in general.

We now collect the formulas necessary to analyze the  $\Delta F = 2$  observables. The effects of axigluons in neutral meson mixing can be described by an effective theory. Assuming alignment in the up-type quark sector, we find in terms of the four-quark operator

$$\mathcal{O}_K = (\bar{s}_L \gamma^\mu d_L)(\bar{s}_L \gamma_\mu d_L), \quad (17)$$

the following axigluon contribution to the effective  $\Delta S = 2$  Hamiltonian

$$\mathcal{H}_K^G = \left(1 - \frac{1}{N_c}\right) \frac{\pi \alpha_s}{M_G^2} (g_L^h - g_L^\ell)^2 (V_{ts}^* V_{td})^2 \mathcal{O}_K = \frac{8\pi \alpha_s}{3M_G^2} \frac{(V_{ts}^* V_{td})^2}{\sin^2(2\theta)} \mathcal{O}_K, \quad (18)$$

which induces  $K$ - $\bar{K}$  mixing. Here we have set  $N_c = 3$  and used (4) to obtain the final result. The strong coupling constant  $\alpha_s = g_s^2/(4\pi)$  entering the above formula is understood to be normalized at the scale  $M_G$ . The expressions for the  $\Delta B = 2$  Hamiltonians, describing  $B_d$ - $\bar{B}_d$  or  $B_s$ - $\bar{B}_s$  mixing, are obtained from (18) by simply replacing  $V_{ts}^* V_{td}$  with  $V_{tb}^* V_{td}$  or  $V_{tb}^* V_{ts}$  and employing the relevant four-quark operator. The  $\Delta C = 2$  observables will receive no correction in this case. Assuming instead alignment in the down-type quark sector, there will be no axigluon contributions to the  $\Delta S = 2$  and  $\Delta B = 2$  transitions, but the prediction for  $D$ - $\bar{D}$  mixing will be altered with respect to its SM expectation. The relevant effective  $\Delta C = 2$  Hamiltonian is obtained from (18) by changing the factor  $V_{ts}^* V_{td}$  into  $V_{cb}^* V_{ub}$  and using again the appropriate four-quark operator.

The tree-level expressions for the Wilson coefficient given in (18) must be evolved, using the renormalization group (RG), down to the low-energy scale  $\mu_K = 2$  GeV in the case of  $K$ - $\bar{K}$  mixing. For the  $B_{d,s}$ - $\bar{B}_{d,s}$  and  $D$ - $\bar{D}$  observables the appropriate low-energy scales are  $\mu_B = 4.6$  GeV and  $\mu_D = 2.8$  GeV, respectively. The running is accomplished by means of the

well-known RG formulas [47]. From  $M_G$  to the top-quark threshold  $m_t$  we use the leading order (LO) approximation, while from  $m_t$  down to the appropriate low-energy scale we work at next-to-leading order (NLO) precision. At the low-energy scale the hadronic matrix element of the operator (17) is customarily expressed in terms of the parameter  $B_K$ . For the operator relevant to our analysis, we write

$$\langle K | \mathcal{O}_K | \bar{K} \rangle = \frac{1}{3} m_K f_K^2 B_K. \quad (19)$$

Analogous definitions are used for the other mesons. In our numerical analysis we will employ  $m_K = 497.6 \text{ MeV}$ ,  $f_K = (155.8 \pm 1.7) \text{ MeV}$ ,  $B_K = 0.527 \pm 0.022$ ,  $m_{B_d} = 5.2796 \text{ GeV}$ ,  $f_{B_d} = (192.8 \pm 9.9) \text{ MeV}$ ,  $B_{B_d} = 0.82 \pm 0.07$ ,  $m_{B_s} = 5.3664 \text{ GeV}$ ,  $f_{B_s} = (238.8 \pm 9.5) \text{ MeV}$ , and  $B_{B_s} = 0.86 \pm 0.04$  [48] to calculate the  $\Delta S = 2$  and  $\Delta B = 2$  observables. In the case of the  $\Delta C = 2$  transition we use instead  $m_D = 1.8645 \text{ GeV}$ ,  $f_D = (212 \pm 14) \text{ MeV}$ , and  $B_D = 0.85 \pm 0.09$  [49].

In order to constrain the axigluon mass  $M_G$  and the mixing angle  $\theta$  in the case of alignment in the up-type quark sector, we will consider the three observables

$$\epsilon_K = \frac{\kappa_\epsilon e^{i\varphi_\epsilon}}{\sqrt{2} (\Delta m_K)_{\text{exp}}} \text{Im} \langle K | \mathcal{H}_K^{\text{SM}} + \mathcal{H}_K^G | \bar{K} \rangle, \quad (20)$$

$$\Delta m_{B_{d,s}} = 2 \left| \langle B_{d,s} | \mathcal{H}_{B_{d,s}}^{\text{SM}} + \mathcal{H}_{B_{d,s}}^G | \bar{B}_{d,s} \rangle \right|,$$

where  $\varphi_\epsilon = (43.51 \pm 0.05)^\circ$ ,  $\kappa_\epsilon = 0.94 \pm 0.02$  [50], and  $(\Delta m_K)_{\text{exp}} = 3.483 \cdot 10^{-12} \text{ MeV}$ , while  $\mathcal{H}_K^{\text{SM}}$  and  $\mathcal{H}_{B_{d,s}}^{\text{SM}}$  denote the SM contributions to the effective  $\Delta S = 2$  and  $\Delta B = 2$  Hamiltonians. We do not attempt a prediction for  $\Delta m_K$ , which is plagued by very large hadronic uncertainties, making it less restrictive than the CP-violating parameter  $\epsilon_K$ .

Since we are dealing with the effect of a single operator only, the resulting expressions for the axigluon contributions to  $|\epsilon_K|$  and  $\Delta m_{B_{d,s}}$  turn out to be very compact. We find the following analytic expressions

$$\begin{aligned} |\epsilon_K|_G &= \frac{\kappa_\epsilon}{\sqrt{2} (\Delta m_K)_{\text{exp}}} \frac{16\pi\alpha_s}{9} \frac{m_K f_K^2 P_K}{M_G^2} \frac{A^4 \lambda^{10} \bar{\eta} (1 - \bar{\rho})}{\sin^2(2\theta)} + \mathcal{O}(\lambda^{12}), \\ (\Delta m_{B_d})_G &= \frac{16\pi\alpha_s}{9} \frac{m_{B_d} f_{B_d}^2 P_{B_d}}{M_G^2} \frac{A^2 \lambda^6 (\bar{\eta}^2 + (1 - \bar{\rho})^2)}{\sin^2(2\theta)} + \mathcal{O}(\lambda^8). \end{aligned} \quad (21)$$

The latter formula also applies to  $B_s - \bar{B}_s$  mixing after obvious replacements. The correct CKM factor reads in this case  $A^2 \lambda^4$ . In our numerical analysis we will use  $\lambda = 0.22543 \pm 0.00077$ ,  $A = 0.812 \pm 0.015$ ,  $\bar{\rho} = 0.148 \pm 0.022$ , and  $\bar{\eta} = 0.344 \pm 0.014$  [51] and will include the full CKM dependence. The factors  $P_M$  with  $M = K, B_d, B_s$  entail the RG effects below  $M_G$  as well as the hadronic parameters  $B_M$  calculated at low energies. In the case of the  $K - \bar{K}$  transition, we obtain

$$P_K = 0.416 \eta_6^{6/21} \approx 0.392 \left[ 1 - 0.024 \ln \left( \frac{M_G}{1 \text{ TeV}} \right) \right], \quad (22)$$

where  $\eta_6 = \alpha_s(M_G)/\alpha_s(m_t)$ . In order to get the result for the case of  $B_d-\bar{B}_d$  ( $B_s-\bar{B}_s$ ) mixing one simply replaces 0.416 by 0.68 (0.416 by 0.72) in the above expression. The rescaling factor 0.944  $[1 - 0.024 \ln(M_G/(1 \text{ TeV}))]$  arising from inserting the leading-logarithmic expression for  $\eta_6$  is universal, *i.e.*, independent from the considered meson.

In order to determine the allowed parameter space in the  $M_G-\theta$  plane, we will compare the ratios  $C_K = |\epsilon_K|_{\text{exp}}/|\epsilon_K|_{\text{SM}}$  and  $C_{B_{d,s}} = (\Delta m_{B_{d,s}})_{\text{exp}}/(\Delta m_{B_{d,s}})_{\text{SM}}$  to the corresponding predictions in our axigluon model. Combining the state-of-the-art SM calculations of  $|\epsilon_K|$  [52] and  $\Delta m_{B_{d,s}}$  [47] with the current experimental results [53], we find

$$C_K = 1.17 \pm 0.16, \quad C_{B_d} = 0.96 \pm 0.14, \quad C_{B_s} = 0.91 \pm 0.09, \quad (23)$$

where the quoted errors have been obtained by adding individual uncertainties of both theoretical and experimental nature in quadrature.

In the case of alignment in the down-type quark sector, we will consider

$$x_D = \frac{2 |\text{Re} \langle D | \mathcal{H}_D^{\text{SM}} + \mathcal{H}_D^{\text{G}} | \bar{D} \rangle|}{\Gamma_D}, \quad (24)$$

to determine the allowed parameter space. Here  $\Gamma_D = 1/\tau_D$  with  $\tau_D$  being the  $D$ -meson lifetime. The axigluon contribution to  $x_D$  reads

$$(x_D)_G = \frac{16\pi\alpha_s}{9} (\tau_D)_{\text{exp}} \frac{m_D f_D^2 P_D}{M_G^2} \frac{A^4 \lambda^{10} (\bar{\eta}^2 - \bar{\rho}^2)}{\sin^2(2\theta)} + \mathcal{O}(\lambda^{12}), \quad (25)$$

where  $(\tau_D)_{\text{exp}} = 0.4101 \text{ ps}$  [53]. The expression for  $P_D$  is obtained from (22) by simply replacing 0.416 by 0.69. Like  $\Delta m_K$  also  $x_D$  is plagued by large theoretical uncertainties. Assuming that there are no accidental cancellations between the SM and the axigluon contributions to  $x_D$ , we bound the axigluon parameters by requiring that the new-physics effects alone do not exceed the measured value of  $x_D$  [54],

$$(x_D)_G \leq (x_D)_{\text{exp}} = (0.419 \pm 0.211) \%. \quad (26)$$

In principle further constraints on the off-diagonal elements of the axigluon couplings  $\Gamma_{L,R}^{u,d}$  also follow from  $\Delta F = 1$  transitions (*i.e.*, radiative and rare weak decays). From the above discussion it should have however become clear that all relevant constraints in the down-type quark sector, *i.e.*,  $B \rightarrow X_s(K^*)\gamma$ ,  $B \rightarrow X_s(K^*)\ell^+\ell^-$ ,  $B_s \rightarrow \mu^+\mu^-$ , and  $K^+ \rightarrow \pi^+\nu\bar{\nu}$ , are readily satisfied by aligning the down-type quark sector. In the case of alignment in the down-type quark sector the axigluon contributions to the short-distance amplitudes of the radiative  $D$ -meson decays  $D \rightarrow \bar{K}^*(\phi)\gamma$  are of the order of  $\alpha_s/(4\pi) m_c/M_G^2 (V_{cb}^*V_{ub})/\sin^2(2\theta)$ . Since radiative charm decays are fully dominated by non-perturbative physics, the strongly suppressed axigluon corrections cannot be separated from the much larger SM long-distance contributions. Similar statements apply to other rare  $D$ -meson decays like  $D \rightarrow \pi(\rho)\ell^+\ell^-$  and  $D \rightarrow \mu^+\mu^-$ . The poor experimental bounds on rare top-quark decays do not lead to any sensible restriction neither. The bottom line is that at present there are no additional constraints on  $M_G$  and  $\theta$  from  $\Delta F = 1$  processes in the up-quark sector beyond those already imposed by the  $\Delta F = 2$  transitions.

## 4 Precision Measurements

The axigluon interactions with the SM quarks give rise to corrections to measurements at  $e^+e^-$  machines as well as hadron colliders. In this and the next section we provide generic calculations of these effects. As already mentioned in Section 2, the presence of a fourth generation of sequential fermions would lead to large one-loop corrections unless the parameters of the model are tuned. For most of the following discussion, we hence consider only the effects of massive color octets and discard the model-dependent contributions from massive fermions beyond those in the SM. We will furthermore neglect possible flavor-violating effects. Assuming an appropriate flavor alignment, such effects are strongly Cabibbo-suppressed.

We begin our survey by studying the axigluon correction to the  $Z$ -boson vertices. The corresponding Feynman diagram involving the virtual exchange of an axigluon between the quark lines is shown in Figure 2. For light quarks ( $q = u, d, s, c, b$ ) the main corrections to the  $Zq_P\bar{q}_P$  couplings ( $P = L, R$ ) occur at second order in the expansion with respect to the external momenta. In terms of effective operators, this means that these corrections are encoded in the Wilson coefficients of the following operators

$$\mathcal{O}_{Q_P W} = (\bar{Q}_P \gamma^\mu \tau^i Q_P) D^\nu W_{\mu\nu}^i, \quad \mathcal{O}_{Q_P B} = (\bar{Q}_P \gamma^\mu Q_P) \partial^\nu B_{\mu\nu}. \quad (27)$$

Here  $\tau^i$  are  $SU(2)_P$  generators,  $D_\mu = 1/2 (\vec{D}_\mu - \overleftarrow{D}_\mu)$  with  $\vec{D}_\mu = \partial_\mu + ig\tau^i W_\mu^i + ig'Y/2B_\mu$  is the covariant derivative with  $g$  ( $g'$ ) denoting the  $SU(2)_L$  ( $U(1)_Y$ ) gauge coupling associated with the field  $W_\mu^i$  ( $B_\mu$ ), and  $W_{\mu\nu}^i$  ( $B_{\mu\nu}$ ) is the corresponding field-strength tensor.

Using the equations of motion in the broken phase of the theory, *i.e.*, including the mass terms of the  $W$  and  $Z$  bosons, the off-shell operators in (27) induce corrections to the current couplings of the light quarks to the electroweak gauge bosons. In the case of the left- and right-handed bottom-quark couplings to the  $Z$  boson, we find that the tree-level  $Zb_P\bar{b}_P$  couplings  $g_P^b$  are modified, yielding

$$\mathcal{G}_P^b \approx g_P^b \left[ 1 - \frac{2}{3} \frac{\alpha_s}{4\pi} C_F (g_P^h)^2 \frac{M_Z^2}{M_G^2} \ln \left( \frac{M_Z^2}{M_G^2} \right) \right], \quad (28)$$

where  $C_F = 4/3$  is the Casimir invariant in the fundamental representation. The expressions for the quarks of the first two generations are obtained from the above formula by simply replacing  $g_P^h$  with  $g_P^\ell$ . The result in (28) implies that the axigluon correction to the current coupling of the  $Z$  boson interferes constructively with the SM for  $M_G > M_Z$ , resulting in  $|\mathcal{G}_P^q| > |g_P^q|$  for all light quarks. Yet, the corrections are flavor non-universal. The new-physics corrections to the  $Zb_L\bar{b}_L$  coupling are enhanced by a factor of  $(g_L^h/g_R^h)^2 = \cot^4 \theta$  relative to those affecting the  $Zb_R\bar{b}_R$  coupling, while for the quarks of the first and second family the pattern of deviations is reversed, given that  $(g_L^\ell/g_R^\ell)^2 = \tan^4 \theta$ . The corrections to the  $Z$ -boson vertex involving bottom quarks are hence dominantly left-handed, while those involving the remaining light quarks are mostly right-handed. We emphasize also that the latter formula, originally derived in [55], contains only the leading-logarithmic corrections in the limit of an infinitely heavy axigluon,  $M_Z^2/M_G^2 \rightarrow 0$ . In consequence, this result can be found by integrating out the axigluon and calculating the anomalous dimension of the “penguin diagram” obtained from the graph in Figure 2 by pinching the axigluon propagator. The full one-loop result

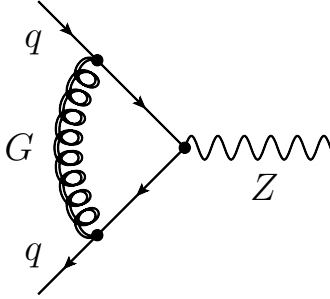


Figure 2: One-loop axigluon contribution to the  $Zq\bar{q}$  vertex.

for the complex effective couplings  $\mathcal{G}_P^q$  is given in Appendix A. From the limiting behavior (A3), we see that non-logarithmic corrections to the formula (28) are not fully negligible for  $M_G = \mathcal{O}(1 \text{ TeV})$ . We will therefore use the full real parts of  $\mathcal{G}_P^q$  in our numerical analysis.

In the case of the top quark, on the other hand, the axigluon corrections to the  $Z$ -boson vertex are contained in the Wilson coefficients of the effective operators

$$\mathcal{O}_{Q_P\phi}^1 = i(\bar{Q}_P\gamma^\mu\tau^i Q_P)\phi^\dagger\tau^i D_\mu\phi, \quad \mathcal{O}_{Q_P\phi}^2 = i(\bar{Q}_P\gamma^\mu Q_P)\phi^\dagger D_\mu\phi. \quad (29)$$

Evaluating the Feynman diagram in Figure 2 with an internal top quark at zero external momenta, we find that after EWSB the matching corrections to the operators in (29) shift the tree-level  $Zt_P\bar{t}_P$  couplings  $g_P^t$  by

$$\mathcal{G}_P^t \approx g_P^t \pm \frac{g}{c_w} \frac{\alpha_s}{4\pi} C_F (g_P^h)^2 \frac{m_t^2}{M_G^2} \ln\left(\frac{m_t^2}{M_G^2}\right), \quad (30)$$

where the plus (minus) sign applies in the case  $P = L$  ( $P = R$ ). Our result agrees with [55] and again contains only the leading-logarithmic corrections in the limit  $m_t^2/M_G^2 \rightarrow 0$ . The complete expression for the  $Z \rightarrow t\bar{t}$  form factor with vanishing external momenta can be found in Appendix A. Like in the case of the on-shell  $Z \rightarrow q\bar{q}$  form factor, non-logarithmic corrections to  $\mathcal{G}_P^t$  are non-negligible and should be included if one aims for precision. Glancing at (30), we see that the one-loop axigluon corrections decrease (increase) the value of the left-handed (right-handed) coupling of the  $Z$  boson to  $t\bar{t}$  pairs, *i.e.*,  $\mathcal{G}_L^t < g_L^t$  ( $\mathcal{G}_R^t > g_R^t$ ). Since  $(g_L^h/g_R^h)^2 = \cot^4\theta$ , the corrections to the left-handed coupling are always more pronounced than those to the right-handed coupling.

Constraints on the  $Z$ -boson couplings to quarks of the first generation are imposed by the measurement of the forward-backward asymmetry of  $e^+e^-$  in  $q\bar{q} \rightarrow Z/\gamma \rightarrow e^+e^-$  and a combined fit to the  $Z$ -boson lineshape, the lepton forward-backward asymmetries, and asymmetry parameters. In the former case one arrives at  $\mathcal{G}_L^u = 0.355 \pm 0.025$ ,  $\mathcal{G}_R^u = -0.147 \pm 0.017$ ,  $\mathcal{G}_L^d = -0.436 \pm 0.008$ , and  $\mathcal{G}_R^d = 0.058 \pm 0.031$  [56], while in the latter case one has  $\mathcal{G}_L^u = 0.356 \pm 0.035$  and  $\mathcal{G}_R^u = -0.11^{+0.30}_{-0.07}$ ,  $\mathcal{G}_L^d = -0.423 \pm 0.012$ , and  $\mathcal{G}_R^d = 0.10^{+0.04}_{-0.06}$  [22]. The limited precision of these extractions makes it impossible to derive any sensible constraint on the  $M_G$ - $\theta$  plane for axigluon masses at the order of a TeV. The situation is improved for what concerns the second family. In the case of the charm quark, precision measurements of the relevant couplings  $\mathcal{G}_L^c = 0.3453 \pm 0.0036$  and  $\mathcal{G}_R^c = -0.1580 \pm 0.0051$  [22] follow from a combination of the

measurements of  $R_c$ ,  $A_c$ , and  $A_{\text{FB}}^c$ . Yet, the obtained constraints on  $M_G$  and  $\theta$  turn out to be less strict than those that derive from the same set of observables in the bottom-quark sector. These will be discussed in a moment. Obvious limitations also precluded measurements of the  $Z$ -boson couplings to top quarks so far. There was insufficient CM energy at LEP to produce top-quark pairs in  $e^+e^- \rightarrow \gamma/Z \rightarrow t\bar{t}$ . At hadron colliders,  $t\bar{t}$  production is fully dominated by the QCD processes  $gg \rightarrow t\bar{t}$  and  $q\bar{q} \rightarrow g \rightarrow t\bar{t}$ , so that it is impossible to extract a signal from the sought couplings entering via  $q\bar{q} \rightarrow \gamma/Z \rightarrow t\bar{t}$ . However, it is feasible to determine the  $Z$ -boson couplings to top quarks via the process of  $gg \rightarrow Zt\bar{t}$  at the LHC with integrated luminosity of at least  $300 \text{ fb}^{-1}$ . The expected relative precision amounts to around 10% (45% to 85%) for the axial-vector (vector) coupling [57, 58, 59]. These uncertainties are too large to allow to derive stringent bounds on the parameter space of the axigluon model.

Important constraints on the  $M_G$ - $\theta$  plane follow from the measurement of the bottom-quark POs performed at LEP and SLC. In the following, we will consider the impact of the one-loop axigluon corrections on the ratio of the  $Z$ -boson decay width into bottom quarks and the total hadronic width,  $R_b$ , the bottom-quark left-right asymmetry,  $A_b$ , and the forward-backward asymmetry for bottom quarks,  $A_{\text{FB}}^b$ . The dependences of these quantities on the left- and right-handed bottom-quark couplings are given by [60]

$$\begin{aligned}
R_b &= \left[ 1 + \frac{4 \sum_{q=u,d} [(\mathcal{G}_L^q)^2 + (\mathcal{G}_R^q)^2]}{\eta_{\text{QCD}} \eta_{\text{QED}} [(1 - 6z_b)(\mathcal{G}_L^b - \mathcal{G}_R^b)^2 + (\mathcal{G}_L^b + \mathcal{G}_R^b)^2]} \right]^{-1}, \\
A_b &= \frac{2\sqrt{1 - 4z_b} \frac{\mathcal{G}_L^b + \mathcal{G}_R^b}{\mathcal{G}_L^b - \mathcal{G}_R^b}}{1 - 4z_b + (1 + 2z_b) \left( \frac{\mathcal{G}_L^b + \mathcal{G}_R^b}{\mathcal{G}_L^b - \mathcal{G}_R^b} \right)^2}, \quad A_{\text{FB}}^b = \frac{3}{4} A_e A_b.
\end{aligned} \tag{31}$$

Radiative QCD and QED corrections are encoded in  $\eta_{\text{QCD}} = 0.9954$  and  $\eta_{\text{QED}} = 0.9997$ , while the parameter  $z_b = m_b^2(M_Z)/M_Z^2 = 0.997 \cdot 10^{-3}$  describes the effects of the non-zero bottom-quark mass.

Since to the considered order axigluon corrections do not affect the asymmetry parameter of the electron,  $A_e$ , we will fix this quantity to its SM value  $(A_e)_{\text{SM}} = 0.1464$ . For the SM couplings, we use  $(\mathcal{G}_L^u)_{\text{SM}} = 0.34665$ ,  $(\mathcal{G}_R^u)_{\text{SM}} = -0.15477$ ,  $(\mathcal{G}_L^d)_{\text{SM}} = -0.42429$ ,  $(\mathcal{G}_R^d)_{\text{SM}} = 0.077379$ ,  $(\mathcal{G}_L^b)_{\text{SM}} = -0.42106$ , and  $(\mathcal{G}_R^b)_{\text{SM}} = 0.077451$  [61].<sup>6</sup> Evaluating the relations (31) using this input, we obtain for the bottom-quark POs

$$\begin{aligned}
(R_b)_{\text{SM}} &= 0.21578 \pm 0.00004, \\
(A_b)_{\text{SM}} &= 0.9347 \pm 0.0001, \\
(A_{\text{FB}}^b)_{\text{SM}} &= 0.1026 \pm 0.0007.
\end{aligned} \tag{32}$$

---

<sup>6</sup>The default flags of ZFITTER version 6.43 are used, except for setting  $\text{ALEM} = 2$  to take into account the externally supplied value of  $\Delta\alpha_{\text{had}}^{(5)} = 0.02758 \pm 0.00035$ . The other relevant input parameters read  $M_Z = (91.1875 \pm 0.0021) \text{ GeV}$ ,  $m_t = (173.3 \pm 1.1) \text{ GeV}$  [62],  $m_h = 150 \text{ GeV}$ , and  $\alpha_s(M_Z) = 0.118 \pm 0.001$ .

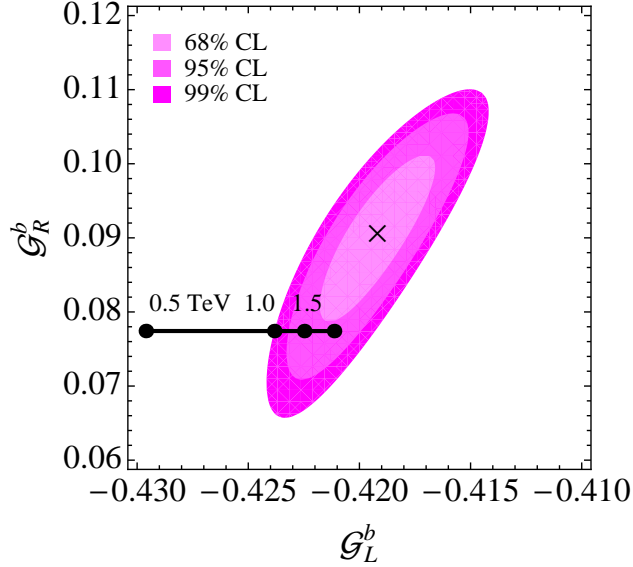


Figure 3: Regions of 68%, 95%, and 99% probability in the  $\mathcal{G}_L^b$ – $\mathcal{G}_R^b$  plane. The black dot without label is the SM expectation for the reference point and the black cross represents the best-fit solution. The black line and the remaining dots indicate the predictions in the flavor non-universal axigluon model. They have been obtained for  $\theta = 15^\circ$  and  $M_G = 0.5$  TeV, 1.0 TeV, 1.5 TeV.

One should compare these numbers with the experimental results [22]

$$\begin{aligned} (R_b)_{\text{exp}} &= 0.21629 \pm 0.00066, \\ (A_b)_{\text{exp}} &= 0.923 \pm 0.020, \\ (A_{\text{FB}}^b)_{\text{exp}} &= 0.0992 \pm 0.0016, \end{aligned} \quad \rho = \begin{pmatrix} 1.00 & -0.08 & -0.10 \\ -0.08 & 1.00 & 0.06 \\ -0.10 & 0.06 & 1.00 \end{pmatrix}, \quad (33)$$

where  $\rho$  is the correlation matrix. While the  $R_b$  and  $A_b$  measurements agree with their SM predictions within  $+0.8\sigma$  and  $-0.6\sigma$  for  $m_h = 150$  GeV, the  $A_{\text{FB}}^b$  measurement is almost  $-2.0\sigma$  away from its SM expectation.<sup>7</sup> Shifts of order  $+20\%$  and  $-0.5\%$  in the right- and left-handed bottom-quark couplings relative to the SM could explain the observed discrepancy. Such a pronounced correction in  $\mathcal{G}_R^b$  would affect  $A_b$  and  $A_{\text{FB}}^b$ , which both depend linearly on the ratio  $\mathcal{G}_R^b/\mathcal{G}_L^b$  in a significant way, while it would not spoil the good agreement in  $R_b \propto (\mathcal{G}_L^b)^2 + (\mathcal{G}_R^b)^2$ .

The possible size of the one-loop new-physics corrections to the effective couplings  $\mathcal{G}_{L,R}^b$  is shown in Figure 3, which displays the regions of 68%, 95%, and 99% CL obtained from a global fit to the bottom-quark POs in (33). The predictions in the flavor non-universal axigluon model are superimposed in black. The shown points correspond to  $\theta = 15^\circ$  and  $M_G = 0.5$  TeV, 1.0 TeV, 1.5 TeV. We see that the axigluon contributions drive  $\mathcal{G}_L^b$  to smaller values with respect to the SM reference point (black dot), while  $\mathcal{G}_R^b$  remains essentially unaffected.<sup>8</sup> For smaller (larger) values of the mixing angle  $\theta$ , the corrections to  $\mathcal{G}_L^b$  are more (less) pronounced due to the presence of the factor  $(g_L^b)^2 = \cot^2 \theta$  in the effective coupling (28). Changing  $\theta$  has only a minor effect on  $\mathcal{G}_R^b$ . This implies that in the considered axigluon

<sup>7</sup>For  $m_h = 115$  GeV the discrepancy in  $A_{\text{FB}}^b$  would amount to around  $-2.4\sigma$ .

<sup>8</sup>The corrections to  $\mathcal{G}_R^b$  are, as anticipated, positive but so small that they are not visible in the figure.

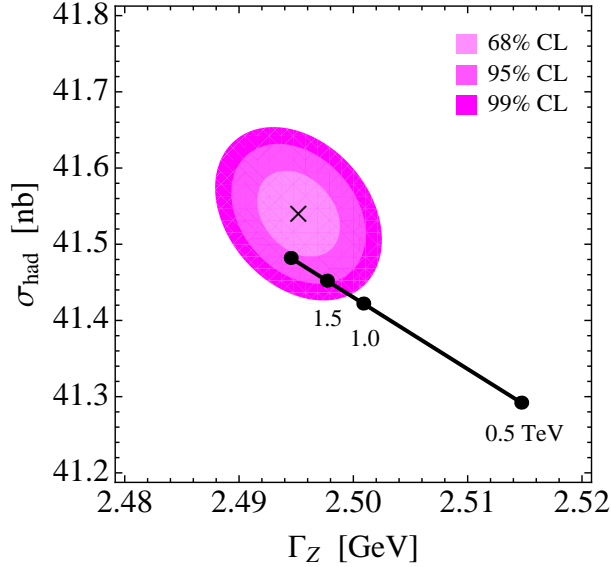


Figure 4: Regions of 68%, 95%, and 99% probability in the  $\Gamma_Z$ - $\sigma_{\text{had}}$  plane. The black dot without label is the SM expectation for the reference point and the black cross represents the best-fit solution. The black line and the remaining dots indicate the predictions in the flavor non-universal axigluon model. They have been obtained for  $\theta = 15^\circ$  and  $M_G = 0.5 \text{ TeV}, 1.0 \text{ TeV}, 1.5 \text{ TeV}$ .

model the quality of the global fit to the bottom-quark POs does not improve with respect to the SM. In particular, the best-fit values  $\mathcal{G}_L^b = -0.41910$  and  $\mathcal{G}_R^b = 0.091044$  (black cross) cannot be obtained in the flavor non-universal axigluon model. The constraints arising from the  $Z \rightarrow b\bar{b}$  couplings on the  $M_G$ - $\theta$  plane will be analyzed in Section 6.

The roles of the total width  $\Gamma_Z$  of the  $Z$  boson and the hadronic pole cross-section  $\sigma_{\text{had}}$  turn out to be even more important in constraining the parameter space of the considered axigluon model than the bottom-quark POs alone. This is due to the fact that the former observables are more sensitive to the altered light-quark couplings. The relevant quantities can be written as

$$\Gamma_Z = \Gamma_{\text{lep}} + \Gamma_{\text{inv}} + \Gamma_{\text{had}}, \quad \sigma_{\text{had}} = \frac{12\pi}{M_Z^2} \frac{\Gamma_e \Gamma_{\text{had}}}{\Gamma_Z^2}, \quad (34)$$

where  $\Gamma_{\text{lep}}$ ,  $\Gamma_{\text{inv}}$ , and  $\Gamma_e$  denote the partial decay width to leptons, the invisible width from  $Z$  decays to neutrinos, and the partial width for electrons, respectively. In our numerical analysis, we will set these partial widths to their SM values,  $(\Gamma_{\text{lep}})_{\text{SM}} = 251.733 \text{ MeV}$ ,  $(\Gamma_{\text{inv}})_{\text{SM}} = 501.579 \text{ MeV}$ , and  $(\Gamma_e)_{\text{SM}} = 83.975 \text{ MeV}$  [61]. This is an excellent approximation, since axigluon corrections affect these observables first at the three-loop level. The hadronic width  $\Gamma_{\text{had}} = \sum_{q \neq t} \Gamma_q$  is given by the sum over all quark final states with mass smaller than  $M_Z$ . The partial  $Z$ -decay widths to quarks  $\Gamma_q$  themselves are defined inclusively, *i.e.*, they contain factorizable QED and QCD final-state corrections encoded in the radiator factors  $R_{V,A}^q$  as well as non-factorizable radiative corrections parametrized by  $\Delta_{\text{EW/QCD}}^q$ . Explicitly, one has

$$\Gamma_q = N_c \frac{G_F M_Z^3}{6\sqrt{2}\pi} \left( R_V^q |\mathcal{G}_L^q + \mathcal{G}_R^q|^2 + R_A^q |\mathcal{G}_L^q - \mathcal{G}_R^q|^2 \right) + \Delta_{\text{EW/QCD}}^q, \quad (35)$$



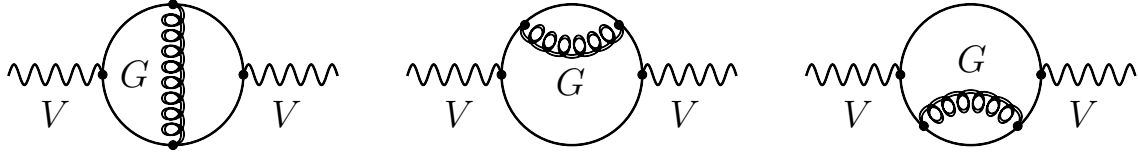


Figure 5: Two-loop axigluon contributions to the oblique parameters. In the case of the  $WW$  selfenergy ( $VV = WW$ ) one has top and bottom quarks in the loop, while in the case of the  $ZZ$  and  $Z\gamma$  selfenergies ( $VV = ZZ, Z\gamma$ ) only top quarks appear as intermediate states.

where  $N_c = 3$  is the number of colors and  $G_F = 1.16637 \cdot 10^{-5} \text{ GeV}^{-2}$  is the Fermi constant. The radiator factors are  $R_V^u = 1.03972$ ,  $R_A^u = 1.04678$ ,  $R_V^{d,s} = 1.03911$ ,  $R_A^{d,s} = 1.03205$ ,  $R_V^c = 1.03974$ ,  $R_A^c = 1.04651$ ,  $R_V^b = 1.03970$ , and  $R_A^b = 1.02544$ , while the relevant non-factorizable corrections amount to  $\Delta_{\text{EW/QCD}}^{u,c} = -0.113 \text{ MeV}$ ,  $\Delta_{\text{EW/QCD}}^{d,s} = -0.160 \text{ MeV}$ , and  $\Delta_{\text{EW/QCD}}^b = -0.040 \text{ MeV}$  [61]. Evaluating the relations (34) and (35) using the input detailed above leads to the following SM predictions

$$(\Gamma_Z)_{\text{SM}} = (2.4945 \pm 0.0007) \text{ GeV}, \quad (\sigma_{\text{had}})_{\text{SM}} = (41.482 \pm 0.006) \text{ nb}. \quad (36)$$

The corresponding experimental extractions and their correlation read [22]

$$\begin{aligned} (\Gamma_Z)_{\text{exp}} &= (2.4952 \pm 0.0023) \text{ GeV}, \\ (\sigma_{\text{had}})_{\text{exp}} &= (41.540 \pm 0.037) \text{ nb}, \end{aligned} \quad \rho = \begin{pmatrix} 1.00 & -0.30 \\ -0.30 & 1.00 \end{pmatrix}. \quad (37)$$

Notice that, while the results for the total width  $\Gamma_Z$  shows agreement with the SM expectation (36) within errors, the experimental value of  $\sigma_{\text{had}}$  is above the SM value by about  $+1.6\sigma$ . After  $A_{\text{FB}}^b$  this is the largest deviation in the global electroweak fit. The principal dependence of  $\sigma_{\text{had}}$  is on the number of light neutrino generations as encoded in  $\Gamma_{\text{inv}}$ , which is constant and equal to three in the SM and in the considered axigluon model.<sup>9</sup>

The regions of 68%, 95%, and 99% CL in the  $\Gamma_Z$ - $\sigma_{\text{had}}$  plane resulting from (37) are shown in Figure 4. The predictions in the flavor non-universal axigluon model are indicated in black. The displayed points correspond to  $\theta = 15^\circ$  and  $M_G = 0.5 \text{ TeV}, 1.0 \text{ TeV}, 1.5 \text{ TeV}$ . We see that the axigluon contributions lead to a correlated shift in  $\Gamma_Z$  and  $\sigma_{\text{had}}$  to higher and lower values, respectively. For smaller (larger) values of the mixing angle  $\theta$ , the corrections to both observables are more (less) pronounced, but the form of the correlation remains unchanged. This tells us that in the flavor non-universal axigluon model the quality of the global fit to  $\Gamma_Z$  and  $\sigma_{\text{had}}$  does not improve relative to the SM. The constraints arising from  $\Gamma_Z$  and  $\sigma_{\text{had}}$  will be combined with those stemming from the bottom-quark POs in Section 6.

We now turn our attention to the axigluon corrections to the oblique (or Peskin-Takeuchi) parameters  $S$ ,  $T$ , and  $U$  [23]. They measure deviations from the electroweak radiative corrections in the SM induced by universal new-physics effects, *i.e.*, those entering through vacuum polarization diagrams. The three parameters are defined as shifts relative to a fixed set of SM

<sup>9</sup>We assume that the mass of the fourth-generation neutrino is larger than the 95% CL LEP II bound, which amounts to  $m_{\nu_4} > 101.5 \text{ GeV}$  [40].

values, so that  $S$ ,  $T$ , and  $U$  are identical to zero at that point. The relevant set of oblique corrections is

$$\begin{aligned} S &= \frac{16\pi s_w^2 c_w^2}{e^2} \left[ \Pi'_{ZZ}(0) + \frac{s_w^2 - c_w^2}{s_w c_w} \Pi'_{Z\gamma}(0) - \Pi'_{\gamma\gamma}(0) \right], \\ T &= \frac{4\pi}{e^2 c_w^2 M_Z^2} \left[ \Pi_{WW}(0) - c_w^2 \Pi_{ZZ}(0) - 2 s_w c_w \Pi_{Z\gamma}(0) - s_w^2 \Pi_{\gamma\gamma}(0) \right], \\ U &= \frac{16\pi s_w^2}{e^2} \left[ \Pi'_{WW}(0) - c_w^2 \Pi'_{ZZ}(0) - 2 s_w c_w \Pi'_{Z\gamma}(0) - s_w^2 \Pi'_{\gamma\gamma}(0) \right], \end{aligned} \quad (38)$$

where  $\Pi_{VV}(p^2) = \Pi_{VV}(0) + p^2 \Pi'_{VV}(0) + \mathcal{O}(p^4)$  with  $VV = WW, ZZ, \gamma\gamma, Z\gamma$  denotes the transversal part of the vacuum polarization tensor of the corresponding selfenergy and  $s_w$  and  $c_w$  are the sine and cosine of the weak mixing angle, respectively. Notice that gauge invariance guarantees that  $\Pi_{\gamma\gamma}(0) = 0$  to all orders in perturbation theory.

The two-loop Feynman diagrams contributing to  $\Pi_{VV}(p^2)$  in the axigluon model are shown in Figure 5. Notice that the mass splitting between the top and the bottom quark provides the source of isospin breaking necessary to generate a non-zero value for  $T$  even so the axigluon physics is isospin preserving. Similarly, non-vanishing contributions to  $S$  and  $U$  are generated at the two-loop level. In the leading-logarithmic approximation, we find the following expressions

$$\begin{aligned} S &\approx S_4 + \frac{2}{9\pi} \frac{\alpha_s}{4\pi} C_F N_c [(g_L^h)^2 + 2(g_R^h)^2] \frac{m_t^2}{M_G^2} \ln^2 \left( \frac{m_t^2}{M_G^2} \right), \\ T &\approx T_4 + \frac{m_t^2}{8\pi s_w^2 c_w^2 M_Z^2} \frac{\alpha_s}{4\pi} C_F N_c [(g_L^h)^2 + 2(g_R^h)^2] \frac{m_t^2}{M_G^2} \ln^2 \left( \frac{m_t^2}{M_G^2} \right), \end{aligned} \quad (39)$$

where  $N_c = 3$  is the number of colors and the mass of the bottom quark has been neglected. Notice that the axigluon contribution to  $T$  is larger by a factor of  $9/(16 s_w^2 c_w^2) m_t^2/M_Z^2 \approx 11.7$  than the one to  $S$ . Since the parameter  $U$  is suppressed with respect to  $T$  by an additional factor of  $M_Z^2/M_G^2$ , we neither quote its analytic result nor use this parameter when constraining the  $M_G$ - $\theta$  plane. We remark that the leading-logarithmic two-loop corrections in (39) can be found by contracting the axigluon propagator to a four-quark interaction and considering only the first diagram in Figure 5. What concerns  $T$ , our leading-logarithmic result agrees with the one presented in [63], while the expression for  $S$  is, to the best of our knowledge, new. The full two-loop results for the set of relevant oblique corrections are given in Appendix B. Although the two-loop axigluon contributions to  $S$  and  $T$  involve double logarithms, it turns out that numerically the leading-logarithmic approximation is not an excellent approximation for the relevant axigluon masses, so that in our numerical analysis we will employ the complete two-loop expressions.

The terms  $S_4$  and  $T_4$  appearing in (39) denote the one-loop contributions of the fourth generation of sequential fermions to the  $S$  and  $T$  parameters. Neglecting inter-generational mixing with the additional generation, these corrections take the well-known form [23, 64]

$$S_4 = \frac{1}{6\pi} \left[ N_c \mathcal{S}(m_{u_4}, m_{d_4}) + \mathcal{S}(m_{\nu_4}, m_{\ell_4}) \right],$$

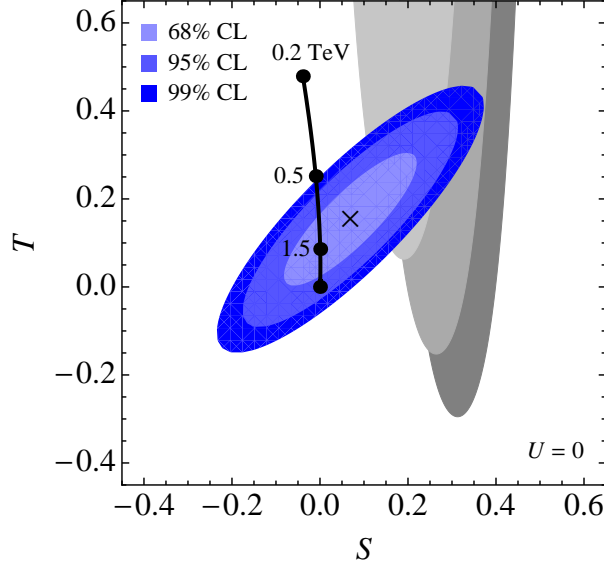


Figure 6: Regions of 68%, 95%, and 99% probability in the  $S$ - $T$  plane. The black dot without label is the SM point and the black cross represents the best-fit solution. The black line and the remaining dots indicate the contribution of a flavor non-universal axigluon. They have been obtained for  $\theta = 15^\circ$  and  $M_G = 0.2$  TeV, 0.5 TeV, 1.5 TeV. The gray areas illustrate the predicted regions for the fourth-generation contributions to  $S$  and  $T$  for three different values of the Higgs-boson mass. See text for further details.

$$T_4 = \frac{1}{16\pi s_w^2 c_w^2 M_Z^2} \left[ N_c \mathcal{T}(m_{u_4}, m_{d_4}) + \mathcal{T}(m_{\nu_4}, m_{\ell_4}) \right], \quad (40)$$

with

$$\mathcal{S}(m_1, m_2) = 1 - 2Y \ln \left( \frac{m_1^2}{m_2^2} \right), \quad \mathcal{T}(m_1, m_2) = m_1^2 + m_2^2 - 2 \frac{m_1^2 m_2^2}{m_1^2 - m_2^2} \ln \left( \frac{m_1^2}{m_2^2} \right). \quad (41)$$

Here  $Y = 1/6$  ( $Y = -1/2$ ) denotes the hypercharge of the left-handed doublet of quarks (leptons). Notice that choosing the masses of the fourth-generation quarks and leptons to be degenerate, which corresponds to the isospin limit, one is left with the finite correction  $S_4 = 2/(3\pi)$  to the  $S$  parameter while the contribution  $T_4$  vanishes identically. This value of  $S$  can be reduced by splitting the multiplets such that  $m_{u_4}/m_{d_4} > 1$  and  $m_{\nu_4}/m_{\ell_4} < 1$ , which in turn leads to a positive shift in  $T$  that is quadratic in the mass splittings. Given that  $\mathcal{T}(m_1, m_2) = \mathcal{T}(m_2, m_1)$  the possible values of  $S_4$  and  $T_4$  thus form an upright parabola-like shaped region in the  $S$ - $T$  plane with a vertex at  $(2/(3\pi), 0)$ .

The experimental 68% CL bounds on the  $S$  and  $T$  parameters, corrected to the present world average of the top-quark mass [62], and their correlation matrix are given by [22]

$$\begin{aligned} S &= 0.07 \pm 0.10, \\ T &= 0.15 \pm 0.10, \end{aligned} \quad \rho = \begin{pmatrix} 1.00 & 0.85 \\ 0.85 & 1.00 \end{pmatrix}. \quad (42)$$

The regions of 68%, 95%, and 99% probability in the  $S$ - $T$  plane are shown in Figure 6. Notice that in the global fit to the LEP and SLC measurements the parameter  $U$  is set to zero. The

$S$ – $T$  error ellipses show that there are no large unexpected electroweak radiative corrections from physics beyond the SM, as the values of the oblique parameters are in agreement with zero. The contributions of a flavor non-universal axigluon to  $S$  and  $T$  are indicated by the black line and points. The shown points have been obtained for the value of the mixing angle fixed to  $\theta = 15^\circ$  and the three different axigluon masses  $M_G = 0.2$  TeV, 0.5 TeV, 1.5 TeV. From the panel as well as the second formula in (39), we see that the axigluon corrections to  $T$  are strictly positive. In contrast, the axigluon contribution to  $S$  changes from positive to negative sign when the axigluon mass is decreased. This feature arises from single logarithms and constant terms not shown in (39) and takes place at  $M_G = 1.25$  TeV for the specific value  $\theta = 15^\circ$  of the mixing angle. For comparison the grayish areas in the latter figure show the possible predictions for  $S_4$  and  $T_4$ , assuming  $m_h = 100$  GeV (light gray), 400 GeV (gray), and 1000 GeV (dark gray). The shifts in  $S$  and  $T$  due to a Higgs-boson mass different from our reference value  $m_h^{\text{ref}} = 150$  GeV are given to leading-logarithmic accuracy by  $\Delta S = 1/(12\pi) \ln(m_h^2/(m_h^{\text{ref}})^2)$  and  $\Delta T = -3/(16\pi c_w^2) \ln(m_h^2/(m_h^{\text{ref}})^2)$  [23]. For each value of the Higgs-boson mass the masses of the fourth-generation fermions have been freely varied in the ranges  $m_{u_4} \in [311, 600]$  GeV,  $m_{d_4} \in [372, 600]$  GeV,  $m_{\nu_4} \in [101.5, 600]$  GeV, and  $m_{\ell_4} \in [101.9, 600]$  GeV. From the plot it is immediately clear that it is not possible to obtain a model-independent bound on  $M_G$  and  $\theta$  from the oblique parameters in the case of a flavor non-universal axigluon. In fact, one has to distinguish three different cases. First, the value of  $T_4$  is below the  $S$ – $T$  ellipse. In this case one can derive a two-side limit on  $M_G$  as a function of  $\theta$ . Second, the prediction for  $T_4$  lies inside the ellipse, which allows one to obtain a lower bound on the axigluon mass for any value of the mixing angle. Third, the prediction for  $T_4$  is above the  $S$ – $T$  ellipse. In this case a flavor non-universal axigluon is at variance with the constraints imposed by the oblique corrections. For illustrative purposes, we will in Section 6 determine the allowed region in the  $M_G$ – $\theta$  plane for the flavor non-universal axigluon model assuming the specific values  $S_4 = 0.15$  and  $T_4 = 0.19$ . For a Higgs boson with a mass  $m_h \in [100, 200]$  GeV such values are obtained for the mass splittings  $m_{\ell_4} - m_{\nu_4} \approx 70$  GeV and  $m_{u_4} - m_{d_4} \approx (1 + 1/3 \ln(m_h^2/(m_h^{\text{ref}})^2)) 45$  GeV with  $m_h^{\text{ref}} = 150$  GeV. A glimpse at Figure 6 tells us that the corresponding point in the  $S$ – $T$  plane lies within the 68% CL of the global fit to the oblique parameters.

## 5 Collider Observables

In this section we will discuss the direct bounds on massive color-octet bosons following from the high- $p_T$  experiments performed at the Tevatron and the LHC. In particular, we will consider top-antitop quark as well as dijet production. In the former case we will combine the available experimental information on the total inclusive  $t\bar{t}$  cross section [13, 14], the invariant mass spectrum [15, 65], and the differential forward-backward asymmetry [16]. In the latter case we explore the constraining power of the searches for dijet resonances [24, 26, 66, 67] and the measurements of the dijet angular distributions [25, 26, 68, 69]. Like before, we will neglect possible effects from flavor-changing axigluon couplings when computing the relevant collider observables. See [30, 31, 34] for other comprehensive studies of color-octet resonances at hadron colliders similar to ours in spirit.

At the Tevatron  $t\bar{t}$  pairs are produced in collisions of protons and antiprotons at an CM

energy of  $\sqrt{s} = 1.96$  TeV. Within the model at hand the hadronic process receives Born-level contributions from quark-antiquark annihilation  $q\bar{q} \rightarrow t\bar{t}$ , associated with tree-level exchange of an axigluon in the  $s$  channel. On the other hand, the gluon-fusion channel  $gg \rightarrow t\bar{t}$  does not contribute at Born level. This result is an important consequence of the gauge invariance of the axigluon model, which forces the  $ggG$  vertex to vanish at tree level. The absence of the  $ggG$  tree-level interactions is a feature of many models with extra massive bosons in the adjoint representation of  $SU(3)_c$ .<sup>10</sup> Beyond tree level or through non-renormalizable operators of dimension six and higher, such a coupling can however be induced. Since the resulting effects are, compared to the contributions from  $q\bar{q} \rightarrow t\bar{t}$ , suppressed by two powers of the new-physics scale and possibly a loop factor, we will not consider contributions to top-quark pair production from gluon fusion in the following.

Constraints on new color-octet resonances in  $t\bar{t}$  production arise from the Tevatron measurements of the total cross section  $\sigma_s$ , the invariant mass spectrum  $d\sigma_s/dM_{t\bar{t}}$ , the forward-backward asymmetry  $A_{\text{FB}}^t$ , and its distribution  $A_{\text{FB}}^t(M_{t\bar{t}})$ . Since the last bin of the available CDF measurement of the differential cross section, *i.e.*,  $M_{t\bar{t}} \in [0.8, 1.4]$  TeV, is most sensitive to the presence of new degrees of freedom with masses of order TeV, we will restrict our attention to this range of invariant masses when calculating  $d\sigma_s/dM_{t\bar{t}}$ . Recently the CDF collaboration has measured the forward-backward asymmetry in two bins of the  $t\bar{t}$  invariant mass, separated at  $M_{t\bar{t}} = 0.45$  TeV. While in the low bin the observed asymmetry agrees with the SM expectation as well as with zero within errors, the result for the upper bin lies more than  $3\sigma$  above the NLO QCD prediction. Similar to the symmetric spectrum, the region of high  $M_{t\bar{t}}$  for the asymmetry is expected to be most sensitive to heavy new physics. In our global analysis of the  $t\bar{t}$  observables, we include both bins of the differential asymmetry, treating the two measurements as fully uncorrelated. This should be a good approximation, since at the moment the measurement of  $A_{\text{FB}}^t(M_{t\bar{t}})$  is statistically limited.

The quantities of interest can all be obtained from the double differential  $t\bar{t}$  cross section,

$$\frac{d^2\sigma}{dM_{t\bar{t}}d\cos\hat{\theta}} = \left( \frac{d^2\sigma}{dM_{t\bar{t}}d\cos\hat{\theta}} \right)_{\text{SM}} + \left( \frac{d^2\sigma}{dM_{t\bar{t}}d\cos\hat{\theta}} \right)_G, \quad (43)$$

by integrating over the invariant mass  $M_{t\bar{t}}$  and the cosine of the scattering angle  $\hat{\theta}$  of the top quark in the partonic CM frame. Here the labels SM and  $G$  denote the SM and axigluon contributions. In particular, the symmetric and asymmetric mass spectra are calculated via

$$\begin{aligned} \frac{d\sigma_s}{dM_{t\bar{t}}} &= \int_{-1}^1 d\cos\hat{\theta} \frac{d^2\sigma}{dM_{t\bar{t}}d\cos\hat{\theta}}, \\ \frac{d\sigma_a}{dM_{t\bar{t}}} &= \int_0^1 d\cos\hat{\theta} \frac{d^2\sigma}{dM_{t\bar{t}}d\cos\hat{\theta}} - \int_{-1}^0 d\cos\hat{\theta} \frac{d^2\sigma}{dM_{t\bar{t}}d\cos\hat{\theta}}, \end{aligned} \quad (44)$$

while the forward-backward asymmetry takes the form  $A_{\text{FB}}^t = \sigma_a/\sigma_s$ . An analog definition holds, of course, in the case of the  $M_{t\bar{t}}$  distribution  $A_{\text{FB}}^t(M_{t\bar{t}})$  of the asymmetry.

---

<sup>10</sup>In the case of warped extra dimensions the absence of the coupling of two gluons to the massive spin-one octet, *i.e.*, the KK gluon, is an artifact of the orthonormality of gauge-boson wave functions [12, 70, 71]. In addition, all gluon-axigluon vertices with an odd number of axigluons can be forbidden by strong parity [5].

Observable	SM	Measurement
$\sigma_s$	$(6.73^{+0.52}_{-0.80})$ pb	$(7.50 \pm 0.48)$ pb [13]
$(d\sigma_s/dM_{t\bar{t}})^{M_{t\bar{t}} \in [0.8, 1.4] \text{ TeV}}$	$(0.061^{+0.012}_{-0.006})$ fb/GeV	$(0.068 \pm 0.034)$ fb/GeV [15]
$(A_{\text{FB}}^t(M_{t\bar{t}}))^{M_{t\bar{t}} < 0.45 \text{ TeV}}$	$(7.0^{+1.0}_{-0.8})\%$	$(-11.6 \pm 15.3)\%$ [16]
$(A_{\text{FB}}^t(M_{t\bar{t}}))^{M_{t\bar{t}} > 0.45 \text{ TeV}}$	$(11.0^{+1.2}_{-1.3})\%$	$(47.5 \pm 11.2)\%$ [16]

Table 2: SM expectations and measurements of the  $t\bar{t}$  observables entering our analysis. The numbers given for the forward-backward asymmetries correspond to the partonic CM frame.

The SM contributions to (43) and (44) are computed at NLO using MCFM [72], which for what concerns  $t\bar{t}$  production is based on the seminal work [73]. For the charge-symmetric observables we employ MSTW2008NLO parton distribution functions (PDFs) [74] with the strong coupling constant  $\alpha_s = 0.120$  as an input, corresponding to  $\alpha_s(m_t) = 0.109$  at two-loop accuracy. Since the charge-asymmetric terms are generated first at the one-loop level, they are computed using MSTW2008LO PDFs and normalized to the LO symmetric cross section. The expectations for the  $t\bar{t}$  observables in the SM along with the corresponding measurements are collected in Table 2. The shown theoretical errors are due to renormalization and factorization scale variations  $\mu_r = \mu_f \in [m_t/2, 2m_t]$  as well as PDF uncertainties. We also mention that the symmetric SM cross section at LO, integrated over the low- and high-mass bin amounts to  $(\sigma_s)^{M_{t\bar{t}} < 0.45 \text{ TeV}} = 4.04$  pb and  $(\sigma_s)^{M_{t\bar{t}} > 0.45 \text{ TeV}} = 2.58$  pb. The axigluon effects in the  $t\bar{t}$  observables are computed by convoluting the well-known matrix element squared for quark-antiquark annihilation induced by axigluon exchange [27, 28] with MSTW2008LO PDFs and fixing  $\mu_r = \mu_f = m_t = 173.3$  GeV. The relevant value of the strong coupling constant is  $\alpha_s(M_Z) = 0.139$ , which translates into  $\alpha_s(m_t) = 0.126$  using LO RG running.

From Table 2 we infer that the measurements of the charge-symmetric observables agree fairly well with their SM predictions, whereas the SM expectation for the asymmetry in the high  $M_{t\bar{t}}$  bin is significantly lower than its measured value. In order to fit the data, an axigluon ought to yield positive contributions to  $(A_{\text{FB}}^t(M_{t\bar{t}}))^> = (A_{\text{FB}}^t(M_{t\bar{t}}))^{M_{t\bar{t}} > 0.45 \text{ TeV}}$ , while leaving  $\sigma_s$ ,  $d\sigma_s/dM_{t\bar{t}}$ , and  $(A_{\text{FB}}^t(M_{t\bar{t}}))^< = (A_{\text{FB}}^t(M_{t\bar{t}}))^{M_{t\bar{t}} < 0.45 \text{ TeV}}$  essentially unaffected. As we will see in Section 6, this leads to a generic tension in the global fit, since the latter observables prefer the new degrees of freedom to be heavy, whereas the asymmetry in the region  $M_{t\bar{t}} > 0.45$  TeV would like to have a low new-physics scale.

Any massive color-octet boson that couples to light  $q\bar{q}$  pairs is also subject to constraints arising from narrow resonance searches in dijet production. Employing an integrated luminosity of only  $3.1 \text{ pb}^{-1}$  [67] and  $2.9 \text{ pb}^{-1}$  [24], ATLAS and CMS have already surpassed the previous most stringent mass limits by CDF [66]. Very recently, ATLAS has presented improved 95% CL upper limits on the product of the resonant production cross section ( $\sigma$ ), branching fraction ( $\mathcal{B}$ ), and acceptance ( $A$ ) for an axigluon coupling decaying democratically to all quark flavors [26]. We will use the latter results, which are based on a data set of  $36 \text{ pb}^{-1}$ ,

to derive the relevant constraints on the allowed parameter space in the non-universal axigluon model.

The tree-level cross section for resonant axigluon production receives only corrections from  $q\bar{q} \rightarrow G$ , and can thus be written as

$$\sigma = \sum_q \mathcal{F}_{q\bar{q}}(M_G^2/s, \mu_f) \frac{C_F}{N_c} \frac{2\pi^2\alpha_s}{s} ((g_L^q)^2 + (g_R^q)^2), \quad (45)$$

where the sum extends over the light quark flavors  $q = u, d, s, c, b$  and  $\sqrt{s} = 7 \text{ TeV}$ . The parton luminosity functions,

$$\mathcal{F}_{ij}(\tau, \mu_f) = \frac{2}{1 + \delta_{ij}} \int_\tau^1 \frac{dx}{x} f_{i/p}(x, \mu_f) f_{j/p}(\tau/x, \mu_f). \quad (46)$$

are evaluated at the parton CM energy corresponding to the resonant production of the axigluon, *i.e.*,  $\tau = M_G^2/s$ . They are obtained from a convolution of the universal non-perturbative PDFs  $f_{i/p}(x, \mu_f)$ , which describe the probability of finding the parton  $i$  in the proton with longitudinal momentum fraction  $x$ . In our analysis we employ MSTW2008L0 PDFs with the renormalization and factorization scales set to  $\mu_r = \mu_f = M_G$ .

The branching ratio for the decay of a heavy spin-one color octet into a pair of light quarks reads  $\mathcal{B}(G \rightarrow q\bar{q}) = \Gamma_q/\Gamma_G$ . The total width in the case of the non-universal axigluon is given by the sum  $\Gamma_G = \sum_q \Gamma_q + \sum_Q \Gamma_Q$  of light- and heavy-quark contributions, where  $Q = t, u_4, d_4$  ( $Q = t$ ) in the case of an flavor non-universal (universal) axigluon. Neglecting the masses of the light quarks, the partial tree-level decay rates are

$$\begin{aligned} \Gamma_q &= \frac{\alpha_s T_F}{6} M_G \left[ (g_L^\ell)^2 + (g_R^\ell)^2 \right], \\ \Gamma_Q &= \frac{\alpha_s T_F}{6} M_G \sqrt{1 - \frac{4m_Q^2}{M_G^2}} \left[ ((g_L^h)^2 + (g_R^h)^2) \left( 1 - \frac{m_Q^2}{M_G^2} \right) + 6g_L^h g_R^h \frac{m_Q^2}{M_G^2} \right], \end{aligned} \quad (47)$$

where  $T_F = 1/2$  and  $m_Q$  denotes the mass of the heavy quarks in the final state. Since dijet resonance searches are based on the narrow-width approximation, they do not apply if the total decay width of the resonance significantly exceeds the mass resolution of the detector. The article [26] lacks the explicit information for which value of  $\Gamma_G/M_G$  the ATLAS axigluon analysis becomes inapplicable.<sup>11</sup> Yet, the presented model-independent limits on Gaussian resonances, which cover the ranges  $M_G \in [0.6, 4.0] \text{ TeV}$  and  $\Gamma_G/M_G \in [3, 15]\%$ , suggest that it should at least apply to cases where the ratio of the resonance width and its mass is below 15%. In order to illustrate the importance of knowing the applicability of the narrow-width approximation, we will consider three different cases  $\Gamma_G/M_G < 10\%, 15\%$ , and  $20\%$ . As we will see in Section 6, these three benchmark scenarios restrict the parameter space to the region where  $\theta \gtrsim 40^\circ, 30^\circ$ , and  $25^\circ$ , respectively. To calculate the total decay width in the non-universal axigluon model, we fix the fourth-generation quark masses to  $m_{u_4} = 311 \text{ GeV}$  [41] and  $m_{d_4} = 372 \text{ GeV}$  [42]. The model dependence introduced by this choice is small.

---

<sup>11</sup>The ATLAS 95% CL exclusion  $M_G \in [0.6, 2.1] \text{ TeV}$  applies to a flavor-universal axigluon that has QCD-like couplings to quarks. Such a color-octet boson has a total width of around 8% to 9% of its mass.

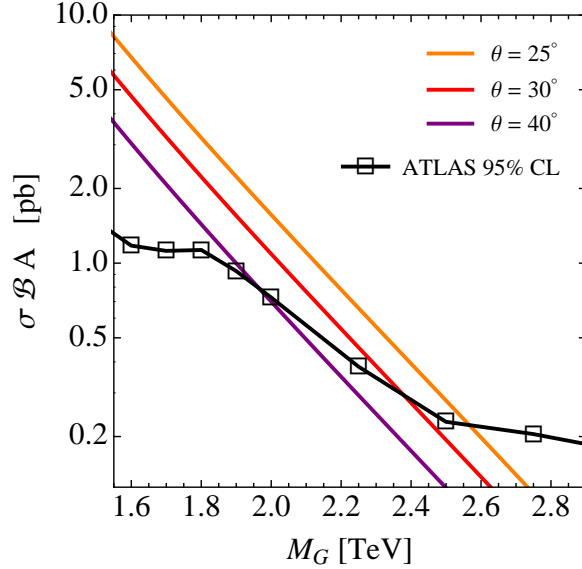


Figure 7: Predictions for resonant axigluon production as a function of  $M_G$  for three different values of the mixing angle. The orange, red, and purple line corresponds to  $\theta = 25^\circ, 30^\circ$ , and  $40^\circ$ , respectively. The black line represents the ATLAS 95% CL upper limit on  $\sigma \mathcal{B} A$  for resonances decaying to  $q\bar{q}$ .

In order to utilize the 95% CL upper limit on  $\sigma \mathcal{B} A$  from ATLAS, we have to correct for perturbative QCD radiation, non-perturbative effects (*i.e.*, hadronization and multi-parton interactions), and the detector acceptance. We achieve this by rescaling our result for the partonic production cross section  $q\bar{q} \rightarrow G \rightarrow q\bar{q}$  by

$$\begin{aligned}
 R &= \frac{(\sigma \mathcal{B} A)_{\text{axigluon}}^{\text{ATLAS}}}{(\sigma \mathcal{B}(G \rightarrow q\bar{q})) \Big|_{\substack{Q \neq u_4, d_4 \\ g_{L,R}^{\ell,h} = \pm 1}}} \\
 &= 0.54 - \frac{0.09}{2.4 \text{ TeV}} (M_G - 0.6 \text{ TeV}) + \left[ \frac{0.99}{2.4 \text{ TeV}} (M_G - 0.6 \text{ TeV}) \right]^2,
 \end{aligned} \tag{48}$$

where the numerator is given by the axigluon prediction of ATLAS, while the denominator is calculated at the partonic level using (45) and (47), including only three generations of quarks, and employing  $g_L^{\ell,h} = 1$  and  $g_R^{\ell,h} = -1$ . Notice that (48) implicitly assumes that the acceptance depends only on  $M_G$  but not on  $\Gamma_G$ . We have explicitly checked that using the limit on a simplified Gaussian signal model presented in [26], which incorporates the dependence on  $\Gamma_G$ , essentially leads to the same exclusions as the rescaling procedure described above.

In Figure 7 we compare the 95% CL upper bound on  $\sigma \mathcal{B} A$  obtained by ATLAS (black line) to our theory predictions for resonant axigluon production employing the three values  $\theta = 25^\circ, 30^\circ$ , and  $40^\circ$  (orange, red, and purple lines) for the mixing angle. Cross sections above the black curve are disfavored by the data. From the intersection of the theory predictions with the ATLAS limit, we derive the following 95% CL bounds  $M_G > 2.5 \text{ TeV}$ ,  $2.4 \text{ TeV}$ , and  $2.0 \text{ TeV}$ . In Section 6 we will compare the constraints on the  $M_G$ - $\theta$  plane following from the recent narrow resonance search at ATLAS with the other available direct constraints.



A second quantity of interest for what concerns dijet production is the jet angular distribution. The differential cross section for a pair of jets with invariant mass  $M_{jj}$  produced at an angle  $\hat{\theta}$  to the beam direction in the jet-jet CM frame, can be written in the following way

$$\frac{d^2\sigma}{dM_{jj}d\cos\hat{\theta}} = \frac{M_{jj}}{s} \sum_{i,j} \mathcal{F}_{ij}(M_{jj}^2/s, \mu_f) \frac{d\sigma_{ij}}{d\cos\hat{\theta}}, \quad (49)$$

with

$$\frac{d\sigma_{ij}}{d\cos\hat{\theta}} = \frac{1}{32\pi M_{jj}^2} \sum_{k,l} \overline{\sum} |\mathcal{M}(ij \rightarrow kl)|^2 \frac{1}{1 + \delta_{kl}}. \quad (50)$$

Here  $\mathcal{M}(ij \rightarrow kl)$  denotes the matrix element for the scattering of the incoming partons  $i, j = q, \bar{q}, g$  into the outgoing partons  $k, l$ . The color and spin indices in (50) are averaged (summed) over initial (final) states as indicated by the symbol  $\overline{\sum}$ . The expressions for the tree-level matrix elements squared appearing in QCD can be found in [75].

Compared to the narrow resonance searches discussed before, the dijet angular distribution (49) has the salient advantage that it also constrains broad  $s$ -channel resonances. This is due to the fact that the dominant channels in QCD dijet production have the familiar Rutherford scattering behavior  $d\sigma_{ij}/d\cos\hat{\theta} \propto 1/\sin^4(\hat{\theta}/2)$  at small angle  $\hat{\theta}$ , which is characteristic for  $t$ -channel exchange of a massless spin-one boson. In order to remove the Rutherford singularity, one usually considers the dijet cross sections differential in

$$\chi = \frac{1 + |\cos\hat{\theta}|}{1 - |\cos\hat{\theta}|}. \quad (51)$$

In the small angle limit, *i.e.*,  $\chi \rightarrow \infty$ , the partonic differential QCD cross section then behaves as  $d\sigma_{ij}/d\chi \propto \text{const.}$  Relative to the QCD background, the production of a heavy resonance leads to additional hard scattering and hence more jets perpendicular to the beam. In turn one expects a deviation from the QCD prediction in form of an enhanced activity of high-energetic jets in the central region of the detector. If the angular distributions receive contributions from the presence of a heavy degree of freedom, one should see an excess of events in  $d\sigma_{ij}/d\chi$  for  $\chi \rightarrow 1$  and large  $M_{jj}$  with respect to the (almost) flat QCD spectrum.

The shape of the normalized dijet angular distribution  $1/\sigma d\sigma/d\chi$  has been studied both at the Tevatron [68] and LHC [25, 26, 69] and found to be in good agreement with the SM prediction. These results put stringent constraints on any non-standard scattering mechanism leading to jet pairs, including scenarios where the new particles are too heavy to be produced directly. In models where the new-physics scale  $\Lambda$  is much larger than the CM energy of the colliding partons, the exchange of new particles is most commonly described in terms of effective four-quark contact interactions (CIs). These consist out of products of left-handed color-singlet quark currents [76, 77],

$$\mathcal{H}_{4q}^{\text{CI}} = \frac{2\pi\xi}{\Lambda^2} \sum_i (\bar{q}_{iL} \gamma^\mu q_{iL})(\bar{q}_{iL} \gamma_\mu q_{iL}). \quad (52)$$

Here  $i$  is a flavor index and  $\xi$  determines whether the interference between the new-physics and the SM contributions is destructive ( $\xi = +1$ ) or constructive ( $\xi = -1$ ). The currently

most stringent 95% CL bound on this type of four-quark interactions amounts to  $\Lambda > 9.5$  TeV for  $\xi = +1$  and is based on  $36 \text{ pb}^{-1}$  of  $\sqrt{s} = 7$  TeV data collected by ATLAS [26].

The ATLAS collaboration determines the bound on the scale  $\Lambda$  entering (52) by studying the fraction of centrally produced dijets versus the total number of observed events for a specified dijet mass range  $M_{jj} \in [M_{jj}^{\min}, M_{jj}^{\max}]$ . Specifically, ATLAS measures

$$F_\chi(M_{jj}) = \frac{\sigma(\chi < 3.32, [M_{jj}^{\min}, M_{jj}^{\max}])}{\sigma(\chi < 30, [M_{jj}^{\min}, M_{jj}^{\max}])}, \quad (53)$$

in 27 different bins of the dijet invariant mass. Utilizing the same amount of data the CMS collaboration obtains the weaker bound  $\Lambda > 5.6$  TeV [25]. The strong constraint by ATLAS is due to the fact that relative to the expected QCD background there are too few observed central events for  $M_{jj}$  around 1.6 TeV and above 2.2 TeV. This feature is illustrated in Figure 8, which shows the central value of the QCD prediction of  $F_\chi(M_{jj})$  (black line) and its total error (gray band) in comparison to the ATLAS data points with their statistical uncertainties (black error bars). To eliminate the possible bias from the downward statistical fluctuations, we will employ the expected limit of  $\Lambda > 5.7$  TeV from the ATLAS collaboration. This more conservative exclusion is comparable to an alternative calculation by ATLAS using Bayesian statistics as well as the aforementioned bound derived by CMS.

Translating the lower limit on  $\Lambda$  into bounds on the parameter space of the axigluon model is complicated by two features. First, the chiral structure of the axigluon interactions is richer than the one of CIs encoded in (52). Second, in the parts of the phase space with  $M_G \lesssim M_{jj}$  a calculation of (53) based on dimension-six operators is not applicable, since the relevant momentum transfer is comparable or larger than the mass of the new state produced in the scattering. We begin by commenting on the first issue. Integrating out the heavy degrees of freedom from the Lagrangian in (7) leads to the following effective tree-level Hamiltonian

$$\mathcal{H}_{4q}^G = \frac{4\pi\alpha_s}{M_G^2} \sum_{i,j} \sum_{P,Q} g_P^\ell g_Q^\ell (\bar{q}_{iP} \gamma^\mu T^a q_{iP}) (\bar{q}_{jQ} \gamma_\mu T^a q_{jQ}), \quad (54)$$

where the sum over  $P, Q = L, R$  includes both left- and right-handed chiral fields. By calculating the partonic differential cross section for the interference of the effective interactions (52) and (54) with the SM and with themselves, one obtains for the dominant channel  $uu \rightarrow uu$  in the former case

$$\left( \frac{d\sigma_{uu}}{d\chi} \right)_{\text{CI}} = \frac{4\pi\alpha_s}{9} \frac{\xi}{\Lambda^2} \frac{1}{\chi} + \mathcal{O}(1/\Lambda^4), \quad (55)$$

while in the latter case one finds

$$\left( \frac{d\sigma_{uu}}{d\chi} \right)_G = \frac{4\pi\alpha_s}{9} \frac{\alpha_s}{3M_G^2} \frac{1}{\chi} \left[ ((g_L^\ell)^2 + (g_R^\ell)^2) + 3g_L^\ell g_R^\ell \frac{1 - \chi + \chi^2}{(1 + \chi)^2} \right] + \mathcal{O}(1/M_G^4). \quad (56)$$

From (56) one observes that the axigluon contribution proportional to the product  $g_L^\ell g_R^\ell$  is sensitive to the relative sign between the couplings to left- and right-handed quarks. It furthermore changes the shape of the angular distribution with respect to (52), which involves only left-handed quarks. This feature is illustrated by the aquamarine (blue) curve in Figure 8,

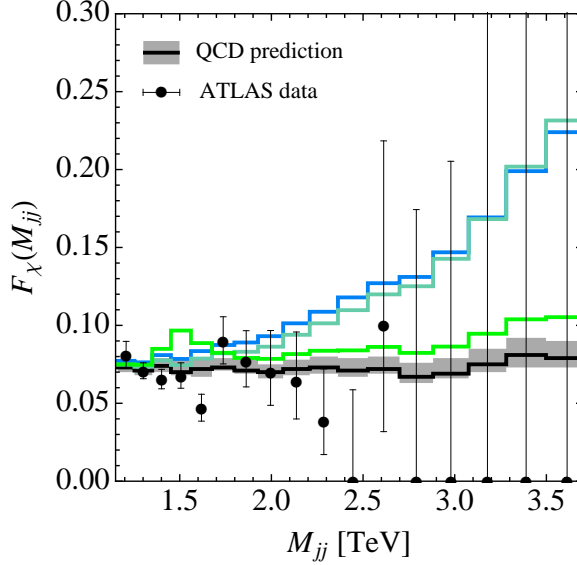


Figure 8: Ratio  $F_\chi(M_{jj})$  as a function of  $M_{jj}$ . The black line and gray band represent the central value of the QCD prediction with its total error. The ATLAS data points with their statistical uncertainties are overlaid as black error bars. The blue, aquamarine, and green lines correspond to QCD plus the effects of a flavor non-universal axigluon with  $M_G = 1.5$  TeV and  $\theta = 45^\circ$  for three different theoretical treatments. The first two curves are obtained in an effective theory, while the third one corresponds to the exact result. The latter prediction employs an axigluon propagator with a Breit-Wigner form and  $\Gamma_G/M_G = 10\%$ . See text for further details.

which corresponds to the prediction for  $F_\chi(M_{jj})$  in the effective theory (54) neglecting (including) contributions proportional to  $g_L^\ell g_R^\ell$ . Both curves have been obtained for  $M_G = 1.5$  TeV and  $\theta = 45^\circ$ . We see that the exact effective theory result predicts less central activity in all bins apart from the last two than the one where the contributions proportional to  $g_L^\ell g_R^\ell$  have been left out. This implies that the actual limits on  $M_G$  obtained from (54) are weaker than the ones derived by simply rescaling the bound on  $\Lambda$  by a factor of  $(\alpha_s((g_L^\ell)^2 + (g_R^\ell)^2)/3)^{1/2}$ .

In order to discuss the range of validity of the effective theory formalism, we have also performed the exact calculation of  $F_\chi(M_{jj})$  for a flavor non-universal axigluon of mass  $M_G$  and width  $\Gamma_G$ . The exact axigluon result assuming  $M_G = 1.5$  TeV,  $\theta = 45^\circ$ , and  $\Gamma_G/M_G = 10\%$  is displayed by the green curve in Figure 8. The corresponding matrix elements are reported in Appendix D. The first noticeable feature of the exact prediction is the relatively wide peak centered at  $M_{jj} \approx 1.5$  TeV corresponding to the onset of resonant axigluon production. In addition, one observes that in contrast to the effective theory result, which scales as  $M_{jj}^2/M_G^2$  for  $M_{jj} \gg M_G$ , the exact  $F_\chi(M_{jj})$  distribution has an almost flat tail for large dijet masses. The different high- $M_{jj}$  behavior of the predictions is readily understood by realizing that the propagator associated with  $s$ -channel axigluon exchange is approximated by  $-1/M_G^2$  in the effective theory, while it behaves like  $1/M_{jj}^2$  in the full theory. In view of the dissimilarity between the exact and the effective theory result in large parts of the phase space, we will use in Section 6 the exact prediction for the dijet angular distribution to determine the allowed parameter space in the  $M_G$ - $\theta$  plane.

Before closing this section, let us finally spend some words on the actual calculation of the dijet angular distributions. Our starting point is the Born-level computation of the QCD expectation for  $F_\chi(M_{jj})$  using MSTW2008L0 PDFs with  $\mu_r = \mu_f = M_{jj}$ .<sup>12</sup> This result is then multiplied by the bin-wise  $K$ -factors computed by the ATLAS collaboration [26] to obtain a reshaped spectrum that includes corrections originating from NLO matrix elements. The detector resolution as well as possible additional non-perturbative QCD effects are incorporated by calculating the ratio between the latter result and the central value of the ATLAS QCD prediction. Numerically, we find that the bin-wise rescaling factor determined in this way lies in the narrow range  $[0.79, 0.91]$  for the relevant kinematic region. Our prediction for  $F_\chi(M_{jj})$  is then obtained by adding the QCD and axigluon results and multiplying the resulting expression by the rescaling factor. Following ATLAS, we apply  $K$ -factors only to the QCD part of the dijet angular distribution.<sup>13</sup> Notice that applying the same rescaling factor to both the QCD and axigluon result is based on the assumption that the event detection and the effects of the Monte Carlo shower depend only on the invariant mass  $M_{jj}$  of the dijet final state, but not on the precise form of the new-physics signal. In order to determine to which extent this assumption is justified would require to perform a dedicated simulation of  $F_\chi(M_{jj})$  including detector effects and parton showering. However, such an analysis is beyond the scope of this work.

## 6 Numerical Analysis

In this section we present the constraints on the parameter space of axigluon models and their look-a-likes that arise from flavor physics, EWPOs, and collider observables. Throughout our analysis, we will require that the couplings of heavy color-octet bosons to quarks remain perturbative. In the flavor non-universal axigluon model, this requirement is fulfilled if the mixing angle lies within  $\theta \in [15^\circ, 45^\circ]$ . Notice that in this parameter region the axigluon forms a distinct resonance, satisfying  $\Gamma_G/M_G \ll 1$ , and that the bounds stemming from fermion condensation [29] are also avoided.

We begin our survey in the flavor sector. A detailed discussion similar to ours has been presented recently in [31]. In Figure 9, we show the constraints on the non-universal axigluon model that follow from neutral meson mixing. The left panel corresponds to flavor alignment in the up-type quark sector (*i.e.*,  $U_u = 1$ ), while the figure on the right-hand side reflects the situation in the case of down-type quark flavor alignment (*i.e.*,  $U_d = 1$ ). We recall that in both cases the resulting FCNCs are purely left-handed (17) and governed by the CKM matrix (18). From the yellow, orange, and red regions in the left plot we infer that in the case of up-type quark flavor alignment, the most stringent bound arises from  $\Delta m_{B_s}$ . The 95% CL

---

<sup>12</sup>In our calculation we respect the rapidity cuts imposed by ATLAS. Effects from cuts on the dijet rapidity boost  $y_B = (y_{j_1} + y_{j_2})/2$  largely cancel in the ratio  $F_\chi(M_{jj})$ , which is designed to be sensitive to the rapidity difference  $|y_{j_1} - y_{j_2}| = \ln \chi$ . Neglecting the ATLAS cut on  $y_B$  leaves the constraints on the axigluon parameters essentially unchanged.

<sup>13</sup>The NLO QCD corrections to dijet production induced by the CIs (52) have been calculated in [78] and shown to lower the exclusion limit on  $\Lambda$  by around 10%. Our analysis neglects NLO corrections in the interference of the axigluon contributions with QCD and with themselves.

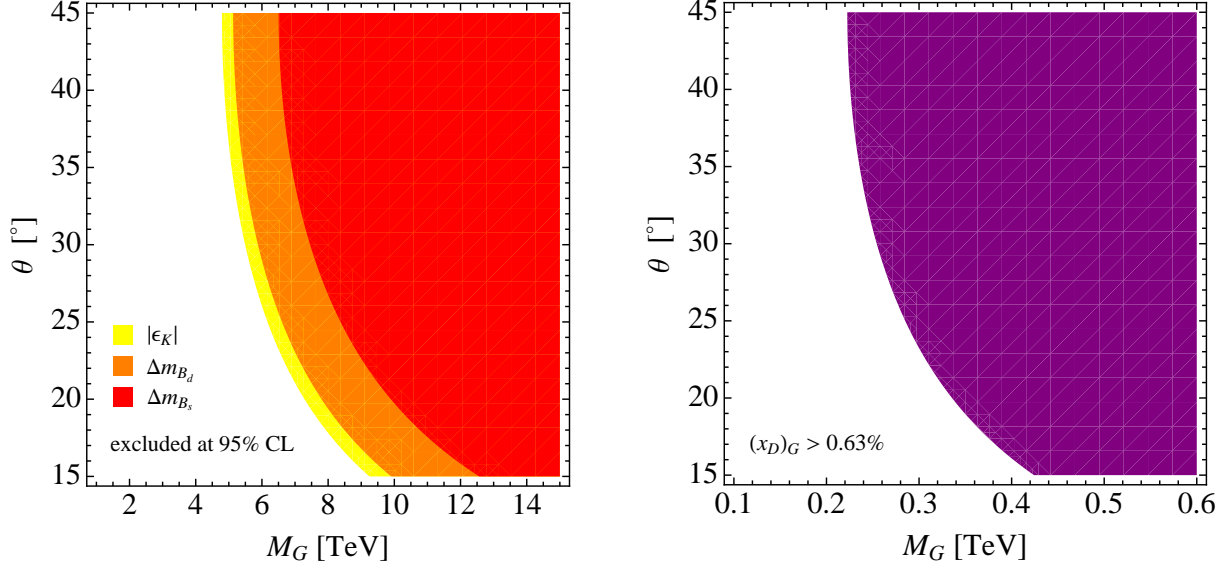


Figure 9: Constraints in the  $M_G$ - $\theta$  plane imposed by the measured amount of flavor violation in the  $\Delta F = 2$  sector. The left (right) panel corresponds to the scenario of up-type (down-type) flavor alignment in the non-universal axigluon model. The regions of parameter space colored white are disfavored by the existing experimental data.

limit reads

$$M_G > \frac{|g_L^h - g_L^\ell|}{2} 6.4 \text{ TeV} = \frac{6.4 \text{ TeV}}{\sin(2\theta)} > 6.4 \text{ TeV}, \quad (57)$$

where in the last step we have inserted the analytic expressions for the left-handed couplings as given in (4). The 95% CL upper limits arising from  $|\epsilon_K|$  and  $\Delta m_{B_d}$  are weaker than the bound quoted in (57) and simply obtained by replacing 6.4 TeV with 4.8 TeV and 5.0 TeV, respectively.<sup>14</sup> Notice that in the presence of new CP phases and/or additional effective operators, the bounds on  $M_G$  following from  $\Delta F = 2$  processes in the down-type quark sector are typically even stronger than the numbers given above. This implies that a flavor non-universal axigluon possessing generic couplings to quarks is experimentally ruled out, unless its mass lies in the multi-TeV range.

Yet, if the underlying theory that determines the pattern of flavor breaking is left unspecified, it is possible to confine FCNC effects to the up-type quark sector by aligning the axigluon couplings to down-type quarks. The purple region in the right panel of Figure 9 shows that in this case the bounds imposed by flavor physics are very weak. Requiring that the axigluon contributions to the  $D$ -meson mixing parameter  $x_D$  do not exceed the measured value, *i.e.*,  $(x_D)_G < 0.63\%$ , we derive the following constraint

$$M_G > \frac{|g_L^h - g_L^\ell|}{2} 0.22 \text{ TeV} = \frac{0.22 \text{ TeV}}{\sin(2\theta)} > 0.22 \text{ TeV}. \quad (58)$$

<sup>14</sup>If the total errors in (23) were enlarged by a factor of 2, the new-physics scales entering the numerator (57) would read 2.8 TeV in the case of  $|\epsilon_K|$  and  $\Delta m_{B_d}$  and 4.0 TeV in the case of  $\Delta m_{B_s}$ .

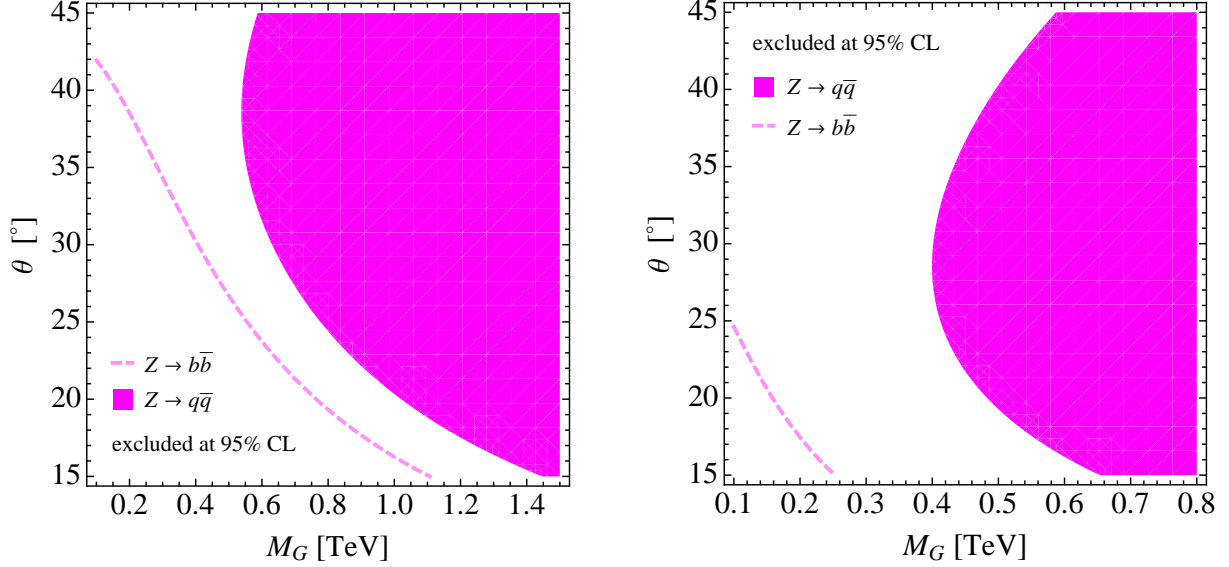


Figure 10: Constraints in the  $M_G$ - $\theta$  plane arising from the precision measurements in the  $Z \rightarrow q\bar{q}$  sector. The left (right) panel corresponds to the flavor non-universal (universal) axigluon model. The magenta colored regions of parameter space are preferred by the global  $\chi^2$  fit to  $R_b$ ,  $A_b$ ,  $A_{\text{FB}}^b$ ,  $\Gamma_Z$ , and  $\sigma_{\text{had}}$ . Parameter sets below the dashed magenta curve are disfavored by the bottom-quark POs alone.

We emphasize that since the latter bound has been obtained by minimizing the constraints from flavor violation in the  $\Delta F = 2$  sector, it is a firm (though quite loose) exclusion limit that has to be satisfied by any flavor non-universal model with extra massive bosons in the adjoint representation of  $SU(3)_c$ . Obviously, flavor universal scenarios are not subject to any flavor constraint by construction.

We now turn our attention to the constraints from the bottom-quark POs (31). The restrictions imposed by a combination of the corresponding measurements (33) are indicated by the dashed magenta curve in the left and right panels of Figure 10 for the case of the flavor non-universal and universal axigluon, respectively. The  $M_G$ - $\theta$  regions below the lines are disfavored at 95% CL. By comparing the two plots, one first observes that the  $Z \rightarrow b\bar{b}$  bound is significantly weaker for a flavor universal axigluon than for a flavor non-universal axigluon. This feature arises since, due to the smallness of the ratios  $(\mathcal{G}_R^u/\mathcal{G}_L^u)^2 \approx 1/5$  and  $(\mathcal{G}_R^d/\mathcal{G}_L^d)^2 \approx 1/30$  of  $Z$ -boson couplings, the dominant observable  $R_b$  measures approximately the difference  $(g_L^h)^2 - (g_L^\ell)^2$ . This combination of axigluon couplings is equal to zero in the flavor universal case, which implies that for fixed  $\theta$  the constraints on  $M_G$  are less severe for a flavor universal than for a non-universal axigluon. A second feature that is clearly visible in the plots is that  $Z \rightarrow b\bar{b}$  does not provide a sound constraint in the limit  $\theta \rightarrow 45^\circ$ . This behavior is readily understood by recalling that the axigluon effects in  $R_b$  vanish in this limit in both variants of the model. Notice further that the less constraining asymmetries  $A_b$  and  $A_{\text{FB}}^b$  are to a good approximation proportional to  $(g_L^h)^2 - (g_R^h)^2$ . This combination also tends

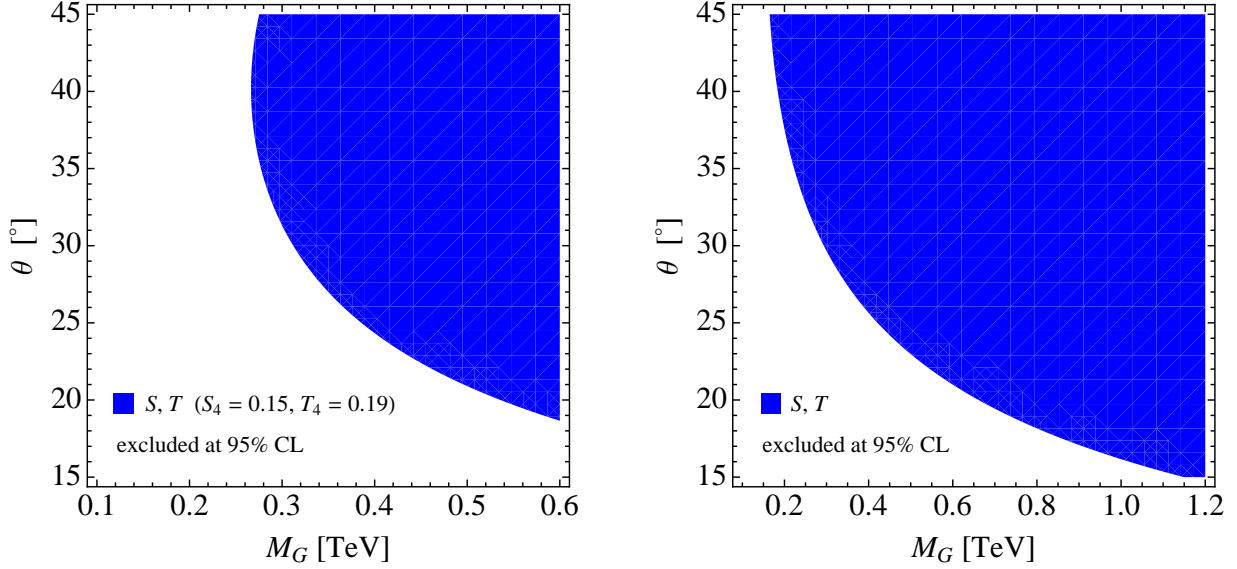


Figure 11: Constraints in the  $M_G$ – $\theta$  plane due to a combined fit to the oblique parameters  $S$  and  $T$ . The left panel shows the results for the case of a flavor non-universal axigluon assuming  $S_4 = 0.15$  and  $T_4 = 0.19$ , while the right plot represents the case of a flavor universal axigluon. The parameter space preferred by the fit is colored blue.

to zero for  $\theta \rightarrow 45^\circ$ , which further impairs the restrictive power of the bottom-quark POs.

While the restrictions imposed by  $R_b$ ,  $A_b$ , and  $A_{\text{FB}}^b$  can thus be avoided, combining them with  $\Gamma_Z$  and  $\sigma_{\text{had}}$ , as defined in (34), turns out to lead to non-trivial constraints on the axigluon mass for any value of the mixing angle. From a combination of the whole set of  $Z \rightarrow q\bar{q}$  observables, we derive in the case of the flavor non-universal axigluon model the following 95% CL limit

$$M_G > \left( 0.67 \sqrt{\tan^2 \theta + 0.40 \cot^2 \theta - 0.35} - 0.10 \right) \text{ TeV} > 0.54 \text{ TeV} . \quad (59)$$

In the case of the flavor universal axigluon, we obtain instead

$$M_G > \left( 0.71 \sqrt{\tan^2 \theta + 0.09 \cot^2 \theta + 0.07} - 0.18 \right) \text{ TeV} > 0.40 \text{ TeV} . \quad (60)$$

For  $\theta = 45^\circ$  the inequalities (59) and (60) imply  $M_G > 0.58 \text{ TeV}$  and  $M_G > 0.59 \text{ TeV}$ , respectively. The parameter regions allowed by  $Z \rightarrow q\bar{q}$  at 95% CL are shown as magenta areas in the left and right panels of Figure 10. The panels show clearly that new color-octet bosons with masses below the electroweak scale and QCD-like axigluon couplings to all quark species are not compatible with the LEP and SLC measurements of the  $Zq\bar{q}$  couplings. Of course, the  $Z \rightarrow q\bar{q}$  constraints can be weakened by assuming that the presence of the axigluon only affects the couplings of a single light quark.

We now discuss the constraints on the  $M_G$ – $\theta$  plane that emerge from the oblique parameters  $S$  and  $T$ . We again distinguish between a flavor non-universal and a universal axigluon.

From Section 4 we know already that in the former case a model-independent bound on  $M_G$  and  $\theta$  cannot be derived, since the fourth-generation contributions  $S_4$  and  $T_4$  can always be chosen in such a way as to compensate for the corrections associated with the axigluon. Studying the constraints for a specific set of fourth-generation contributions to  $S$  and  $T$  is nevertheless a useful exercise to get a feeling of how stringent the bounds on the  $M_G$ – $\theta$  plane can be. Taking  $S_4 = 0.15$  and  $T_4 = 0.19$  as motivated in Section 4, we obtain the following 95% CL bound

$$M_G > \left( 1.68 \sqrt{\tan^2 \theta + 0.50 \cot^2 \theta + 56.3} - 12.5 \right) \text{ TeV} > 0.27 \text{ TeV} . \quad (61)$$

This lower limit is displayed in the left plot in Figure 11. Since the axigluon contribution to  $T$  is strictly positive and larger by an order of magnitude than the one to  $S$ , a stronger (weaker) bound is obtained if a value  $T_4 > 0.19$  ( $T_4 < 0.19$ ) inside the 68% probability region of the  $S$ – $T$  ellipse is chosen. We conclude from this exercise that in the context of the flavor non-universal axigluon the oblique parameters are typically able to probe values of  $M_G$  at and beyond the electroweak scale.

One can be more specific in the case of a flavor universal axigluon, since the model is anomaly-free without the introduction of extra matter. This feature allows one to derive a model-independent bound on  $M_G$  as a function of  $\theta$  from  $S$  and  $T$ . At 95% CL we find

$$M_G > \left( 0.88 \sqrt{\tan^2 \theta + 1.23 \cot^2 \theta + 34.0} - 5.13 \right) \text{ TeV} > 0.16 \text{ TeV} . \quad (62)$$

This limit is shown in the right panel of Figure 11. For  $\theta = 45^\circ$  the latter inequality yields  $M_G > 0.17 \text{ TeV}$ . We see again that the oblique parameters, despite the fact that they are first affected at the two-loop level by the presence of the axigluon, rule out the possibility of masses  $M_G$  significantly below the electroweak scale. Notice however that the limits from  $T$  can become quite pesky, if the top quark couples very strongly to the massive color-octet vector. In view of the enhancement of  $(g_R^h)^2$  relative to  $(g_L^h)^2$  by a factor of 2 in the expression (39), this statement applies in particular to models where the right-handed top quark is (fully) composite. In such a case the parameter  $T$  receives unacceptably large positive corrections even for axigluon masses in the TeV range.

After this detailed discussion of the indirect probes of the axigluon parameter space through high-intensity experiments, we now move to the direct bounds stemming from the energy frontier. We start with the constraints imposed by the narrow resonance searches in dijet production. In Figure 12 we display the 95% CL upper bounds in the  $M_G$ – $\theta$  plane for the flavor non-universal (left) and universal (right) axigluon model. The area to the left of the dashed black curve is disfavored by the latest ATLAS measurement of the product  $\sigma \mathcal{B} A$  involving the resonant production cross section, the branching fraction, and the acceptance. As explained in Section 5, resonance search analyses are only applicable if the total decay width  $\Gamma_G$  is sufficiently small, so that the axigluon forms a distinct resonance. The excluded regions are obtained for fixed ratios  $\Gamma_G/M_G < 10\%$  (purple),  $\Gamma_G/M_G < 15\%$  (red), and  $\Gamma_G/M_G < 20\%$  (orange), corresponding to mixing angles of  $\theta \gtrsim 40^\circ$ ,  $30^\circ$ , and  $25^\circ$ , respectively. The blank area features  $\Gamma_G/M_G > 20\%$ . Comparing the two panels, one observes that the bound on  $M_G$  is weaker if the axigluon has flavor non-universal couplings. This is due to the presence



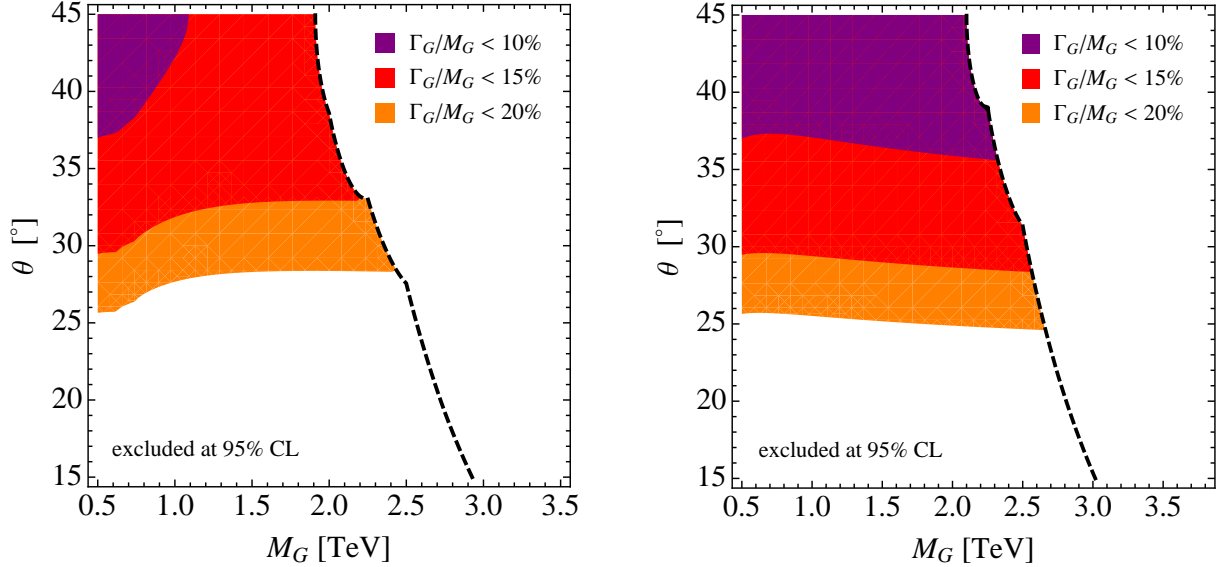


Figure 12: Constraints from the latest ATLAS narrow resonance search in dijet production on the flavor non-universal (left) and universal (right) axigluon model. The 95% CL contour is represented by the dashed black line. Excluded regions of parameter space are displayed in color for fixed relative axigluon decay widths  $\Gamma_G/M_G < 10\%$  (purple),  $\Gamma_G/M_G < 15\%$  (red), and  $\Gamma_G/M_G < 20\%$  (orange).

of the extra fermion generation, which lowers the axigluon branching ratio into light quarks, and hence allows for a bigger production cross section for fixed values of  $\sigma\mathcal{B}A$ . Yet, a larger resonant production cross section goes along with a lower axigluon mass. Notice that the presence of the additional decay channels into  $u_4\bar{u}_4$  and  $d_4\bar{d}_4$  manifests itself even more clearly if one considers the contours in the  $M_G$ - $\theta$  plane corresponding to constant values of  $\Gamma_G/M_G$ . We see that the resonance search is applicable to a wider range of parameter space in the flavor universal model. In the limit  $\theta \rightarrow 45^\circ$ , we find for a flavor non-universal axigluon the following 95% CL bound<sup>15</sup>

$$M_G > 1.9 \text{ TeV} , \quad (63)$$

while in the flavor universal case we obtain the somewhat stronger constraint

$$M_G > 2.1 \text{ TeV} . \quad (64)$$

The values of  $\Gamma_G/M_G$  corresponding to these limits amount to almost 11% and a little bit more than 8%, respectively. Although the publication [26] does not state explicitly for which values of  $\Gamma_G/M_G$  their axigluon analysis is applicable, we conclude from the model-independent ATLAS limits on Gaussian resonances, which cover relative widths up to 15%, that the derived

<sup>15</sup>Since the narrow resonance search of ATLAS includes only dijet events with  $M_{jj} > 0.6 \text{ TeV}$ , the mass window below 0.6 TeV is strictly speaking also allowed by this measurement. Older dijet searches [79, 80] extend the disfavored region down to around 0.15 TeV.

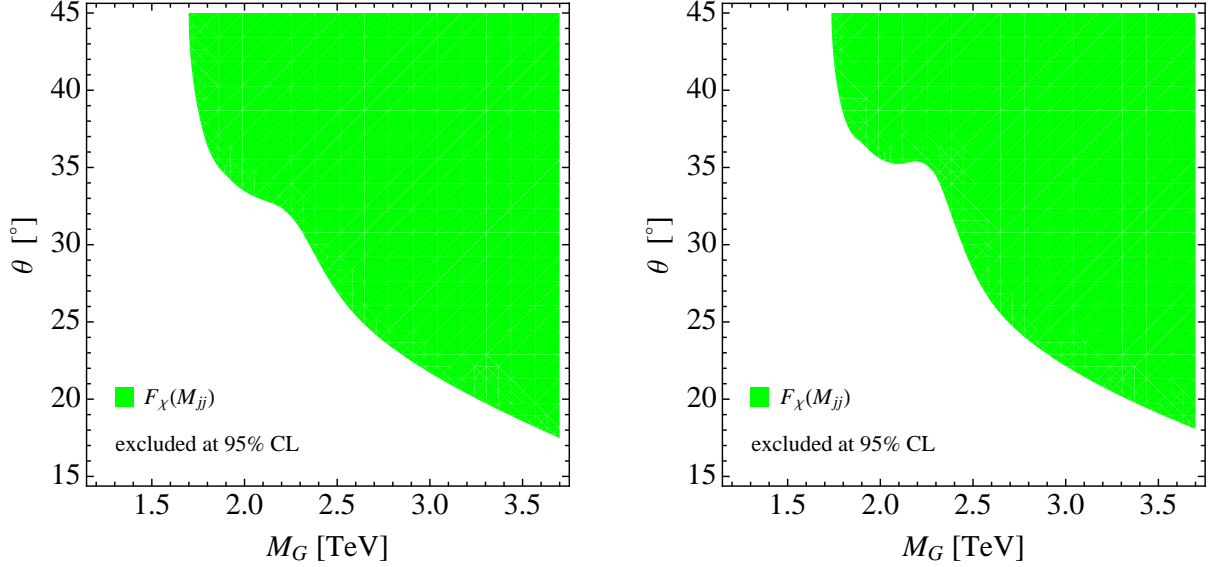


Figure 13: Constraints on  $M_G$ – $\theta$  arising from the angular distribution in dijet production in the non-universal (left) and universal (right) axigluon model. The green areas show the parameter region in accordance with the ATLAS data at 95% CL.

dijet resonance bounds (63) and (64) are robust. We also remark that the dependence of (63) on the masses of the fourth-generation quarks is rather mild. If instead of  $m_{u_4} = 311$  GeV and  $m_{d_4} = 372$  GeV one would use  $m_{u_4} = m_{d_4} = 600$  GeV, the former bound would strengthen slightly and read  $M_G > 2.0$  TeV.

The angular distribution in dijet production allows one to derive constraints on the axigluon parameter space without restricting to the narrow-width approximation. As described at the end of Section 5, we perform a fit of the axigluon prediction for the centrality ratio  $F_\chi(M_{jj})$  in (53) by constructing a likelihood following the procedure outlined in [26]. Our analysis uses the ATLAS data for  $F_\chi(M_{jj})$  in 17 different bins, covering dijet masses of  $M_{jj} \in [1.2, 3.7]$  TeV. Due to the low statistics at high  $M_{jj}$  the fit is however essentially driven by the bins below 2.5 TeV. The resulting constraints on the axigluon parameters in the  $M_G$ – $\theta$  plane are shown in Figure 13 for the non-universal (left) and universal (right) axigluon model. The white areas are excluded at 95% CL. Notice the distortion of the exclusion contour at  $M_G \approx 2.2$  TeV. The constraints are strengthened in this region due to the strong decline of the measured  $F_\chi(M_{jj})$  spectrum starting at this value of  $M_{jj}$ , as displayed in Figure 8. In the limit  $\theta \rightarrow 45^\circ$ , the 95% CL bound reads<sup>16</sup>

$$M_G > 1.7 \text{ TeV} , \quad (65)$$

for both the flavor non-universal and universal axigluon model. Since the matrix elements for axigluon production are symmetric under the exchange of left- and right-handed couplings, the difference between the contours is due to the presence of the fourth generation in the

<sup>16</sup>The quoted number is based on the expected ATLAS limit of  $\Lambda > 5.7$  TeV. If instead the observed limit  $\Lambda > 9.5$  TeV is used, one finds  $M_G > 2.4$  TeV.

non-universal case only. The additional contributions to the width broaden the resonance in the spectrum  $F_\chi(M_{jj})$ , yielding a slightly weaker constraint. The dependence of (65) on the masses of the extra quarks themselves is however negligible.

We emphasize that the recent measurement of the dijet angular distribution also puts constraints on axigluons with masses below 0.5 TeV, where no ATLAS data is available, since light axigluons enhance the tail of the  $F_\chi(M_{jj})$  distribution with respect to the QCD expectation. This feature is clearly visible in the left panel of Figure 14, which shows the axigluon predictions for  $M_G = 0.3$  TeV (red curve),  $M_G = 0.6$  TeV (green curve), and  $M_G = 1.2$  TeV (blue curve). All lines have been obtained assuming QCD-like couplings and  $\Gamma_G/M_G = 10\%$ . Performing a likelihood fit to the set of the first 22 invariant mass bins,<sup>17</sup> we find that the parameter space with  $M_G > 0.17$  TeV is disfavored at 95% CL in the case of both the flavor non-universal and universal axigluon. Axigluon masses down to 0.25 TeV are also excluded directly by an earlier analysis of angular distributions at the Tevatron [68]. These results indicate that color-octet resonances with QCD-like couplings to light and heavy quarks and masses at and below the electroweak scale are in general in conflict with existing constraints arising from angular distributions in dijet production.

Let us also spend some words on how the bounds on the new-physics scale  $M_G$  change if dijet production can only proceed via  $u\bar{u} \rightarrow G$  scattering. First recall that it is more likely to find an up quark than any other light quark in the proton. In fact, the up-quark luminosity  $\mathcal{L}_{u\bar{u}}(M_G^2/s, \mu_f)$ , which is a measure of this probability, amounts to 60% to 92% of the total quark luminosity  $\sum_q \mathcal{L}_{q\bar{q}}(M_G^2/s, \mu_f)$  for axigluon masses  $M_G \in [0.5, 4.0]$  TeV and  $pp$  collisions at  $\sqrt{s} = 7$  TeV. These numbers imply that the sensitivity to  $M_G$  is largely unchanged if the axigluon has  $\mathcal{O}(1)$  couplings to up quarks only. On the right-hand side of Figure 14, we show the bound on  $M_G$  as a function of  $\Gamma_G/M_G$  that arises from the model-independent limits on resonances with Gaussian shape presented by ATLAS [26]. The area allowed at 95% CL is colored red. One observes that the limit on  $M_G$  depends only very weakly on the relative width of the resonance and amounts to around 1.9 TeV to 2.0 TeV over the whole range of  $\Gamma_G/M_G$ . The shown exclusion region has been obtained assuming  $g_L^u = g_R^u = 1$ , but translating it to other couplings just requires to perform a simple rescaling by  $((g_L^u)^2 + (g_R^u)^2)/2$ . To give an example, a color-octet resonance interacting only with right-handed up quarks, a coupling strength of  $g_R^u = 2$ , and  $\Gamma_G/M_G < 15\%$  is disfavored at 95% CL if its mass is below 4.0 TeV. The situation is different in the case of the dijet angular distribution. For an axigluon that couples only to up quarks, the effect on the centrality ratio  $F_\chi(M_{jj})$  is significantly reduced. In particular, the enhancement of the tail at high  $M_{jj}$  is very mild, such that an axigluon with  $M_G < 0.5$  TeV cannot be excluded by the LHC measurements. Axigluons with a mass in the accessibility range of the ATLAS detector are visible as a sharp resonance in the  $F_\chi(M_{jj})$  spectrum only if their relative width does not exceed a few percent. Broader axigluon resonances escape the constraints set by the angular distribution.

We finally explore the constraints on axigluons from top-antitop quark production. In Figure 15 we compare the inclusive cross section  $\sigma_s$  and its high- $M_{t\bar{t}}$  bin,  $(d\sigma_s/dM_{t\bar{t}})^> = (d\sigma_s/dM_{t\bar{t}})^{M_{t\bar{t}} \in [0.8, 1.4] \text{ TeV}}$ , with the forward-backward asymmetry in two bins separated at

---

<sup>17</sup>We do not include the last 5 bins of the recent ATLAS measurement in the fit, because their central values are all zero and they have large statistical errors.

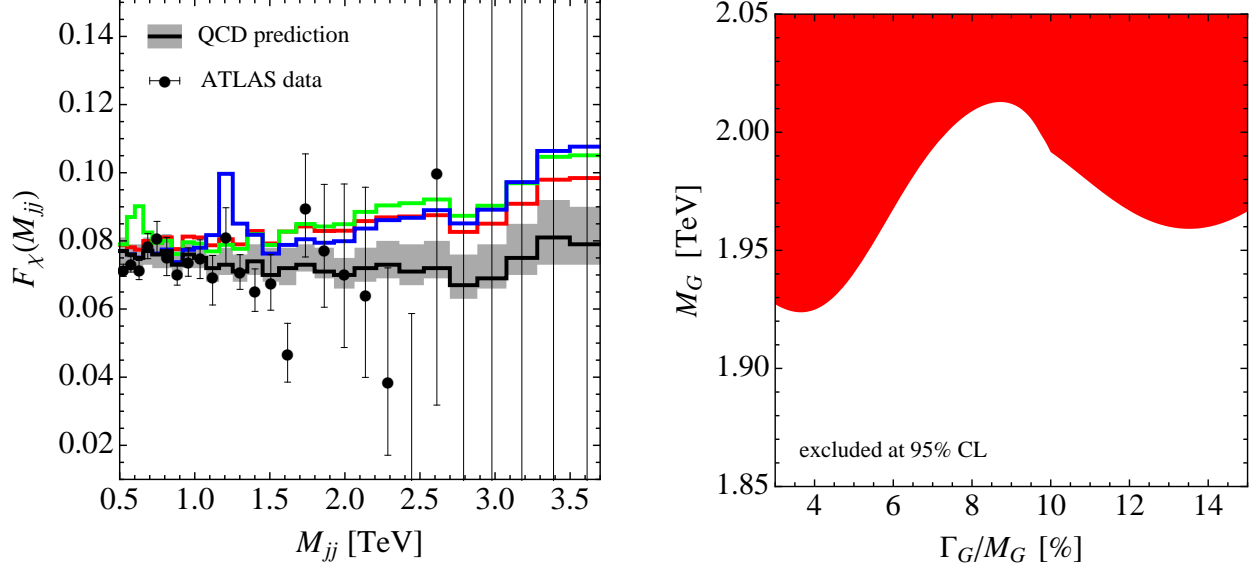


Figure 14: Left: Ratio  $F_\chi(M_{jj})$  as a function of  $M_{jj}$  for three different axigluons with  $M_G = 0.3$  TeV (red line),  $M_G = 0.6$  TeV (green line), and  $M_G = 1.2$  TeV (blue line). The shown predictions correspond to QCD-like couplings and  $\Gamma_G/M_G = 10\%$ . For comparison the QCD prediction with errors (black line and gray band) and the ATLAS measurement (black error bars) are also shown. Right: Constraints from the latest ATLAS narrow resonance search in dijet production on a color-octet boson with relative width  $\Gamma_G/M_G$  that only couples to up quarks. The blank region is excluded at 95% CL for  $g_L^u = g_R^u = 1$ . See text for details.

$M_{t\bar{t}} = 0.45$  TeV (see Table 2 for the SM predictions and experimental values of the relevant  $t\bar{t}$  observables). As anticipated in Section 5, the large measured values of the asymmetry are in tension with the remaining observables, which are well described by QCD. This tension is most pronounced in the region of high  $M_{t\bar{t}}$ , which is most sensitive to contributions from new physics. From the upper and lower right panels it becomes apparent that the asymmetry  $(A_{\text{FB}}^t(M_{t\bar{t}}))^>$  favors an axigluon with a mass around 1 TeV, while the symmetric cross section  $(d\sigma_s/dM_{t\bar{t}})^>$  is in agreement with the measurement within errors for  $M_G \gtrsim 1.5$  TeV. Notice that the observable  $(A_{\text{FB}}^t(M_{t\bar{t}}))^>$  prefers large mixing angles  $\theta$ , corresponding to axigluon couplings that are mostly axial-vector-like. This maximizes the contribution that arises from the axigluon interference with the SM amplitude, proportional to  $-g_A^q g_A^t$ . Axial-vector-like couplings are also preferred by  $(d\sigma_s/dM_{t\bar{t}})^>$ , as in this case the axigluon-gluon interference is suppressed and, in addition, the different terms that stem from the interference of the new-physics contribution with itself tend to cancel. These features can be read off from the model-independent formulas presented in Appendix C. The asymmetry at low  $M_{t\bar{t}}$ , as shown in the lower left panel, disfavors constructive axigluon contributions, but is subject to large statistical errors, rendering its restrictive power marginal at present. Finally, since the QCD prediction is below the measurement, the total cross section displayed on the upper left leaves

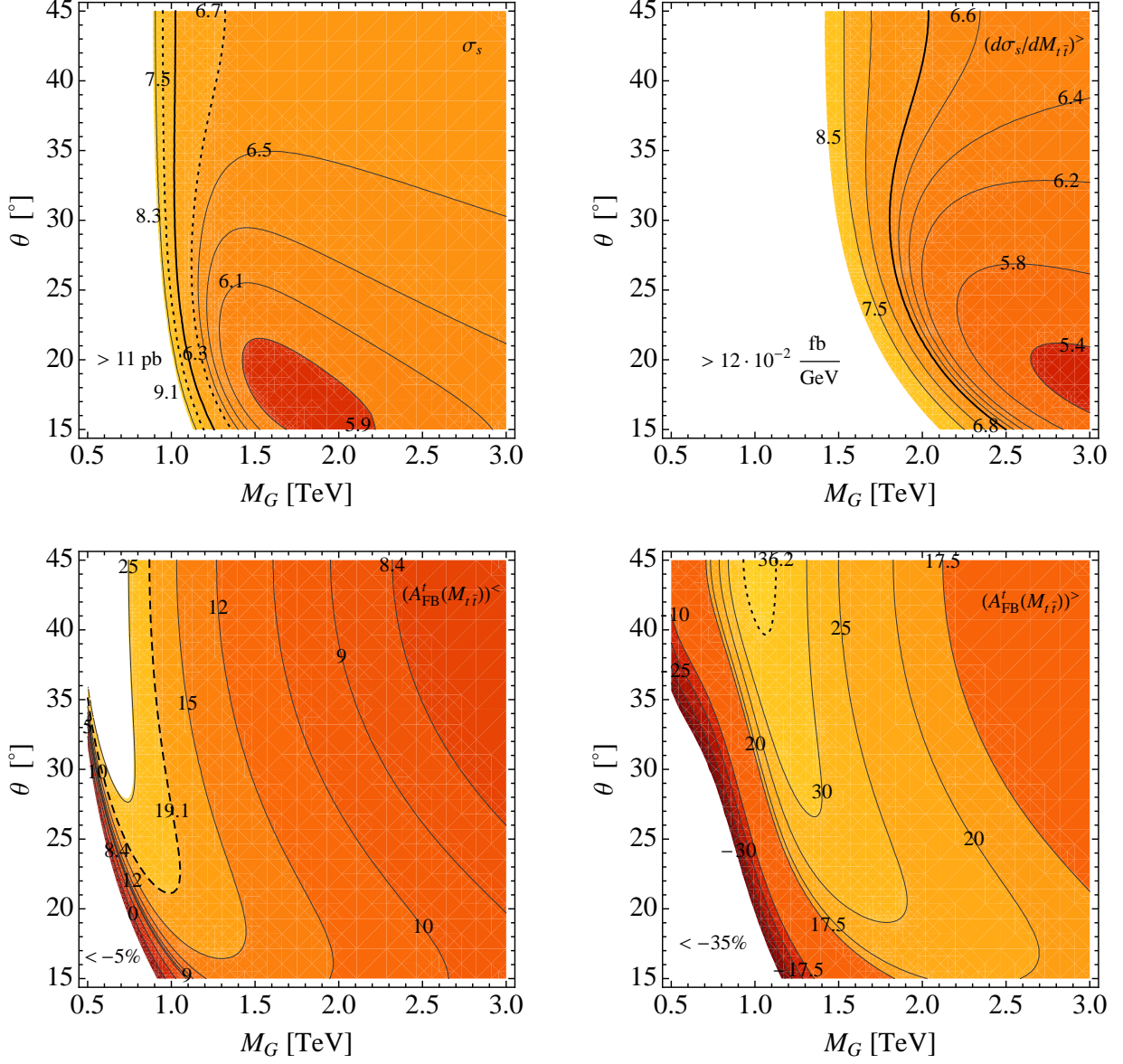


Figure 15: Predictions for the observables in  $t\bar{t}$  production obtained in the non-universal axigluon model. From the upper left to the lower right  $\sigma_s$ ,  $(d\sigma_s/dM_{t\bar{t}})^>$ ,  $(A_{\text{FB}}^t(M_{t\bar{t}}))^<$ , and  $(A_{\text{FB}}^t(M_{t\bar{t}}))^>$  are shown. The central values of the measurements are displayed as solid black contours, while the  $1\sigma$  ( $2\sigma$ ) total error ranges are indicated by the dotted (dashed) lines. See text for further details.

space for moderate positive axigluon contributions. Such moderate enhancements are in fact predicted in the flavor non-universal model for values of  $\theta$  close to maximal and  $M_G \gtrsim 1$  TeV.

The constraints that derive from  $t\bar{t}$  production are presented in Figures 16 and 17. Let us first focus on the charge-symmetric observables, namely  $\sigma_s$  and  $(d\sigma_s/dM_{t\bar{t}})^>$ . The corre-

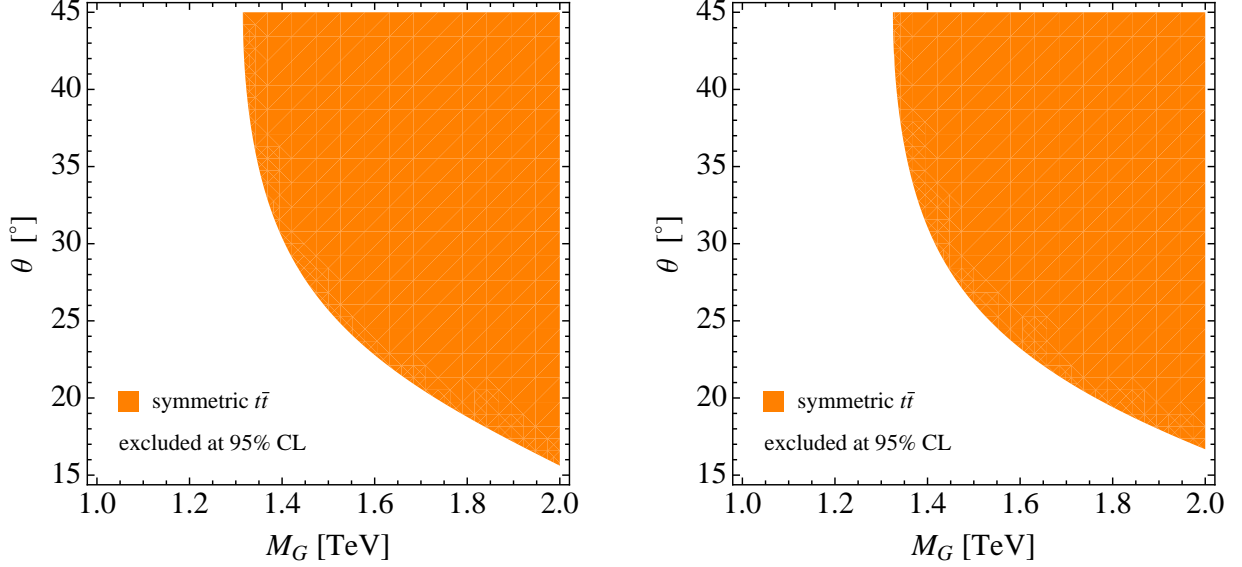


Figure 16: Constraints in the  $M_G$ – $\theta$  plane imposed by the charge-symmetric observables in  $t\bar{t}$  production in the flavor non-universal (left) and universal (right) axigluon model. The regions below the orange area are excluded at 95% CL.

sponding  $M_G$ – $\theta$  planes are displayed in the left and right panels of Figure 16 for the case of a flavor non-universal and universal axigluon, respectively. The regions below the orange areas are excluded at 95% CL. For a given mixing angle  $\theta$ , we derive the following mass bound on a non-universal axigluon,

$$M_G > (0.45 + 0.47 \tan \theta + 0.40 \cot \theta) \text{ TeV} > 1.3 \text{ TeV} , \quad (66)$$

while in the flavor universal case we obtain

$$M_G > (0.27 + 0.61 \tan \theta + 0.46 \cot \theta) \text{ TeV} > 1.3 \text{ TeV} , \quad (67)$$

at 95% CL. Notice that the axigluon contributions to the symmetric  $t\bar{t}$  cross section in both models differ only marginally as a result of the changed axigluon width. Due to the low sensitivity on the width, the bound in (66) is robust and to first approximation independent from the masses of the extra quarks  $u_4$  and  $d_4$ . We also emphasize that our fit to  $\sigma_s$  and  $(d\sigma_s/dM_{t\bar{t}})^>$  excludes masses down to 0.2 TeV, irrespectively of whether a flavor non-universal or universal axigluon is considered.

In order to gauge how the presence of an axigluon affects the overall consistency of the data in the  $t\bar{t}$  sector, we perform a  $\chi^2$  fit to the four observables  $\sigma_s$ ,  $(d\sigma_s/dM_{t\bar{t}})^>$ ,  $(A_{\text{FB}}^t(M_{t\bar{t}}))^<$ , and  $(A_{\text{FB}}^t(M_{t\bar{t}}))^>$ . We treat the individual measurements as fully uncorrelated. The left (right) panel in Figure 17 shows the constraint in the  $M_G$ – $\theta$  plane for the non-universal (universal) axigluon model. The white area of the parameter space is excluded at 99% CL (99.5% CL). The orange (yellow) area in the left panel shows clearly that agreement with the

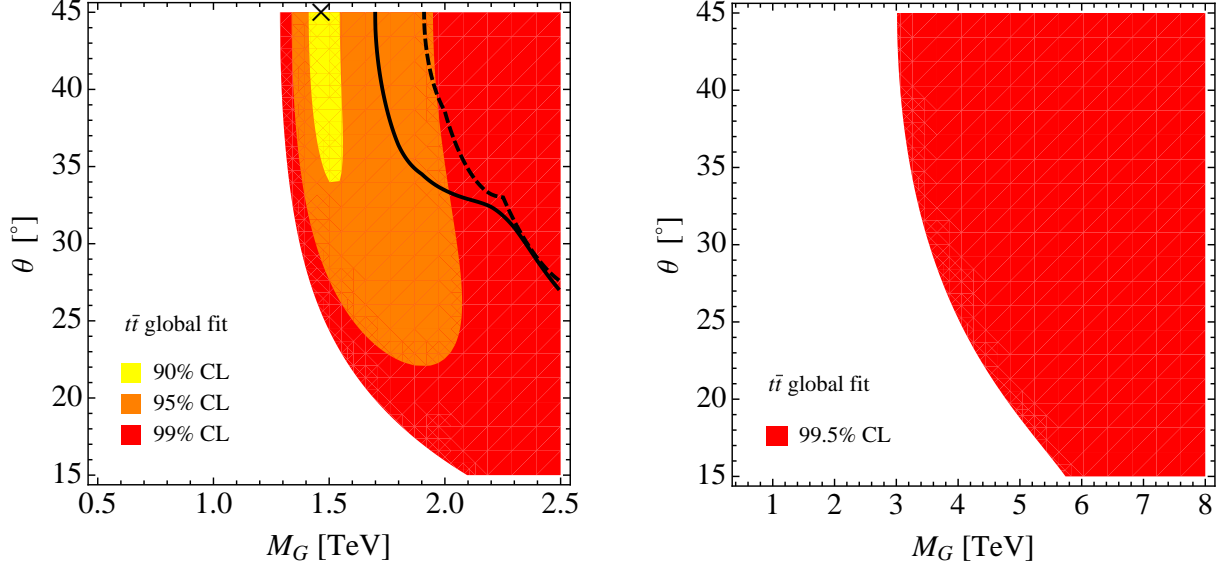


Figure 17: Confidence regions in the  $M_G$ – $\theta$  plane resulting from a fit to the  $t\bar{t}$  observables in the flavor non-universal (left) and universal (right) case. For comparison the constraints from the dijet resonance search (angular distribution) is also shown in the left panel as a dashed (solid) black line. The areas to the left of the curves are disfavored at 95% CL.

data at 95% CL (90% CL) is only achieved for a flavor non-universal axigluon with a mass in the range of  $1.3 \text{ TeV} \lesssim M_G \lesssim 2.1 \text{ TeV}$  ( $1.4 \text{ TeV} \lesssim M_G \lesssim 1.5 \text{ TeV}$ ). In the global fit, the lower bound on the axigluon mass is essentially determined by the two charge-symmetric  $t\bar{t}$  observables, while the upper limit arises from the requirement to accommodate large values of  $(A_{\text{FB}}^t(M_{t\bar{t}}))^>$ . In fact, due to the tension between the asymmetry in the high- $M_{t\bar{t}}$  bin with the remaining observables, it is not possible to obtain a fit to the data with a CL of 68%. The best fit to the  $t\bar{t}$  data, as indicated by the black cross, is achieved for the axigluon parameters  $M_G = 1.5 \text{ TeV}$  and  $\theta = 45^\circ$ . It has  $\chi_G^2/\text{ndf} = 7.6/4$ . Compared to the goodness of the fit in the SM,  $\chi_{\text{SM}}^2/\text{ndf} = 13.1/4$ , the presence of a non-universal axigluon thus provides a significant improvement from 99% CL to 90% CL. The central values of the total cross section, the cross section in the highest  $M_{t\bar{t}}$  bin, the total asymmetry in the parton frame, and the asymmetry at large  $M_{t\bar{t}}$  corresponding to the best-fit point are shown on the left-hand side in Figure 18. We see that large positive values of the  $t\bar{t}$  asymmetries are indeed possible in the flavor non-universal axigluon model without impairing the overall consistency with the symmetric observables. Relative to the SM, the shifts in  $\sigma_s$ ,  $(d\sigma_s/dM_{t\bar{t}})^>$ ,  $A_{\text{FB}}^t$ , and  $(A_{\text{FB}}^t(M_{t\bar{t}}))^>$  amount to around 1%, 46%, 94%, and 133%. For the best-fit point the central value of the asymmetry in the low  $M_{t\bar{t}}$  bin reads  $(A_{\text{FB}}^t(M_{t\bar{t}}))^< = 10.7\%$ . It is not included in the figure.

The region of parameter space that is preferred by the  $t\bar{t}$  data in the case of a flavor non-universal axigluon is consistent with the indirect constraints from flavor physics and EWPOs



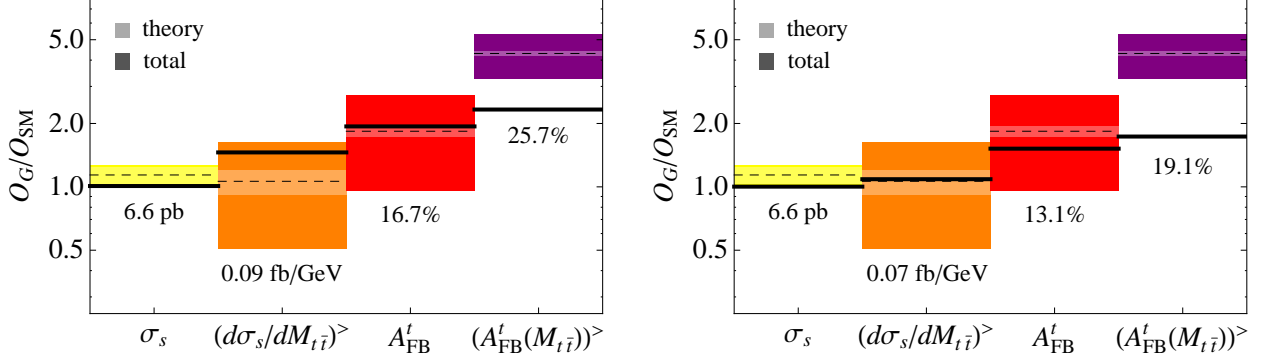


Figure 18: Predictions for the  $t\bar{t}$  observables in the flavor non-universal axigluon model (thick black lines and numbers) corresponding to the best fit before (left) and after (right) including dijet constraints. For comparison the central values of the associated measurements (dashed black lines) are also shown. All predictions have been normalized to the SM expectations. The light colored bars illustrate the theoretical uncertainties, while the combined experimental and theoretical errors as displayed in bright colors. See text for further details.

that have been discussed above. Large parts of it are however disfavored by the recent results on dijet production at the LHC. This feature is illustrated by the dashed and solid black lines in the left panel of Figure 17 corresponding to the 95% CL limits from the resonance search and the angular distribution measurement in dijet production at ATLAS. These constraints exclude the best-fit solution and allow only for a reduced compatibility with the  $t\bar{t}$  data at 95% CL. Notice that, by taking into account the constraints from dijet production, the axigluon mass is confined to the narrow range of  $1.9 \text{ TeV} \lesssim M_G \lesssim 2.0 \text{ TeV}$ . The maximal axigluon effects in the asymmetries are thus obtained for  $M_G = 1.9 \text{ TeV}$  and  $\theta = 45^\circ$ . The predictions for the relevant  $t\bar{t}$  observables corresponding to this set of parameters are presented on the right in Figure 18. The quoted values correspond to  $\chi_G^2/\text{ndf} = 9.3/4$ , still yielding a considerably better fit than within the SM. With respect to the SM prediction the symmetric observables  $\sigma_s$  and  $(d\sigma_s/dM_{t\bar{t}})^>$  change by 0.2% and 9%. Both the total charge asymmetry as well as the prediction for the high- $M_{t\bar{t}}$  bin exhibit a large enhancement of 52% and 73% relative to the SM. It is important to realize that, compared to the best-fit values, the asymmetries are not only smaller, but also the value of the cross section in the highest  $M_{t\bar{t}}$  has come down. This shows the strong positive correlation between these observables. The forward-backward asymmetry at low  $M_{t\bar{t}}$  amounts to 9.1% for the latter set of parameters. We conclude from these numbers, that an axigluon with QCD-like couplings to all quarks, able to explain the top forward-backward asymmetry and to simultaneously evade the bounds from dijet production, should have a mass of 2 TeV and hence is expected to be soon discovered at the LHC.

In the left panel of Figure 19, we show the prediction for the  $M_{t\bar{t}}$  spectrum of the asymmetry at the Tevatron corresponding to the best-fit solution before (red curve) and after (blue curve) imposing the latest dijet constraints. The QCD prediction with its theoretical uncertainty,



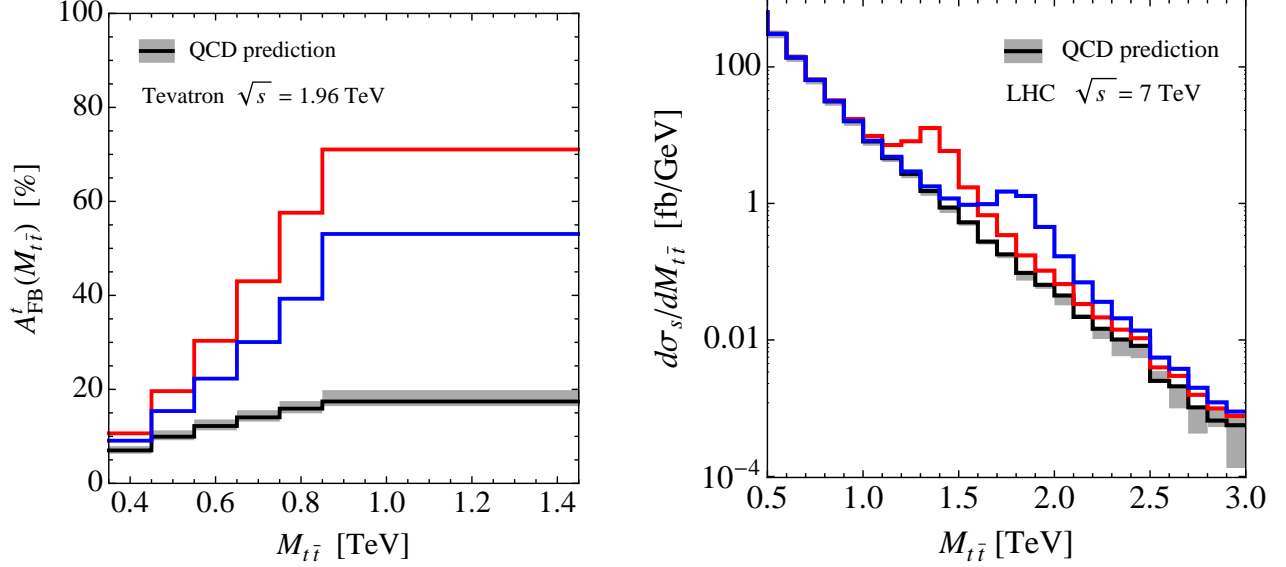


Figure 19: Left: Prediction for the  $t\bar{t}$  forward-backward asymmetry at the Tevatron as a function of  $M_{t\bar{t}}$ . The red (blue) curve represents the result for a flavor non-universal axigluon with  $\theta = 45^\circ$  and  $M_G = 1.5$  TeV ( $M_G = 1.9$  TeV). The central value and uncertainty of the QCD expectation are indicated by the black line and the gray band, respectively. Right: Prediction for the  $t\bar{t}$  cross section differential in  $M_{t\bar{t}}$  for  $pp$  collisions at  $\sqrt{s} = 7$  TeV. The red (blue) line corresponds to a flavor non-universal axigluon with  $\theta = 45^\circ$  and  $M_G = 1.5$  TeV ( $M_G = 1.9$  TeV). For comparison the SM expectation with its uncertainty is also shown (black line and gray band).

obtained by varying the renormalization and factorization scales in the range  $\mu_r = \mu_f \in [m_t/2, 2m_t]$ , is displayed as a black line on top of a gray band. We see that for the preferred axigluon parameters  $A_{\text{FB}}^t(M_{t\bar{t}})$  is predicted to be strictly positive and a factor of around 3 to 4 above the SM expectation for  $M_{t\bar{t}} > 0.85$  TeV. Notice that the former behavior is characteristic for the presence of a heavy  $s$ -channel resonance with  $g_A^q g_A^t < 0$ . In fact, the interference term in  $A_{\text{FB}}^t(M_{t\bar{t}})$  only changes sign across a resonance, switching from positive to negative (negative to positive) values in going from  $M_{t\bar{t}}$  below to above the pole for  $g_A^q g_A^t < 0$  ( $g_A^q g_A^t > 0$ ). Given the high sensitivity of the differential asymmetry to the precise nature of the underlying physics, a more precise measurement of this quantity should be a primary goal of the Tevatron experiments and pursued with great vigor. Further information on the possible origin of the anomaly in  $A_{\text{FB}}^t$  is expected to come in the near future from the measurement of the distribution of the  $t\bar{t}$  cross section at the LHC. On the right of Figure 19, we depict the prediction for  $d\sigma_s/dM_{t\bar{t}}$  corresponding to the best-fit solution before (red curve) and after (blue curve) incorporating the ATLAS dijet constraints. The QCD prediction including its scale variation is displayed for comparison (black line and gray band). The relatively wide axigluon resonances are clearly visible in the figure. By integrating over the range  $M_{t\bar{t}} \in [1.0, 3.0]$  TeV, we find that the presence of an axigluon with  $\theta = 45^\circ$  and  $M_G = 1.5$  TeV ( $M_G = 1.9$  TeV)

leads to an enhancement of the tail of the spectrum by a factor of around 2.5 (1.3). From this observation, we conclude that if the anomaly in  $A_{\text{FB}}^t$  persists and is due to a new heavy color-octet resonance, then a notable enhancement of the  $t\bar{t}$  cross section with respect to the SM should be observed at the LHC. The synergy/complementarity of Tevatron and LHC measurements has also been stressed in [30, 31, 32, 34, 36].

It is possible to circumvent the dijet constraints by relaxing the conditions on the axigluon couplings present in the simplest chiral color model. Since the  $t\bar{t}$  observables are mostly sensitive to the product of the couplings to the light quarks and the top quark, a simple rescaling

$$g_{L,R}^q \rightarrow \xi g_{L,R}^q, \quad g_{L,R}^t \rightarrow g_{L,R}^t/\xi, \quad (68)$$

leaves the goodness of the global fit essentially unchanged. This freedom can be exploited to suppress the couplings to light quarks that govern effects in dijet production. In order to reach the axigluon best-fit point for  $t\bar{t}$  production around  $M_G = 1.5$  TeV and simultaneously evade the bounds from resonance searches in dijet production, one needs a suppression factor of  $\xi \lesssim 0.85$ . For the minimal suppression the resulting couplings are hence  $g_L^q = -g_R^q \approx 0.85$  and  $g_L^t = -g_R^t \approx -1.2$ , which implies that  $\Gamma_G/M_G \approx 9\%$ , if only SM quark decay modes are open. For such a resonance, we find  $A_{\text{FB}}^t = 13.7\%$ ,  $(A_{\text{FB}}^t(M_{t\bar{t}}))^< = 10.7\%$ , and  $(A_{\text{FB}}^t(M_{t\bar{t}}))^> = 25.6\%$ . The total cross section is SM-like, while  $(d\sigma_s/dM_{t\bar{t}})^> = 0.09$  fb/GeV shows the previously mentioned characteristic enhancement with respect to the QCD prediction. The corresponding results for  $A_{\text{FB}}^t(M_{t\bar{t}})$  and  $d\sigma_s/dM_{t\bar{t}}$  essentially resemble the blue curves in the left and right panels of Figure 19. Relaxing the conditions further to  $|g_L^q| \neq |g_R^q|$  and/or  $|g_L^t| \neq |g_R^t|$  does not improve the fit to the  $t\bar{t}$  data, since it enhances the effects on the symmetric cross section for fixed contributions to the asymmetry. From these general considerations we conclude that the predictions of the asymmetries presented in the left panel of Figure 18 represent, in fact, the maximal values that can be obtained in any model of new physics, where  $t\bar{t}$  production receives the dominant corrections from  $s$ -channel exchange of a color-octet resonance.<sup>18</sup>

Let us finally also briefly comment on the global fit to the  $t\bar{t}$  observables in presence of an axigluon with flavor universal couplings to quarks. The allowed parameter region is displayed in the right panel of Figure 17. While the effects on the symmetric observables are essentially the same as in the non-universal case, the contributions to the asymmetric cross section now interfere destructively with QCD, driving the asymmetry  $(A_{\text{FB}}^t(M_{t\bar{t}}))^>$  below the SM value. A flavor universal axigluon is therefore excluded at 99.5% CL by the global fit to the  $t\bar{t}$  data unless its mass is above 3.0 TeV. Notice also that the obtained fit is always worse than the one in the SM, and that the  $t\bar{t}$  observables provide a constraint that is notably stronger than the bound that follows from dijet production as well as from any indirect constraints.

---

<sup>18</sup>It might be possible to lever out these arguments and evade the constraints from both  $t\bar{t}$  and dijet production by introducing more than one color-octet boson with almost degenerate masses and arrange for the couplings so that the individual contributions in the symmetric observables cancel each other to a large extent.

## 7 Conclusions

In this article we have performed a comprehensive study of direct and indirect constraints on massive color-octet vector bosons and their impact on top-quark pair production. Motivated by the observation of large effects in asymmetric  $t\bar{t}$  production at the Tevatron, we have focused on axigluons with flavor non-universal couplings to quarks in the framework of chiral color. However, it is straightforward to apply our general results and formulas to other strongly-coupled  $s$ -channel resonances with arbitrary couplings to quarks.

We have pointed out that any model with a heavy color-octet boson that possesses flavor non-universal couplings to quarks inevitably features FCNC interactions at tree level. In the case of generic flavor violation in the down-quark sector, we found that neutral meson mixing rules out axigluons with masses below several TeV. Without specifying an underlying theory that fixes the pattern of flavor breaking, the FCNC effects can however be confined to the up-quark sector and aligned such that they are of MFV type. Minimal constraints are thus derived from the mass difference in the neutral  $D$ -meson sector and yield the rather weak bound of  $M_G > 0.22$  TeV. This bound has to be fulfilled by any axigluon with flavor non-universal couplings of QCD strength to quarks. In contrast, models with flavor universality are not constrained by flavor physics at all.

The precision observables at the  $Z$  pole are sensitive to one-loop effects in the  $Zq\bar{q}$  couplings associated to the virtual exchange of massive color-octet bosons. Constraints from the bottom-quark POs are largely avoided if  $|g_L^b| = |g_L^q|$  and  $|g_L^b| = |g_R^b|$ . In the axigluon model these conditions are both fulfilled for a mixing angle of  $\theta = 45^\circ$ . Axigluon effects in the total  $Z$ -boson decay width  $\Gamma_Z$  and the hadronic cross section  $\sigma_{\text{had}}$ , on the other hand, cannot be decoupled for any choice of the mixing angle. From the combined fit to all five  $Z \rightarrow q\bar{q}$  observables, we derive the mass bounds  $M_G > 0.54$  TeV in the flavor non-universal and  $M_G > 0.40$  TeV in the universal axigluon model. Colored resonances with QCD-like couplings to all quark flavors and a mass around the electroweak scale are therefore highly disfavored. In fact, the presence of an axigluon worsens the quality of the global fit to the  $Zq\bar{q}$  couplings with respect to the SM and, in particular, does not allow to reduce the long-standing discrepancy in the bottom-quark asymmetry  $A_{\text{FB}}^b$ .

Heavy-gluon corrections affect the Peskin-Takeuchi parameters  $S$  and  $T$  first at the two-loop level. Since the  $T$  parameter measures isospin violation, axigluon effects to it are enhanced relative to  $S$  by a chiral factor  $m_t^2/M_Z^2$ . In the flavor non-universal axigluon model, the presence of a sequential fourth generation of fermions leads to non-zero one-loop effects to  $S$  and  $T$ , making it impossible to derive a model-independent bound on the parameter space. For a given set of typical fourth generation parameters, it however turns out that the oblique parameters probe axigluon masses at and slightly above the scale of EWSB. In the case of an axigluon with flavor universal QCD-like couplings, the absence of extra fermions allows to derive a firm bound on the axigluon mass of  $M_G > 0.16$  TeV. The limits from isospin violation can however become competitive or even more restrictive than those arising from the other indirect constraints, if the top quark couples very strongly to the new colored boson. In particular, in models where the right-handed top quark is fully composite,  $T$  can receive unacceptably large positive corrections even for axigluon masses in the TeV range.

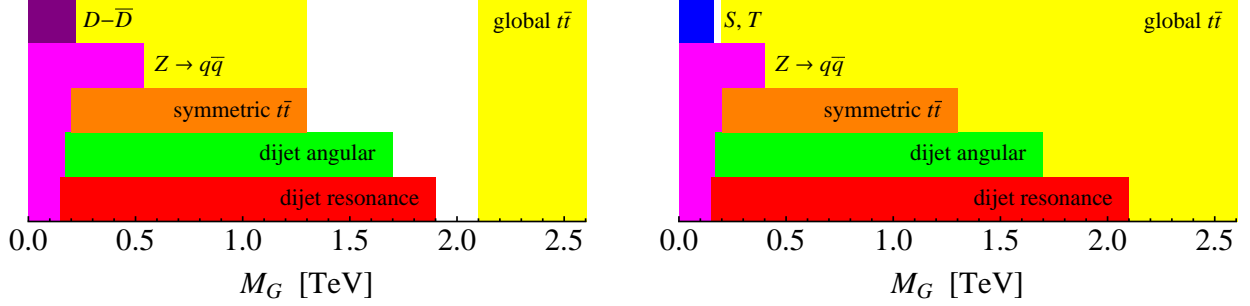


Figure 20: Bounds on  $M_G$  in the flavor non-universal (left) and universal (right) axigluon model. Colored regions are excluded at 95% CL by  $D-\bar{D}$  mixing (purple),  $Z \rightarrow q\bar{q}$  (magenta),  $S$  and  $T$  (blue),  $\sigma_s$  and  $(d\sigma_s/dM_{t\bar{t}})^>$  (orange), dijet angular distributions (green) and resonances searches (red) at the LHC, and by the global fit to the Tevatron  $t\bar{t}$  data (yellow).

The most stringent constraints on the axigluon parameter space stem from the production of massive color-octet bosons decaying to dijets at the LHC. Searches for narrow resonances in the dijet invariant mass spectrum exclude the mass window  $0.6 \text{ TeV} < M_G < 1.9 \text{ TeV}$  in the flavor non-universal model. The lower bound is due to the limited detector sensitivity to dijet events with small invariant masses  $M_{jj}$ . Earlier resonance searches exclude axigluon masses down to around 0.15 TeV. In the flavor universal model, the axigluon width  $\Gamma_G$  is smaller due to the absence of the fourth generation, which results in a stronger exclusion limit of  $0.6 \text{ TeV} < M_G < 2.1 \text{ TeV}$ . These bounds are only relevant in the case of narrow resonances with  $\Gamma_G/M_G \lesssim 15\%$ . Constraints from the angular distribution of dijets are applicable for broad resonances as well. In this context, we have shown that the inclusion of width effects is important to obtain reliable bounds from the analysis of the angular distribution, since the shape of the centrality ratio of the jet pairs depends significantly on them. We found that, by probing the enhancement of jets in the central region, one can exclude the mass range of  $0.17 \text{ TeV} < M_G < 1.7 \text{ TeV}$  for both the case of a flavor non-universal and universal axigluon. The excluded range extends well below the region  $M_{jj} > 0.5 \text{ TeV}$  directly probed by ATLAS, because light axigluons enhance the central activity also at  $M_{jj} \gg M_G$ .

We have finally studied the possible effects of a massive color-octet vector boson in top-quark pair production. Our analysis shows that there is a generic tension between having large effects in the asymmetric and small effects in the symmetric  $t\bar{t}$  cross sections, because these observables are positively correlated. While the anomalously large forward-backward asymmetry can in principle be accommodated by a color octet with strong flavor non-universal axial-vector couplings to quarks and a mass  $M_G \approx 1 \text{ TeV}$ , such a possibility is disfavored by a combined fit to the total cross section  $\sigma_s$  and its spectrum  $(d\sigma_s/dM_{t\bar{t}})^>$  at high invariant mass, which excludes masses in the range  $0.2 \text{ TeV} < M_G < 1.3 \text{ TeV}$ , independently from flavor (non-)universality. The tension between the different observables also limits the goodness of a global  $t\bar{t}$  fit. For masses satisfying  $1.3 \text{ TeV} < M_G < 2.1 \text{ TeV}$ , agreement with the Tevatron data is found at 95% CL. The best fit has  $\chi^2/\text{ndf} = 7.6/4$  (corresponding to 90% CL) and is

achieved for a flavor non-universal axigluon with  $M_G = 1.5$  TeV and  $\theta = 45^\circ$ . This solution hence represents a significant improvement with respect to the SM ( $\chi^2/\text{ndf} = 13.1/4$ ), giving rise to asymmetries of  $A_{\text{FB}}^t = 16.7\%$  and  $(A_{\text{FB}}^t(M_{t\bar{t}}))^> = 25.7\%$ . A flavor universal axigluon, on the other hand, does not provide an acceptable fit to the  $t\bar{t}$  data, since it fails to yield large positive values of the asymmetry.

The various mass constraints are summarized in Figure 20 for the flavor non-universal (left) and universal (right) axigluon model. In the non-universal case the best-fit point for the  $t\bar{t}$  observables at  $M_G = 1.5$  TeV is at variance with the constraints arising from dijet production, resulting in a narrow window of allowed masses around 2 TeV. Axigluon effects in the  $t\bar{t}$  asymmetry are in this mass window reduced to at most  $A_{\text{FB}}^t = 13.1\%$  and  $(A_{\text{FB}}^t(M_{t\bar{t}}))^> = 19.1\%$ . We have also emphasized that the bounds from dijet production can be evaded by relaxing the conditions on the axigluon couplings arising in models of chiral color. For the rescaled couplings  $g_L^q = -g_R^q \approx 0.85$  and  $g_L^t = -g_R^t \approx -1.2$ , the best-fit point to the  $t\bar{t}$  data at  $M_G = 1.5$  TeV becomes viable again. It however turns out that the fit cannot be further improved by allowing for  $|g_L^q| \neq |g_R^q|$  and/or  $|g_L^t| \neq |g_R^t|$ . These general arguments imply that the presence of a single color-octet boson cannot raise the prediction for the top-quark forward-backward asymmetry  $(A_{\text{FB}}^t(M_{t\bar{t}}))^>$  above 26%. In conclusion, our findings suggest that a consistent explanation of the Tevatron  $t\bar{t}$  data by a massive color-octet boson predicts a resonance of 1.5 TeV to 2 TeV in the spectrum of top-quark pair production at the LHC. Combined with improved Tevatron determinations of the top-quark properties and an explicit measurement of the  $t\bar{t}$  charge asymmetry by ATLAS, CMS, and possibly LHCb, this should allow to confirm or rule out the axigluon hypothesis in the near future.

## Acknowledgments

It is a pleasure to thank Giulia Zanderighi for providing the analytic result for one of the integrals needed for the calculations presented in this article. Useful discussions and correspondence with Roberto Barcelo, Mads Frandsen, Barbara Jäger, Alex Kagan, Jürgen Rohrwild, and Jose Santiago are also acknowledged. We are finally grateful to Volker Büscher, Regina Demina, Sebastian Eckweiler, Rhorry Gauld, Adam Gibson, Weina Ji, Lucia Masetti, Andrei Nomerotski, and Christian Schmitt for helpful discussions about experimental aspects of top-antitop and/or dijet production.

## A Form Factors for $Z \rightarrow q\bar{q}$

Below we present the analytic expressions for the one-loop  $Z \rightarrow q\bar{q}$  form factor describing the virtual exchange of a color-octet spin-one state. For light quarks ( $q = u, d, s, c, b$ ) the given expressions correspond to the limit of an on-shell  $Z$  boson and on-shell external quarks with vanishing mass, while in the case of the top quark we evaluate the form factor at zero momentum transfer. Throughout the calculation we will ignore possible flavor-violating effects.

The one-loop axigluon corrections to the couplings of the  $Z$  boson to light quarks lead to a shift in the tree-level couplings  $g_P^q$  with  $P = L, R$ . In the case of the bottom quark, the

resulting effective couplings can be written as

$$\mathcal{G}_P^b = g_P^b \left[ 1 + \frac{\alpha_s}{4\pi} C_F (g_P^h)^2 \mathcal{K}(x_Z) \right], \quad (\text{A1})$$

where the real and imaginary parts of the complex form factor  $\mathcal{K}(x_Z)$  take the following form

$$\begin{aligned} \text{Re} \mathcal{K}(x_Z) &= -\frac{4+7x_Z}{2x_Z} + \frac{2+3x_Z}{x_Z} \ln x_Z - \frac{2(1+x_Z)^2}{x_Z^2} [\ln x_Z \ln(1+x_Z) + \text{Li}_2(-x_Z)], \\ \text{Im} \mathcal{K}(x_Z) &= \left[ -\frac{2+3x_Z}{x_Z} + \frac{2(1+x_Z)^2}{x_Z^2} \ln(1+x_Z) \right] \pi. \end{aligned} \quad (\text{A2})$$

The above result agrees with the analytic expression given in [81, 82]. Here  $x_Z = M_Z^2/M_G^2$  and  $\text{Li}_2(z) = -\int_0^z dt \ln(1-t)/t$  denotes the dilogarithm. We remark that in the decoupling limit  $x_Z \rightarrow 0$ , the real and imaginary parts of the form factor  $\mathcal{K}(x_Z)$  behave as

$$\text{Re} \mathcal{K}(x_Z) \rightarrow x_Z \left( -\frac{2}{3} \ln x_Z + \frac{11}{9} \right), \quad \text{Im} \mathcal{K}(x_Z) \rightarrow \frac{2\pi}{3} x_Z. \quad (\text{A3})$$

Notice finally that the imaginary components which are not logarithmically enhanced, have been ignored in the discussion of the  $Z \rightarrow q\bar{q}$  constraints on the parameter space of the axigluon model. In particular, the expression (28) contains only the leading-logarithmic corrections.

In the case of the top quark, we find instead

$$\mathcal{G}_P^t = g_P^t \pm \frac{g}{c_w} \frac{\alpha_s}{4\pi} C_F (g_P^h)^2 G(x_t), \quad (\text{A4})$$

where the plus (minus) sign applies in the case  $P = L$  ( $P = R$ ) and  $x_t = m_t^2/M_G^2$ . The short-distance coefficient  $G(x_t)$  is given by

$$G(x_t) = \frac{x_t}{1-x_t} + \frac{x_t}{(1-x_t)^2} \ln x_t. \quad (\text{A5})$$

It obeys  $G(x_t) \rightarrow x_t (\ln x_t + 1)$  for  $x_t \rightarrow 0$ .

## B Corrections to Oblique Parameters

In this appendix we give the analytic results for the two-loop corrections to the Peskin-Takeuchi parameters  $S$  and  $T$  arising in the considered axigluon model. The calculation has been performed in the on-shell renormalization scheme and the bottom-quark mass has been neglected throughout. Effects from the fourth generation of fermions, needed to make the model anomaly-free, are ignored in the following. Finally, flavor-violating effects that are strongly CKM suppressed in the case of flavor alignment are neglected.

Our result for the  $S$  parameter reads

$$S = \frac{2}{9\pi} \frac{\alpha_s}{4\pi} C_F N_c \left[ (g_L^h)^2 s_{LL}(x_t) + (g_R^h)^2 s_{RR}(x_t) + g_L^h g_R^h s_{LR}(x_t) \right], \quad (\text{B1})$$

where the functions  $s_{LL}(x_t)$ ,  $s_{RR}(x_t)$ , and  $s_{LR}(x_t)$  are given by

$$\begin{aligned}
s_{LL}(x_t) &= \frac{2 - 21x_t + 80x_t^2 - 152x_t^3 + 60x_t^4}{8(1 - 4x_t)^2 x_t} \\
&\quad + \frac{1 - 16x_t + 98x_t^2 - 240x_t^3 + 30x_t^4 + 400x_t^5 - 120x_t^6}{8(1 - 4x_t)^3 x_t^2} \ln x_t \\
&\quad + \frac{1 - 2x_t}{4x_t} \psi(x_t) + \frac{4x_t - 29x_t^2 + 34x_t^3 - 18x_t^4 + 60x_t^5}{4(1 - 4x_t)^3} \phi\left(\frac{1}{4x_t}\right), \\
s_{RR}(x_t) &= \frac{2 - 21x_t + 76x_t^2 - 136x_t^3 + 60x_t^4}{8(1 - 4x_t)^2 x_t} \\
&\quad + \frac{1 - 16x_t + 98x_t^2 - 240x_t^3 + 6x_t^4 + 496x_t^5 - 120x_t^6}{8(1 - 4x_t)^3 x_t^2} \ln x_t \\
&\quad + \frac{1 - 2x_t}{4x_t} \psi(x_t) + \frac{8x_t - 79x_t^2 + 230x_t^3 - 258x_t^4 + 60x_t^5}{4(1 - 4x_t)^3} \phi\left(\frac{1}{4x_t}\right), \\
s_{LR}(x_t) &= \frac{8 - 79x_t + 178x_t^2 - 60x_t^3}{4(1 - 4x_t)^2} \\
&\quad + \frac{2 - 28x_t + 131x_t^2 - 256x_t^3 + 118x_t^4 + 60x_t^5}{2(1 - 4x_t)^3 x_t} \ln x_t \\
&\quad + 2\psi(x_t) - \frac{9x_t^2 - 42x_t^3 + 54x_t^4 + 30x_t^5}{(1 - 4x_t)^3} \phi\left(\frac{1}{4x_t}\right).
\end{aligned} \tag{B2}$$

The function  $\psi(z)$  arises from the one-loop top-quark selfenergy entering the counterterm contribution and takes the form

$$\psi(z) = \begin{cases} \frac{\sqrt{1-4z}}{z} \tanh^{-1}(\sqrt{1-4z}), & z < 1/4, \\ -\frac{\sqrt{4z-1}}{z} \left[ \tan^{-1}\left(\frac{2z-1}{\sqrt{4z-1}}\right) + \cot^{-1}(\sqrt{4z-1}) \right], & z > 1/4. \end{cases} \tag{B3}$$

The function  $\phi(z)$  stems from the two-loop scalar tadpole with two different masses. The corresponding analytic expression reads [83]

$$\phi(z) = \begin{cases} 4\sqrt{\frac{z}{1-z}} \text{Cl}_2(2\sin^{-1}(\sqrt{z})), & z < 1, \\ \frac{-4\text{Li}_2\left(\frac{1}{2}\left[1 - \sqrt{1-z^{-1}}\right]\right) + 2\ln^2\left(\frac{1}{2}\left[1 - \sqrt{1-z^{-1}}\right]\right) - \ln^2(4z) + \frac{\pi^2}{3}}{\sqrt{1-z^{-1}}}, & z > 1, \end{cases} \tag{B4}$$

where  $\text{Cl}_2(z) = \text{Im}[\text{Li}_2(e^{iz})]$  denotes the Clausen function.

The formulas in (B2) are not very illuminating. We therefore also give explicit expressions for the coefficient functions in the limit  $x_t \rightarrow 0$ , corresponding to an infinitely heavy axigluon. We obtain

$$\begin{aligned} s_{LL}(x_t) &\rightarrow x_t \left( \ln^2 x_t + 5 \ln x_t + \frac{\pi^2}{3} + \frac{7}{6} \right), \\ s_{RR}(x_t) &\rightarrow x_t \left( 2 \ln^2 x_t + 5 \ln x_t + \frac{2}{3} \pi^2 + \frac{2}{3} \right), \\ s_{LR}(x_t) &\rightarrow x_t \left( -\frac{9}{2} \ln x_t - \frac{11}{4} \right), \end{aligned} \quad (\text{B5})$$

which implies that, if one is interested only in the leading-logarithmic behavior for  $x_t \rightarrow 0$ , one simply has  $s_{LL}(x_t) \approx x_t \ln^2 x_t$ ,  $s_{RR}(x_t) \approx 2s_{LL}(x_t)$ , and  $s_{LR}(x_t) \approx 0$ . These approximate formulas have been used in (39).

In the case of the  $T$  parameter, we find instead

$$T = \frac{m_t^2}{8\pi s_w^2 c_w^2 M_Z^2} \frac{\alpha_s}{4\pi} C_F N_c \left[ (g_L^h)^2 t_{LL}(x_t) + (g_R^h)^2 t_{RR}(x_t) + g_L^h g_R^h t_{LR}(x_t) \right], \quad (\text{B6})$$

The coefficient functions  $t_{LL}(x_t)$ ,  $t_{RR}(x_t)$ , and  $t_{LR}(x_t)$  are given by

$$\begin{aligned} t_{LL}(x_t) &= -\frac{9-8x_t}{2x_t} + \frac{1-x_t}{6x_t^3} \pi^2 - \frac{1-20x_t+64x_t^2-24x_t^3}{4(1-4x_t)x_t^2} \ln x_t + \frac{1-x_t}{2x_t^3} \ln^2 x_t \\ &\quad + \frac{2-7x_t+8x_t^2-3x_t^3}{x_t^3} \text{Li}_2\left(\frac{x_t-1}{x_t}\right) - \frac{1-2x_t}{2x_t} \psi(x_t) \\ &\quad + \frac{1-12x_t+50x_t^2-83x_t^3+50x_t^4-12x_t^5}{2(1-4x_t)x_t^3} \phi\left(\frac{1}{4x_t}\right), \\ t_{RR}(x_t) &= -\frac{3-4x_t}{2x_t} - \frac{1-12x_t+32x_t^2-24x_t^3}{4(1-4x_t)x_t^2} \ln x_t - \frac{1-2x_t+x_t^2}{x_t^2} \text{Li}_2\left(\frac{x_t-1}{x_t}\right) \\ &\quad - \frac{1-2x_t}{2x_t} \psi(x_t) - \frac{1-8x_t+19x_t^2-18x_t^3+12x_t^4}{2(1-4x_t)x_t^2} \phi\left(\frac{1}{4x_t}\right), \\ t_{LR}(x_t) &= -7 + \frac{\pi^2}{6x_t^2} - \frac{2-14x_t+12x_t^2}{(1-4x_t)x_t} \ln x_t + \frac{\ln^2 x_t}{2x_t^2} + \frac{2-4x_t+2x_t^2}{x_t^2} \text{Li}_2\left(\frac{x_t-1}{x_t}\right) \\ &\quad - 4\psi(x_t) + \frac{1-10x_t+32x_t^2-32x_t^3+24x_t^4}{2(1-4x_t)x_t^2} \phi\left(\frac{1}{4x_t}\right). \end{aligned} \quad (\text{B7})$$



In the limit  $x_t \rightarrow 0$ , the coefficients given in (B7) behave as

$$\begin{aligned}
t_{LL}(x_t) &\rightarrow x_t \left( \ln^2 x_t + \frac{7}{3} \ln x_t + \frac{\pi^2}{3} + \frac{35}{36} \right), \\
t_{RR}(x_t) &\rightarrow x_t \left( 2 \ln^2 x_t + \frac{11}{3} \ln x_t + \frac{2}{3} \pi^2 + \frac{5}{18} \right), \\
t_{LR}(x_t) &\rightarrow x_t (6 \ln x_t - 1).
\end{aligned} \tag{B8}$$

so that for  $x_t \rightarrow 0$  and leading-logarithmic accuracy,  $t_{LL}(x_t) \approx x_t \ln^2 x_t$ ,  $t_{RR}(x_t) \approx 2 t_{LL}(x_t)$ , and  $t_{LR}(x_t) \approx 0$ . The latter relations have been employed in (39).

## C Contributions to $t\bar{t}$ Observables

Below we present approximate formulas that allow for a model-independent global analysis of the  $t\bar{t}$  observables measured at the Tevatron. In terms of the following combinations

$$\begin{aligned}
c_{gG}^\pm &= (g_L^\ell \pm g_R^\ell) (g_L^h \pm g_R^h), \\
c_{GG}^\pm &= ((g_L^\ell)^2 \pm (g_R^\ell)^2) ((g_L^h)^2 \pm (g_R^h)^2), \\
c_{GG} &= ((g_L^\ell)^2 + (g_R^\ell)^2) g_L^h g_R^h,
\end{aligned} \tag{C1}$$

of the coupling strengths (4), we find

$$\begin{aligned}
(\sigma_s)_G &\approx \left\{ \left[ - \left( \frac{803 \text{ GeV}}{M_G} \right)^2 - \left( \frac{642 \text{ GeV}}{M_G} \right)^4 - \left( \frac{579 \text{ GeV}}{M_G} \right)^6 - \left( \frac{710 \text{ GeV}}{M_G} \right)^8 \right] c_{gG}^+ \right. \\
&\quad + \left[ \left( \frac{494 \text{ GeV}}{M_G} \right)^4 + \left( \frac{659 \text{ GeV}}{M_G} \right)^6 - \left( \frac{773 \text{ GeV}}{M_G} \right)^8 + \left( \frac{882 \text{ GeV}}{M_G} \right)^{10} \right] c_{GG}^+ \\
&\quad \left. + \left[ \left( \frac{462 \text{ GeV}}{M_G} \right)^4 + \left( \frac{556 \text{ GeV}}{M_G} \right)^6 - \left( \frac{553 \text{ GeV}}{M_G} \right)^8 + \left( \frac{734 \text{ GeV}}{M_G} \right)^{10} \right] c_{GG} \right\} \text{ pb}, \\
\left( \frac{d\sigma_s}{dM_{t\bar{t}}} \right)_G^{M_{t\bar{t}} \in [0.8, 1.4] \text{ TeV}} &\approx \left\{ \left[ - \left( \frac{181 \text{ GeV}}{M_G} \right)^2 - \left( \frac{429 \text{ GeV}}{M_G} \right)^4 + \left( \frac{494 \text{ GeV}}{M_G} \right)^6 - \left( \frac{733 \text{ GeV}}{M_G} \right)^8 \right] c_{gG}^+ \right. \\
&\quad + \left[ \left( \frac{241 \text{ GeV}}{M_G} \right)^4 + \left( \frac{712 \text{ GeV}}{M_G} \right)^6 - \left( \frac{896 \text{ GeV}}{M_G} \right)^8 + \left( \frac{955 \text{ GeV}}{M_G} \right)^{10} \right] c_{GG}^+ \\
&\quad \left. + \left[ \left( \frac{202 \text{ GeV}}{M_G} \right)^4 + \left( \frac{515 \text{ GeV}}{M_G} \right)^6 - \left( \frac{691 \text{ GeV}}{M_G} \right)^8 + \left( \frac{783 \text{ GeV}}{M_G} \right)^{10} \right] c_{GG} \right\} \frac{\text{fb}}{\text{GeV}},
\end{aligned}$$

$$\begin{aligned}
\left(\frac{d\sigma_s}{dM_{t\bar{t}}}\right)_G^{M_{t\bar{t}} < 0.45\text{TeV}} &\approx \left\{ \left[ -\left(\frac{1660\text{ GeV}}{M_G}\right)^2 - \left(\frac{846\text{ GeV}}{M_G}\right)^4 + \left(\frac{481\text{ GeV}}{M_G}\right)^6 - \left(\frac{671\text{ GeV}}{M_G}\right)^8 \right] c_{gG}^+ \right. \\
&\quad + \left[ \left(\frac{567\text{ GeV}}{M_G}\right)^4 + \left(\frac{702\text{ GeV}}{M_G}\right)^6 - \left(\frac{688\text{ GeV}}{M_G}\right)^8 + \left(\frac{674\text{ GeV}}{M_G}\right)^{10} \right] c_{GG}^+ \\
&\quad \left. + \left[ \left(\frac{618\text{ GeV}}{M_G}\right)^4 + \left(\frac{729\text{ GeV}}{M_G}\right)^6 - \left(\frac{703\text{ GeV}}{M_G}\right)^8 + \left(\frac{688\text{ GeV}}{M_G}\right)^{10} \right] c_{GG} \right\} \frac{\text{fb}}{\text{GeV}}, \\
\left(\frac{d\sigma_s}{dM_{t\bar{t}}}\right)_G^{M_{t\bar{t}} > 0.45\text{TeV}} &\approx \left\{ \left[ -\left(\frac{487\text{ GeV}}{M_G}\right)^2 - \left(\frac{536\text{ GeV}}{M_G}\right)^4 - \left(\frac{522\text{ GeV}}{M_G}\right)^6 - \left(\frac{673\text{ GeV}}{M_G}\right)^8 \right] c_{gG}^+ \right. \\
&\quad + \left[ \left(\frac{418\text{ GeV}}{M_G}\right)^4 + \left(\frac{609\text{ GeV}}{M_G}\right)^6 - \left(\frac{735\text{ GeV}}{M_G}\right)^8 + \left(\frac{847\text{ GeV}}{M_G}\right)^{10} \right] c_{GG}^+ \\
&\quad \left. + \left[ \left(\frac{365\text{ GeV}}{M_G}\right)^4 + \left(\frac{500\text{ GeV}}{M_G}\right)^6 - \left(\frac{535\text{ GeV}}{M_G}\right)^8 + \left(\frac{704\text{ GeV}}{M_G}\right)^{10} \right] c_{GG} \right\} \frac{\text{fb}}{\text{GeV}}, \\
(\sigma_a)_G &\approx \left\{ \left[ -\left(\frac{497\text{ GeV}}{M_G}\right)^2 - \left(\frac{527\text{ GeV}}{M_G}\right)^4 - \left(\frac{508\text{ GeV}}{M_G}\right)^6 - \left(\frac{668\text{ GeV}}{M_G}\right)^8 \right] c_{gG}^- \right. \\
&\quad \left. + \left[ \left(\frac{436\text{ GeV}}{M_G}\right)^4 + \left(\frac{619\text{ GeV}}{M_G}\right)^6 - \left(\frac{745\text{ GeV}}{M_G}\right)^8 + \left(\frac{855\text{ GeV}}{M_G}\right)^{10} \right] c_{GG}^- \right\} \text{pb}, \\
\left(\frac{d\sigma_a}{dM_{t\bar{t}}}\right)_G^{M_{t\bar{t}} < 0.45\text{TeV}} &\approx \left\{ \left[ -\left(\frac{840\text{ GeV}}{M_G}\right)^2 - \left(\frac{601\text{ GeV}}{M_G}\right)^4 - \left(\frac{338\text{ GeV}}{M_G}\right)^6 - \left(\frac{565\text{ GeV}}{M_G}\right)^8 \right] c_{gG}^- \right. \\
&\quad \left. + \left[ \left(\frac{477\text{ GeV}}{M_G}\right)^4 + \left(\frac{589\text{ GeV}}{M_G}\right)^6 - \left(\frac{590\text{ GeV}}{M_G}\right)^8 + \left(\frac{612\text{ GeV}}{M_G}\right)^{10} \right] c_{GG}^- \right\} \frac{\text{fb}}{\text{GeV}}, \\
\left(\frac{d\sigma_a}{dM_{t\bar{t}}}\right)_G^{M_{t\bar{t}} > 0.45\text{TeV}} &\approx \left\{ \left[ -\left(\frac{340\text{ GeV}}{M_G}\right)^2 - \left(\frac{447\text{ GeV}}{M_G}\right)^4 - \left(\frac{522\text{ GeV}}{M_G}\right)^6 - \left(\frac{596\text{ GeV}}{M_G}\right)^8 \right] c_{gG}^- \right. \\
&\quad \left. + \left[ \left(\frac{358\text{ GeV}}{M_G}\right)^4 + \left(\frac{649\text{ GeV}}{M_G}\right)^6 - \left(\frac{815\text{ GeV}}{M_G}\right)^8 + \left(\frac{880\text{ GeV}}{M_G}\right)^{10} \right] c_{GG}^- \right\} \frac{\text{fb}}{\text{GeV}}.
\end{aligned} \tag{C2}$$

Notice that the coefficients in (C1) labelled by  $gG$  and  $GG$  arise from the interference of the gluon with the axigluon and the interference of the axigluon with itself. In order to obtain the above formulas, the total decay width of the axigluon has been fixed to  $\Gamma_G/M_G = 10\%$ , which is a typical value for massive color-octet bosons with QCD-like couplings to quarks.

In the specific axigluon model taken as a benchmark in the main body of this work, one has  $\Gamma_G/M_G \approx 10\%$  in the regime of  $M_G \approx 1$  TeV,  $\theta \gtrsim 35^\circ$ , and fourth-generation quark masses above the Tevatron bounds [41, 42]. For smaller values of the mixing angle  $\theta$  the total decay width becomes significantly larger, thereby effectively suppressing the size of the axigluon contributions. In this case the formulas (C2) should not be applied, since they typically lead to constraints in the  $M_G$ – $\theta$  plane that are too restrictive. In our numerical analysis presented in Section 6, we have therefore included the exact dependence on  $\Gamma_G$ , employing the expressions for the partial widths given in (47).

## D Matrix Elements for Dijet Production

This appendix contains the new-physics corrections to the dijet tree-level matrix elements squared. Possible flavor-violating effects are neglected throughout. In terms of the couplings (4) and the partonic Mandelstam variables  $\hat{s}$ ,  $\hat{t}$ , and  $\hat{u}$ , we obtain the following results

$$\begin{aligned} \left( \overline{\sum} |\mathcal{M}(q_i \bar{q}_i \rightarrow q_i \bar{q}_i)|^2 \right)_G &= \frac{4}{9} g_s^4 \left\{ 2g_L^\ell g_R^\ell \left[ \frac{\hat{t}^2(\hat{s} - M_G^2)}{\hat{s}((\hat{s} - M_G^2)^2 + \Gamma_G^2 M_G^2)} + (\hat{s} \leftrightarrow \hat{t}) \right] \right. \\ &\quad + ((g_L^\ell)^2 + (g_R^\ell)^2) \left[ \frac{\hat{u}^2(\hat{s} - M_G^2)}{(\hat{s} - M_G^2)^2 + \Gamma_G^2 M_G^2} \left( \frac{1}{\hat{s}} - \frac{1}{3\hat{t}} \right) + (\hat{s} \leftrightarrow \hat{t}) \right] \\ &\quad + \frac{1}{2} \frac{((g_L^\ell)^4 + (g_R^\ell)^4) \hat{u}^2}{(\hat{s} - M_G^2)^2 + \Gamma_G^2 M_G^2} \left[ 1 + \frac{(\hat{s} - M_G^2)^2 + \Gamma_G^2 M_G^2}{(\hat{t} - M_G^2)^2 + \Gamma_G^2 M_G^2} \right. \\ &\quad \left. \left. - \frac{2}{3} \frac{(\hat{s} - M_G^2)(\hat{t} - M_G^2) + \Gamma_G^2 M_G^2}{(\hat{t} - M_G^2)^2 + \Gamma_G^2 M_G^2} \right] \right\}, \quad (\text{D1}) \\ \left( \overline{\sum} |\mathcal{M}(q_i \bar{q}_j \rightarrow q_i \bar{q}_j)|^2 \right)_G &= \frac{4}{9} g_s^4 \left\{ [((g_L^\ell)^2 + (g_R^\ell)^2) \hat{u}^2 + 2g_L^\ell g_R^\ell \hat{s}^2] \frac{\hat{t} - M_G^2}{\hat{t}((\hat{t} - M_G^2)^2 + \Gamma_G^2 M_G^2)} \right. \\ &\quad \left. + \frac{1}{2} ((g_L^\ell)^4 + (g_R^\ell)^4) \frac{\hat{u}^2}{(\hat{t} - M_G^2)^2 + \Gamma_G^2 M_G^2} \right\}, \end{aligned}$$

where  $g_s$  denotes the strong coupling constant. The result for  $q_i q_i \rightarrow q_i q_i$  ( $q_i q_j \rightarrow q_i q_j$ ) follows from the expression in the first (second) line by simply interchanging  $\hat{s}$  with  $\hat{u}$ , while the result for  $q_i \bar{q}_i \rightarrow q_j \bar{q}_j$  is obtained by interchanging  $\hat{s}$  with  $\hat{t}$  in the second line. The matrix elements in terms of  $\chi = (1 + |\cos \hat{\theta}|)/(1 - |\cos \hat{\theta}|)$  and  $M_{jj}$  are easily obtained using  $\hat{s} = M_{jj}^2$ ,  $\hat{t} = -(1 - \cos \hat{\theta}) \hat{s}/2$ , and  $\hat{u} = -(1 + \cos \hat{\theta}) \hat{s}/2$ . In order to obtain the matrix elements after integrating out the axigluon, one simply neglects the width  $\Gamma_G$  and expands around the limit  $\hat{s}, \hat{t}, \hat{u} \ll M_G^2$ .

## References

- [1] L. Randall and R. Sundrum, Phys. Rev. Lett. **83**, 3370 (1999) [arXiv:hep-ph/9905221].

- [2] C. T. Hill and E. H. Simmons, Phys. Rept. **381**, 235 (2003) [Erratum-ibid. **390**, 553 (2004)] [arXiv:hep-ph/0203079].
- [3] P. H. Frampton and S. L. Glashow, Phys. Lett. B **190**, 157 (1987).
- [4] P. H. Frampton and S. L. Glashow, Phys. Rev. Lett. **58**, 2168 (1987).
- [5] J. Bagger, C. Schmidt and S. King, Phys. Rev. D **37**, 1188 (1988).
- [6] C. T. Hill, Phys. Lett. B **266**, 419 (1991).
- [7] C. T. Hill, Phys. Lett. B **345**, 483 (1995) [arXiv:hep-ph/9411426].
- [8] C. T. Hill and S. J. Parke, Phys. Rev. D **49**, 4454 (1994) [arXiv:hep-ph/9312324].
- [9] R. S. Chivukula, A. G. Cohen and E. H. Simmons, Phys. Lett. B **380**, 92 (1996) [arXiv:hep-ph/9603311].
- [10] K. Agashe, A. Delgado, M. J. May and R. Sundrum, JHEP **0308**, 050 (2003) [arXiv:hep-ph/0308036].
- [11] K. Agashe, A. Belyaev, T. Krupovnickas, G. Perez and J. Virzi, Phys. Rev. D **77**, 015003 (2008) [arXiv:hep-ph/0612015].
- [12] B. Lillie, L. Randall and L. T. Wang, JHEP **0709**, 074 (2007) [arXiv:hep-ph/0701166].
- [13] E. Thomson *et al.* [CDF Collaboration], Conference Note 9913, October 19, 2009, [http://www-cdf.fnal.gov/physics/new/top/2009/xsection/ttbar\\_combined\\_46invfb/](http://www-cdf.fnal.gov/physics/new/top/2009/xsection/ttbar_combined_46invfb/)
- [14] DØ Collaboration, Conference Note 5907-CONF, March 12, 2009, <http://www-d0.fnal.gov/Run2Physics/WWW/results/prelim/TOP/T79/>
- [15] T. Aaltonen *et al.* [CDF Collaboration], Phys. Rev. Lett. **102**, 222003 (2009) [arXiv:0903.2850 [hep-ex]].
- [16] T. Aaltonen *et al.* [CDF Collaboration], arXiv:1101.0034 [hep-ex].
- [17] T. A. Schwarz, FERMILAB-THESIS-2006-51, UMI-32-38081.
- [18] V. M. Abazov *et al.* [DØ Collaboration], Phys. Rev. Lett. **100**, 142002 (2008) [arXiv:0712.0851 [hep-ex]].
- [19] T. Aaltonen *et al.* [CDF Collaboration], Phys. Rev. Lett. **101**, 202001 (2008) [arXiv:0806.2472 [hep-ex]].
- [20] DØ Collaboration, Conference Note 6062-CONF, July 23, 2010, <http://www-d0.fnal.gov/Run2Physics/WWW/results/prelim/TOP/T90/>
- [21] CDF Collaboration, CDF Note 10398, March 10, 2011, <http://www-cdf.fnal.gov/physics/new/top/2011/DilAfb/>

- [22] S. Schael *et al.* [ALEPH Collaboration], Phys. Rept. **427**, 257 (2006) [arXiv:hep-ex/0509008].
- [23] M. E. Peskin and T. Takeuchi, Phys. Rev. D **46** (1992) 381.
- [24] V. Khachatryan *et al.* [CMS Collaboration], Phys. Rev. Lett. **105**, 211801 (2010) [arXiv:1010.0203 [hep-ex]].
- [25] V. Khachatryan *et al.* [CMS Collaboration], Phys. Rev. Lett. **106**, 201804 (2011) [arXiv:1102.2020 [hep-ex]].
- [26] G. Aad *et al.* [ATLAS Collaboration], New J. Phys. **13**, 053044 (2011) [arXiv:1103.3864 [hep-ex]] additional material available at <https://atlas.web.cern.ch/Atlas/GROUPS/PHYSICS/PAPERS/exoticsdijets2010/>
- [27] P. H. Frampton, J. Shu and K. Wang, Phys. Lett. B **683**, 294 (2010) [arXiv:0911.2955 [hep-ph]].
- [28] Q. H. Cao, D. McKeen, J. L. Rosner, G. Shaughnessy and C. E. M. Wagner, Phys. Rev. D **81**, 114004 (2010) [arXiv:1003.3461 [hep-ph]].
- [29] R. S. Chivukula, E. H. Simmons and C. P. Yuan, Phys. Rev. D **82**, 094009 (2010) [arXiv:1007.0260 [hep-ph]].
- [30] T. Han, I. Lewis and Z. Liu, JHEP **1012**, 085 (2010) [arXiv:1010.4309 [hep-ph]].
- [31] Y. Bai, J. L. Hewett, J. Kaplan and T. G. Rizzo, JHEP **1103**, 003 (2011) [arXiv:1101.5203 [hep-ph]].
- [32] J. A. Aguilar-Saavedra and M. Perez-Victoria, JHEP **1105**, 034 (2011) [arXiv:1103.2765 [hep-ph]].
- [33] M. I. Gresham, I. W. Kim and K. M. Zurek, arXiv:1103.3501 [hep-ph].
- [34] J. L. Hewett, J. Shelton, M. Spannowsky, T. M. P. Tait and M. Takeuchi, arXiv:1103.4618 [hep-ph].
- [35] R. Barcelo, A. Carmona, M. Masip and J. Santiago, arXiv:1105.3333 [hep-ph].
- [36] J. A. Aguilar-Saavedra and M. Perez-Victoria, arXiv:1105.4606 [hep-ph].
- [37] O. Antunano, J. H. Kühn, and G. Rodrigo, Phys. Rev. D **77**, 014003 (2008), [arXiv:0709.1652 [hep-ph]].
- [38] P. Ferrario and G. Rodrigo, Phys. Rev. D **78**, 094018 (2008) [arXiv:0809.3354 [hep-ph]].
- [39] P. Ferrario and G. Rodrigo, Phys. Rev. D **80**, 051701 (2009) [arXiv:0906.5541 [hep-ph]].
- [40] P. Achard *et al.* [L3 Collaboration], Phys. Lett. B **517**, 75 (2001) [arXiv:hep-ex/0107015].

- [41] A. Lister [CDF Collaboration], arXiv:0810.3349 [hep-ex].
- [42] T. Aaltonen *et al.* [CDF Collaboration], Phys. Rev. Lett. **106**, 141803 (2011) [arXiv:1101.5728 [hep-ex]].
- [43] S. Chatrchyan *et al.* [CMS Collaboration], arXiv:1102.4746 [hep-ex].
- [44] G. Buchalla, G. Burdman, C. T. Hill and D. Kominis, Phys. Rev. D **53**, 5185 (1996) [arXiv:hep-ph/9510376].
- [45] G. Burdman, K. D. Lane and T. Rador, Phys. Lett. B **514**, 41 (2001) [arXiv:hep-ph/0012073].
- [46] A. Martin and K. Lane, Phys. Rev. D **71**, 015011 (2005) [arXiv:hep-ph/0404107].
- [47] A. J. Buras, S. Jäger and J. Urban, Nucl. Phys. B **605**, 600 (2001) [arXiv:hep-ph/0102316].
- [48] J. Laiho, E. Lunghi and R. S. Van de Water, Phys. Rev. D **81**, 034503 (2010) [arXiv:0910.2928 [hep-ph]].
- [49] V. Lubicz and C. Tarantino, Nuovo Cim. B **123**, 674 (2008) [arXiv:0807.4605 [hep-lat]].
- [50] A. J. Buras, D. Guadagnoli and G. Isidori, Phys. Lett. B **688**, 309 (2010) [arXiv:1002.3612 [hep-ph]].
- [51] J. Charles *et al.* [CKMfitter Group], Eur. Phys. J. C **41**, 1 (2005) [arXiv:hep-ph/0406184], updated results available at <http://ckmfitter.in2p3.fr>
- [52] J. Brod and M. Gorbahn, Phys. Rev. D **82**, 094026 (2010) [arXiv:1007.0684 [hep-ph]].
- [53] K. Nakamura *et al.* [Particle Data Group], J. Phys. G **37**, 075021 (2010), updated results available at <http://pdglive.lbl.gov>
- [54] D. Asner *et al.* [The Heavy Flavor Averaging Group], arXiv:1010.1589 [hep-ex], updated results available at <http://www.slac.stanford.edu/xorg/hfag>
- [55] C. T. Hill and X. m. Zhang, Phys. Rev. D **51**, 3563 (1995) [arXiv:hep-ph/9409315].
- [56] V. Abazov *et al.* [DØ Collaboration], arXiv:1104.4590 [hep-ex].
- [57] U. Baur, A. Juste, L. H. Orr and D. Rainwater, Phys. Rev. D **71**, 054013 (2005) [arXiv:hep-ph/0412021].
- [58] U. Baur, A. Juste, D. Rainwater and L. H. Orr, Phys. Rev. D **73**, 034016 (2006) [arXiv:hep-ph/0512262].
- [59] E. L. Berger, Q. H. Cao and I. Low, Phys. Rev. D **80**, 074020 (2009) [arXiv:0907.2191 [hep-ph]].

- [60] J. H. Field, Mod. Phys. Lett. A **13**, 1937 (1998) [arXiv:hep-ph/9801355].
- [61] A. B. Arbuzov *et al.*, Comput. Phys. Commun. **174**, 728 (2006) [arXiv:hep-ph/0507146].
- [62] The Tevatron Electroweak Working Group [CDF and DØ Collaboration], arXiv:1007.3178 [hep-ex].
- [63] G. Burdman, R. S. Chivukula and N. J. Evans, Phys. Rev. D **61**, 035009 (2000) [arXiv:hep-ph/9906292].
- [64] H. J. He, N. Polonsky and S. f. Su, Phys. Rev. D **64**, 053004 (2001) [arXiv:hep-ph/0102144].
- [65] A. Bridgeman, FERMILAB-THESIS-2008-50.
- [66] T. Aaltonen *et al.* [CDF Collaboration], Phys. Rev. D **79**, 112002 (2009) [arXiv:0812.4036 [hep-ex]].
- [67] G. Aad *et al.* [ATLAS Collaboration], Phys. Rev. Lett. **105**, 161801 (2010) [arXiv:1008.2461 [hep-ex]].
- [68] V. M. Abazov *et al.* [DØ Collaboration], Phys. Rev. Lett. **103**, 191803 (2009) [arXiv:0906.4819 [hep-ex]].
- [69] G. Aad *et al.* [ATLAS Collaboration], Phys. Lett. B **694**, 327 (2011) [arXiv:1009.5069 [hep-ex]].
- [70] L. Randall and M. D. Schwartz, JHEP **0111**, 003 (2001) [arXiv:hep-th/0108114].
- [71] M. Bauer, F. Goertz, U. Haisch, T. Pfoh and S. Westhoff, JHEP **1011**, 039 (2010) [arXiv:1008.0742 [hep-ph]].
- [72] J. Campbell and R. K. Ellis, <http://mcfm.fnal.gov>
- [73] P. Nason, S. Dawson and R. K. Ellis, Nucl. Phys. B **303**, 607 (1988).
- [74] A. D. Martin, W. J. Stirling, R. S. Thorne and G. Watt, Eur. Phys. J. C **63**, 189 (2009) [arXiv:0901.0002 [hep-ph]].
- [75] R. K. Ellis, W. J. Stirling and B. R. Webber, Camb. Monogr. Part. Phys. Nucl. Phys. Cosmol. **8**, 1 (1996).
- [76] E. Eichten, K. D. Lane and M. E. Peskin, Phys. Rev. Lett. **50**, 811 (1983).
- [77] K. D. Lane, arXiv:hep-ph/9605257.
- [78] J. Gao, C. S. Li, J. Wang, H. X. Zhu and C. P. Yuan, Phys. Rev. Lett. **106**, 142001 (2011) [arXiv:1101.4611 [hep-ph]].
- [79] C. Albajar *et al.* [UA1 Collaboration], Phys. Lett. B **209**, 127 (1988).

- [80] F. Abe *et al.* [CDF Collaboration], Phys. Rev. Lett. **71**, 2542 (1993).
- [81] C. D. Carone and H. Murayama, Phys. Rev. Lett. **74**, 3122 (1995) [arXiv:hep-ph/9411256].
- [82] B. Holdom, Phys. Lett. B **351**, 279 (1995) [arXiv:hep-ph/9502273].
- [83] A. I. Davydychev and J. B. Tausk, Nucl. Phys. B **397**, 123 (1993).